AN IMPROVED FINITE ELEMENT MODEL FOR VIBRATION AND CONTROL SIMULATION OF SMART COMPOSITE STRUCTURES WITH EMBEDDED PIEZOELECTRIC SENSOR AND ACTUATOR

MARINO KEKANA

A THESIS SUBMITTED TO

THE FACULTY OF ENGINEERING AND APPLIED SCIENCE

IN CANDIDACY FOR THE DEGREE OF DOCTOR OF TECHNOLOGY

AT TECHNIKON NATAL

APPROVED FOR FINAL SUBMISSION

11 Dec 2001

SUPERVISOR

Dr P. Tabakov

DATE

DURBAN, SOUTH AFRICA

DECEMBER, 2001

Summary

This thesis details a study conducted to investigate the dynamic stability of an existing active control model (ACF1) of a composite structure embedded with a piezoelectric sensor and actuator for the purpose of vibration measurement and control. Criteria for stability are established based on the second method of Lyapunov which considers the energy of the system. Results show that ACF1 is asymptotically stable although piezoelectric control effects persist when the feedback gain is set to zero. Meanwhile, it is required that there should be no control effects occurring through the piezoelectric actuator when the gain is set to zero.

In this study, a new active control model (ACF2) is developed to satisfy the stability criteria, which satisfies the requirement of no piezoelectric control effects when the gain is set to zero. In ACF2 – as well as ACF1 – the displacement and potential fields are discretised using the finite element method. In light of the locking phenomena associated with discrete displacements – which is expected to be pronounced in the case of discrete potentials due to their element geometry, ACF2-mixed is developed. ACF2 and ACF2-mixed control methodologies are similar except that in ACF2 both the displacement and potential field are discretised whereas in ACF2-mixed, only the displacement field is discretised and the potential field is continuous. Consequent to ACF2 and ACF2-mixed, stability analysis of the resulting time integration scheme is investigated as well.

The results show that the damping forces due to the piezoelectric effect do not add energy to the structure. Hence, asymptotic stability is achieved. The time integration scheme yielded a small error, consistent with the literature.

Numerical results revealed that ACF1 exhibits a high degree of locking which is relaxed in ACF2 whereas ACF2-mixed exhibits envisaged results when compared with the other two models. Therefore, the ACF2 and ACF2-mixed will provide engineers with an alternative simulation model to solve actively controlled vibration problems hitherto.

Declaration

I, Marino Kekana, declare that this thesis is essentially my own work except where due acknowledgement is made to others and has not been submitted previously for any other degree or examination.

M Kekana December 2001

Declaration

I, Marino Kekana, declare that this thesis is essentially my own work except where due acknowledgement is made to others and has not been submitted previously for any other degree or examination.

M Kekana December 2001

Table of contents

List of figures

List of tables

Nomenclature

Ψ	Residual force vector
σ	Stress vector
ε	Strain vector
$\boldsymbol{C}$	Elastic constants matrix
$\boldsymbol{D}$	Electric displacement vector
$\boldsymbol{E}$	Electric field vector
$\boldsymbol{L}$	Differential operator matrix
$\boldsymbol{N}$	Shape function matrix
$\boldsymbol{P}$	Mechanical load vector
$\boldsymbol{e}$	Piezoelectric constants matrix
$\boldsymbol{g}$	Dielectric constants matrix
$\boldsymbol{u}$	Displacement field vector
ϕ	Potential field
ρ	Mass density
A	Feedback gain
Q	Electric charge
t	Time

Embellishments

$\dot{\boldsymbol{u}}$	Time derivative
$\tilde{\boldsymbol{u}}$	Discrete values
$\overline{\boldsymbol{u}}$	Predictor values (for variables)
$\overline{\boldsymbol{e}}$	Transformed material properties (for constants)

1 Introduction

1.1 Overview

The use of composite materials in structural design has gained popularity due to several advantages that they offer compared to other materials. One of the reasons is their high strength-to-weight and stiffness-to-weight ratios, which can be tailored to match design requirements. Composite structures are also known to perform better under cyclic loads than metallic structures because of their fatigue resistance.

Composite structures are widely used in modern engineering. Their virtues related to environmental requirements may include structural integrity, weather durability and dimensional stability. Their theoretical investigations date back to the 1920s and the earliest paper cited was published by Shtayerman in 1924.

Jones (1975) classifies composite materials into three common types, namely fibrous, particulate and laminated composites. The fibrous composites consist of strong, stiff fibres held together by a matrix. The particulate composites consist of randomly dispersed hard particles of one or more materials in a matrix of another material. Laminated composites consist of two or more laminae bonded together and each lamina consists of fibres and a matrix. Lamination is used to combine the best aspects of constituent layers. These types of composite materials are also described and discussed in Gürdal *et al* (1999), amongst others. Laminated composite materials are commonly used in spacecraft and aircraft design even though they can be more susceptible to impact damage than similar metallic structures.

The weight saving characteristics of composites coupled with flexibility in the manufacturing scheme make them attractive structural materials compared to metals, in industrial, military and commercial applications. The high strength-to-weight ratio has stimulated widespread use of composites in the design of spacecraft and aircraft structures (see Middleton, 1990). In addition, the operational environment of these crafts, in particular, is characterised by fast motion and high-speed manoeuvre. This may induce uncontrolled vibration due to low structural and environmental damping. Key structural components may be subjected to fatigue and impact damage caused by space debris or bird strikes.

Recently, the study conducted by Hou and Jeronimidis (2000) showed that the main damage modes of fibre reinforced laminated composites, after an impact, are matrix cracking and delamination. Fibre failure is also observed at high input energies. Margueres, Meraghni and Beneggagh (2000) found the same results in a study conducted to investigate the threshold energy of impact on a composite consisting of resin reinforced by continuous and randomly dispersed glass fibres. Wu and Chang (1989), Sun and Liou (1989), Abrate (1998), Chun and Lam (1998) developed and studied models simulating the dynamic behaviour of composite plates under transverse impact.

It is known that whenever the vibration frequency of excitation coincides with the natural frequency of the structure, resonance occurs (see Weaver, Timoshenko and Young, 1990; Rao, 1990 and Inman, 1997). In most applications, the excitation frequency cannot be controlled since it is imposed by the functional requirements of the system. To avoid resonance, attention may be focused on controlling the natural frequency of the structure. This can be changed by either varying the mass or the stiffness. Frequently, the mass is

determined by the functional requirements of the structure, i.e. weight saving. Hence, stiffness is the property that is often changed. In laminated composite structures, this is achieved by varying the orientation of the fibre in the construction of the laminate. Gürdal *et al* (1999), Adali *et al* (1996), Walker (2000) and Walker *et al* (1996 & 1997) studied optimal design for maximum strength by varying the ply angles of laminates.

There are cases where the structure may be required to operate over a range of frequencies. In such instances, it may not be possible to avoid resonance – as well as prolonged oscillations – under all operating conditions. In such cases, damping is introduced into the structure to reduce, but not eliminate, the effects of the dynamic forces that causes vibration. This has been achieved, for example, by bonding visco-elastic material onto the structure to control its transient and/or steady state response. This material has high internal damping characteristics. The study of effects of visco-elastic damping on distributed structures is found in Inman (1994), Macé (1994), Bhimaraddi (1995), Cupia and Nizio (1995), Fung, Huang and Chen (1996), Kung and Singh (1998) and Nakra (1998). The challenge with the use of visco-elastic material is that their properties change with temperature, frequency and strain.

Also, Fung *et al* (1996) studied the dynamic stability of a simply supported visco-elastic beam subjected to harmonic and parametric excitations. The Routh-Hurwitz criterion was used to investigate the stability of the non-linear effects of the spring, mass and damping terms. The results show that increasing the visco-elastic behaviour of the beam improves the stability of the system. In addition, increasing the non-linear effects of the spring stiffness or decreasing the mass makes the system more stable.

The approaches mentioned so far, for tailoring the response of a structure, are regarded as passive control, since the output has no effect in controlling the response of the structure. It is, however, desirable to control the response of the structure with respect to its behaviour, i.e. active control. The envisaged outcome is a truly smart structure which can adapt in real time to minimise the effects of the forces causing vibration. This requires the structure to have control elements consisting of sensors and actuators. Among materials with adaptable properties - such as piezoelectric polymers and ceramics, shape memory alloys, electro-rheological fluids and optical fibres – piezoelectric materials can be used both as sensors and actuators. As a result of this capability, developments have emerged with regards the usage of piezoelectric materials to control and minimise the dynamic response of a structure for the purpose of increasing the operational life of key structural components.

1.2 Piezoelectricity

In 1880 Pierre and Jacques Curie discovered that some crystals produce a voltage which is proportional to the applied stress. Their experiment consisted of measurement of voltage appearing in specially prepared crystals which were subjected to mechanical stress. This effect was named piezoelectricity in order to distinguish it from phenomenological experience such as contact electricity (friction generated static electricity) and pyroelectricity (heat generated electricity). This effect is generally known as the direct piezoelectric effect.

In 1881 Lippmann deduced from fundamental thermodynamic principles the converse effect. That is, stress is developed in response to an applied voltage. Pierre and Jacques Curie confirmed the existence of the converse effect. They continued the investigation to obtain

quantitative proof of the complete reversibility of deformations in piezoelectric crystals. In 1910 Voigt formulated the thermodynamic potential of piezoelectricity which became the standard reference work. The challenge faced in this science then was that the mathematics required to understand it was complicated; and no visible applications of the piezoelectric crystals were apparent. Comparing piezoelectric science to electro-magnetism, which at the time was maturing from a science to a technology, fuelled the challenge (Cady, 1946).

The first serious application work with piezoelectric devices took place during World War I. The classic piezoelectric applications that are familiar now - such as microphones, ultrasonic transducers and bender element actuators – were conceived and implemented. During World War II, improvements to these applications were made.

Rapid development in aerospace exploration, structural dynamics and control of distributed mechanical systems has drawn much attention in the past two decades. The lack of structural and environmental damping experienced by aircraft/spacecraft in fast motion and high-speed manoeuvring led to reduced life of certain key structural components. It was desirable to control the vibration and to stabilise the structure after any manoeuvre. Hence, the development of active vibration control was considered.

Research on vibration sensing and active control of piezo-elastic structures has presented a challenge, both in theory and practice. Current simulation models derived through laminate formulations are based on the assumed variation of the displacement field through the laminate thickness. In the equivalent single layer (ESL) theories, the heterogeneous laminated plate/shell/beam is implicitly treated as a single homogeneous layer whose

stiffness and inertia properties are equivalent to those of the original heterogeneous laminate, by reducing the 3-D continuum problem to a 2-D or 1-D representation.

The reduction of the order of the problem is based on the assumed variation of the displacement field. The simplest theory used, in the reduction process, is the classical laminate theory based on Kirchhoff's hypothesis. It assumes that straight lines normal to the mid-plane before deformation remain straight and normal to the mid-plane after deformation. The Kirchhoff assumptions neglects the shear transverse and normal transverse deformation effects, making it inadequate in modelling laminated composite structures, unless they are very thin. Hwang and Park (1993) and Salemi and Golnarghi (1997) used this theory in conjunction with piezoelectric theory to study the active vibration control of piezo-elastic composite beams.

Catering for transverse shear deformation effects, the simplest theory used is the first order shear deformation theory, known as Mindlin (1951) theory. It extends the kinematics of Kirchhoff theory by including the transverse shear deformation effects, where the transverse shear strain is assumed to be constant along the thickness co-ordinate. This theory assumes that straight lines normal to the mid-plane before deformation remain straight but not normal to the mid-plane after deformation. The approach requires a constant, which is not known for arbitrarily laminated composite structures, to be inserted as a correction factor to account for the fact that the transverse shear stress in not uniform. The study of this theory in conjunction with piezoelectric theory is found in Tzou and Tseng (1991) and Liao and Wang (1997) for beam structures.

Higher order deformation theories are developed based on displacement fields using Taylor series expansions of the displacement components in the thickness co-ordinate. The third order shear deformation theory of Reddy (1984) assumes a quadratic variation of the transverse shear strains in the thickness co-ordinate vanishing off at the top and at the bottom of the general laminate. Reddy's theory is a special case of the third order shear deformation theory proposed by Lo, Christensen and Wu (1977). The Lo *et al* theory has higher order terms, not included by Reddy, corresponding to the transverse displacement. Chandrashekhara and Donthireddy (1997) studied active vibration control of composite beams using piezoelectric theory in conjunction with the Reddy theory.

Further research on the development of mathematical models simulating plate and shell structures with embedded piezoelectric films was conducted by Detwiler, Shen and Venkayya, (1995), Mitchell and Reddy (1995), Ray and Baz (1997), Tzou, Bao and Venkayya (1996) and Tzou and Zhong *et al* (1993 & 1993b). It is noted that these researchers used the finite element method to predict the response of the piezo-elastic structure.

The use of conventional finite elements has not been always suitable for modelling structural behaviour. Piezo-elastic structures are no exception to this. Under certain conditions, conventional elements tend to lock, resulting in an ill-conditioned problem and an inaccurate analysis. This is shown in Hughes (1987), Bathe (1996) and Kekana and Badur (2000). Tzou and Tseng (1990 & 1991) tackled the locking phenomena by introducing elements with incompatible modes. Kekana and Badur (2000) tackled the same by introducing reduced integration, and Kekana (1996) improved the accuracy of the solution through the use of

adaptive mesh refinement. The former modelled the plate with sensors/actuators using hexahedron solid elements. This made the problem large and required special techniques, i.e. Guyan (1965) reduction, to reduce the total degrees of freedom. Other problems associated with these solid elements in the analysis of thin structures are the excessive shear strain energy and high stiffness coefficients in the thickness direction, as the thickness is reduced.

On the design aspects, Miller *et al* (1995) proposed a design strategy for fully anisotropic plates using an analytical approach, based on Lyapunov's stability criteria. This required that for each piezoelectric actuator layer above the mid-plane of the plate, a corresponding sensor layer should exist below the mid-plane. Also, the input to the actuator layer must be proportional and opposite in sign to the corresponding sensor layer. The study shows that the design prerequisites may be relaxed significantly in the absence of bending-stretching coupling. Chen, Wang and Liu (1997) studied dynamic stability and the effect of active vibration control of a piezoelectric plate element by introducing the state space equations. In the study, it was shown that the displacement decay amplitude and the damping ratio increases as the feedback gain increases.

The research highlighted so far has been directed at the behaviour of structures subject to isothermal conditions. An increasing number of investigations have addressed non-isothermal responses. The work density function for crystal plates which considers pyro-thermo-piezo-elastic effects is presented in Cady (1946). A review of theoretical developments in thermopiezoelasticity with relevance to smart composite structures is presented in Tauchert *et al* (1998). Among the earliest papers cited in this field are those by Tiersten (1971) on polarised, deformable, heat conducting medium in interaction with an

electric field, and Mindlin (1974) on vibrations of plates with coupled deformation, temperature and electric fields. Further developments in the study of thermopiezoelastic plates includes classical bending theory (Tauchert, 1992), first order shear deformation theory (Jonnalagadda *et al*, 1994) and higher order shear deformation theory (Tauchert *et al*, 2000).

Other investigations in the application of piezoelectric continua in conjunction with structures include visco-piezo-elastic effects (Liao & Wang, 1997 and Ray & Baz, 1997), artificial intelligence-based control (Yang & Lee, 1997) and design optimisation (Mota Soares *et al*, 2000).

With regards to the electric signal, two approaches have been adopted. One approach assumes the signal from the sensor(s) to be the electric current thus closed circuit mode (see Miller *et al*, 1995). The other approach assumes the signal from the sensor(s) to be the potential thus open circuit mode (see Tzou and Tseng, 1990 & 1991).

The control model developed through assuming a closed circuit mode has been studied extensively by Miller *et al* (1995). Results of the study show that applying suitable potentials on the piezoelectric elements via an amplifier can effect control of a structure. At zero gain, the structure is free from any piezoelectric control. Thus, the control model resembles the passive structure at this state.

Research conducted on the active control model of the open circuit mode has also shown that control can be effected through the piezoelectric elements by applying suitable potentials

(see Tzou and Tseng, 1990 & 1991). However, these studies have not considered the bearing of the active control model at zero gain.

This study shows through stability analysis that piezoelectric effects persist at zero gain for the current active control model of the open circuit mode. As a result, a control model of the open circuit mode which resembles the passive structure at zero gain is proposed and developed. With the aid of an example, the current and proposed models are compared numerically.

The outline of the thesis is as follows: Chapter 2 presents some fundamental aspects of elasticity. These will be used in the formulation of the equations of motion describing the motion of the laminated composite structure embedded with piezoelectric materials.

In Chapter 3, the finite element formulation of the equations of motion, in which both the displacement and the potential are discretised, is presented. The conditions under which stability exists are investigated.

In Chapter 4, the basis for modelling the potential as the difference between the electrodes is presented. The equations of motion resulting from using this approach are formulated. The de-coupled dynamic equation is presented in Chapter 5. The conditions under which stability exists are also investigated.

In Chapter 6, the algorithm developed for sampling the equations of motion through the Newton-Raphson method combined with the Newmark's time integration scheme is

presented. The stability, accuracy, and convergence criteria of this algorithm are investigated as well. Numerical results are presented in Chapter 7.

1.3 References

1. ABRATE S [1998], *Impact on Composite Structures*, pub. Cambridge University Press.
2. ADALI S, WALKER M AND VERIJENKO V E [1996], Multiobjective optimization of laminated plates for maximum prebuckling, buckling and postbuckling strength using continuous and discrete ply angles, *Composite Stuctures*, **35**, 117-130.
3. BATHE K [1996] *Finite Element Procedures*, pub. Prentice Hall.
4. BHIMARADDI A [1995], Sandwich beam theory and the analysis of constrained layer damping, *Journal of Sound and Vibration*, **179**, no. 4, 591-602.
5. CADY W G [1946], *Piezoelectricity*, pub. McGraw-Hill.
6. CHANDRASHEKHARA K AND DONTHIREDDY P [1997], Vibration suppression of composite beams with piezoelectric devices using a higher order theory, *Eur. J. Mech., A/Solids*, **16**, no. 4, 709-721.
7. CHEN S –H, WANG Z –D AND LIU X –H [1997], Active vibration control and suppression for intelligent structures, *Journal of Sound and Vibration*, **200**, no. 2, 167-177.
8. CHUN L AND LAM K Y [1998], Dynamic response of fully-clamped laminated composite plates subjected to low-velocity impact of a mass, *Int. J. Solids Structures*, **35**, no. 11, 963-979.
9. CUPIA P AND NIZIO J [1995], Vibration and damping analysis of a three-layered composite plate with a viscoelastic mid-layer, *Journal of Sound and Vibration*, **183**, no. 1, 99-114.
10. DETWILER D T, SHEN M H H AND VENKAYYA V B [1995], Finite element analysis of laminated composite structures containing distributed piezoelectric actuators and sensors, *Finite Elements in Analysis and Design*, **20**, 87-100.
11. FUNG R -F, HUANG J -S AND CHEN W -H [1996], Dynamic stability of viscoelastic beam subjected to harmonic and parametric excitations simultaneously, *Journal of Sound and Vibration*, **198**, no. 1, 1-16.
12. GÜRDAL Z, HAFTKA R T AND HAJELA P [1999], *Design and Optimisation of Laminated Composite Materials*, pub. John Wiley & Sons.
13. GUYAN R J [1965] Reduction of stiffness and mass matrices, *AIAA*, **3**, 380.
14. HOU J P AND JERONIMIDIS G [2000], Bending stiffness of composite plates with delamination, *Composites: Part A*, **31**, 121-132.

15. HUGHES T J R [1987], *The Finite Element Method: Linear Static and Dynamic Finite Element Analysis*, pub. Prentice-Hall.

16. HWANG W S AND PARK H C [1993], Finite element modeling of piezoelectric sensor and actuators, *AIAA Journal*, **31**, no. 5, 930-937.

17. INMAN D J [1994], *Engineering Vibration*, pub. Prentice Hall.

18. JONES R M [1975], *Mechanics of Composite Materials*, pub. McGraw-Hill.

19. JONNALAGADDA K D, BLANDFORD G E AND TAUCHERT T R (1994), Piezothermoelastic composite plate analysis using first-order shear deformation theory, *Computers & Structures*, **51**, 79-89.

20. KEKANA M [1996], *An Adaptive Mesh Generation Technique for non-Newtonian Flow*, Masters Dissertation, Peninsula Technikon, South Africa.

21. KEKANA M AND BADUR J [2000], Modelling of beams using the reduced integration technique: statics and free vibrations, *R & D Journal*, **16**, no. 1, 9-15.

22. KUNG S W AND SINGH R [1998], Vibration analysis of beams with multiple constrained layer damping patches, *Journal of Sound and Vibration*, **212**, no. 5, 781-805.

23. LESIEUTRE G A AND LEE U [1996], A finite element for beams having segmented active constrained layers with frequency-dependent viscoelastic, *Smart Materials and Structures*, **5**, 615-627.

24. LIAO W H AND WANG K W [1997], On the analysis of viscoelastic materials for active constrained layer damping treatments, *Journal of Sound and Vibration*, **207**, no. 3, 319-334.

25. LO K H, CHRISTENSEN R M AND WU E M [1977], A higher order theory of plate deformation, *Journal of Applied Mechanics*, **44**, 663-676.

26. MACÉ M [1994], Damping of beam vibrations by means of a thin constrained viscoelastic layer: Evaluation of a new theory, *Journal of Sound and Vibration*, **172**, no. 5, 577-591.

27. MARGUERES P H, MERAGHNI F AND BENZEGGAGH [2000], Comparison of stiffness measurements and damage investigation techniques for a fatigued and post-impact fatigued GFRP composite obtained by RTM process, *Composites: Part A*, **31**, 151-163.

28. MIDDLETON D H [1990], *Composite materials in Aircraft Structures*, Longman Scientific & Technical.

29. MILLER S E, ABRAMOVICH H AND OSHMAN Y [1995], Active distributed vibration control of anisotropic piezoelectric laminated plates, *Journal of Sound and Vibration*, **183**, no. 5, 797-817.

30. MINDLIN R D [1951], Influence of rotary inertia and shear on flexural motion of isotropic, elastic plates, *Journal of Applied Mechanics*, **18**, 31-38.

31. MINDLIN R D [1974], Equations of high frequency vibrations of thermopiezoelectric crystal plates, *Int. J. Solids and Structures*, **10**, 625-637.

32. MITCHELL J A AND REDDY J N [1995], A refined hybrid plate theory for composite laminates with piezoelectric laminae, *Int. J. Solids Structures*, **32**, no. 16,2345-2367.

33. MOTA SOARES C A, MOTA SOARES C M AND FRANCO CORREIA [2000], *Modelling and Design of Laminated Composite Structures with Integrated Sensors and Actuators*, in Computational Mechanics for the Twenty-first Century edited by B H V Topping, pub. Saxe-Coburg Publications, 165-185.

34. NAKRA B C [1998], Vibration control in machines and structures using viscoelastic damping, *Journal of Sound and Vibration*, **211**, no. 3, 449-466.

35. RAO S S [1990], *Mechanical Vibrations*, pub. Addison-Wesly.

36. RAY M C AND BAZ A [1997], Optimization of energy dissipation of active constrained layer damping treatments of plates, *Journal of Sound and Vibration*, **208**, no. 3, 391-406.

37. REDDY J N [1984], A simple higher-order theory for laminated composite plates, *Journal of Applied Mechanics*, **51**, 745-752.

38. SALEMI P AND GOLNARAGHI M F [1997], Active control of forced and unforced structural vibration, *Journal of Sound and Vibration*, **208**, no. 1, 15-32.

39. SARAVANOS D A, HEYLIGER P R AND HOPKINS D A [1997], Layerwise mechanics and finite element for the dynamic analysis of piezoelectric composites plates, *Int. J. Solids Structures*, 34, no. 3, 359-378.

40. SHTAYERMAN I YA [1924], Theory of symmetrical deformation of anisotropic elastic shells, *Izvertia Kievsk. Politekh. Inst.*, 54-72.

41. SUN C T AND LIOU W J [1989], Investigation of laminated composite plates under impact dynamic loading using a three-dimensional hybrid stress finite element method, *Computers & Structures*, **33**, no. 3, 879-884.

42. TAUCHERT T R [1992], Piezothermoelastic behaviour of laminated plate, *J. Thermal Stresses*, **15**, 25-37.

43. TAUCHERT T R, ASHIDA F, NODA N, ADALI S AND VERIJENKO V [1998], Developments in thermopiezoelasticity with relevance to smart composite structures, *Proc. of 2nd Int. Conf. on Composite Science and Technology*, 17-29.

44. TAUCHERT T R, VERIJENKO V AND ADALI S [2000], High-order displacement formulation for a circular plate containing piezothermoelastic layers, *Proc. of 3rd Int. Conf. on Composite Science and Technology*, 343-348.

45. TIERSTEN H F (1971), On the nonlinear equations of thermoelectroelasticity, *Int. J. Engineering Science*, **9**, 587-604.

46. TZOU H S, BAO Y AND VENKAYYA V B [1996], Parametric study of segmented transducers laminated on cylindrical shells, part 1: sensor patches, *Journal of Sound and Vibration*, **197**, no. 2, 207-224.

47. TZOU H S AND GADRE [1989], Theoretical analysis of a multilayered thin shell coupled with piezoelectric shell actuators for distributed vibration controls, *Journal of Sound and Vibration*, **132**, no. 3, 433-450.

48. TZOU H S AND TSENG C I [1990], Distributed piezoelectric sensor/actuator design for dynamic measurement/control of distributed parameter systems: A piezoelectric finite element approach, *Journal of Sound and Vibration*, **138**, no. 1, 17-34.

49. TZOU H S AND TSENG C I [1991], Distributed vibration control and identification of coupled elastic/piezoelectric systems: finite element formulation and applications, *Mechanical Systems and Signal Processing*, **5**, no. 3, 215-231.

50. TZOU H S AND ZHONG J P [1993], Adaptive piezoelectric shell structures: Theory and experiments, *Mechanical Systems and Signal Processing*, **7**, no. 4, 307-319.

51. TZOU H S AND ZHONG J P [1993], Electromechanics and vibrations of piezoelectric shell distributed systems, *Journal of Dynamic Systems, Measurement and Control*, **115**, 506-517.

52. WALKER M [2000], A method for optimally designing laminated plates subject to fatigue loads for minimum weight using a cumulative damage constraint, *Composite Structures*, **48**, 213-218.

53. WALKER M, ADALI S AND VERIJENKO V [1996], Optimization of symmetric laminates for maximum buckling load including the effects of bending-twisting coupling, *Computers & Structures*, **58**, no. 2, 313-319.

54. WALKER M, REISS T AND ADALI S [1997], Optimal design of symmetrically laminated plates for minimum deflection and weight, *Composite Structures*, **39**, 337-346.

55. WEAVER W, TIMOSHENKO S D AND YOUNG D H [1990], *Vibration Problems in Engineering*, 5th, pub. John Wiley & sons.

56. WU H Y T AND CHANG F K [1989], Transient dynamic analysis of laminated composite plates subjected to transverse impact, *Computers & Structures*, **31**, no. 3, 453-466.

57. YANG S M AND LEE G S [1997], Vibration control of smart structures by using neural networks, *Journal of Dynamics Systems, Measurement and Control*, **119**, March, 34-39.

58. YELLIN J M AND SHEN I Y [1996], A self-sensing active constrained layer damping treatment for a Euler-Bernoulli beam, *Smart Mater. Struct.*, **5**, 628-637.

2 Theoretical background

2.1 Introduction

This chapter presents the framework which will be used as the basis for a description of qualitative and quantitative phenomena which occur in the physical world. The framework embodies a means of measuring physical quantities and, in particular, is equipped to monitor the relative positions of points in space and the progress of time (Ogden, 1984). This framework will be used in the variational formulation of the equations of motion of laminated composite structures embedded with piezoelectric films. These materials exhibit linear elastic deformation from the initial until failure occurs, i.e. fracture or plasticity. As a result, the study will focus on linear material properties within the elastic region.

2.2 Kinematics

Denote by E a three-dimensional Euclidean space and R a set of real numbers in which physical phenomena and times are observed, respectively. Consider a body B occupying a region of the Euclidean space E. Denote with $\mathbf{O}$ a common origin of two rectangular Cartesian co-ordinate systems $\boldsymbol{E}_M$ and $\boldsymbol{e}_i$ such that a generic particle P has co-ordinates i $(i = x, y, z)$ relative to $\mathbf{O}$ and basis $\boldsymbol{e}_i$ or co-ordinates M $(M = X, Y, Z)$ relative to the basis $\boldsymbol{E}_M$ (see Figure 2.1). Identify with $(\boldsymbol{X}, t_0)$ the position vector of a particle P at time t_0. During the motion of B from time t_0 to time t, its position at time $t > t_0$ is given as

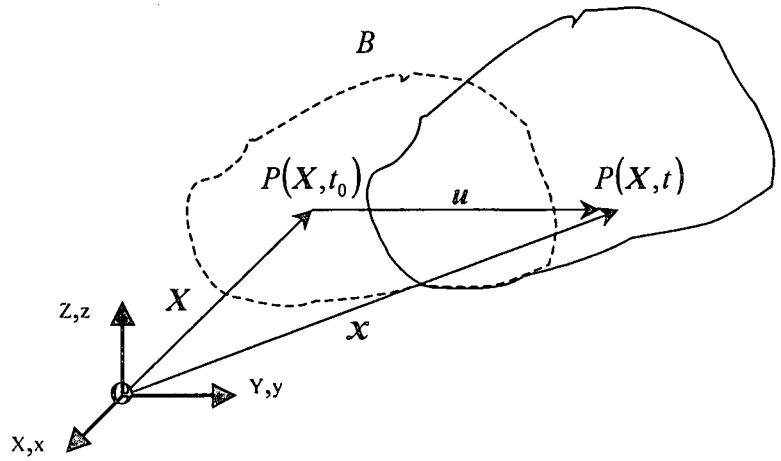

Figure 2.1 *Motion of a body in a three dimensional space. Dotted lines indicate B before displacement and deformation.*

$$x = \chi(X,t) \tag{2.1}$$

Identify with (X,t_0) and $x = \chi(X,t)$ a configuration called the reference configuration and deformed configuration, respectively. Consequently, the displacement of P from time t_0 to time t is given as

$$u = x - X = \chi(X,t) - X(t_0) \tag{2.2}$$

Thus u gives the displacement of each point in the body from the reference configuration to the deformed configuration. The displacement u may be expressed in terms of the Lagrangian co-ordinates (X,t), in which case it expresses the displacement from the position (X,t) in the reference configuration to the deformed configuration $\chi(X,t)$. On the other hand u can equally be expressed in terms of $\chi(X,t)$, the Eulerian co-ordinates, in which case it expresses the displacement that must have taken place to get to the position $\chi(X,t)$ from the reference configuration.

2.3 Deformation and strain

Consider the deformation of the body B from the reference configuration to the deformed configuration. The two configurations are taken to be independent of time such that intermediate stages will not be required. Also, the orthonormal bases $\boldsymbol{E}_M$ and $\boldsymbol{e}_i$, where $M = X,Y,Z$ and $i = x,y,z$, designate the reference and deformed configuration, respectively. Taking the differential of equation (2.1) with respect to space, yields

$$d\boldsymbol{x} = \frac{\partial \boldsymbol{x}}{\partial \boldsymbol{X}} d\boldsymbol{X} = \boldsymbol{F} d\boldsymbol{X} \tag{2.3}$$

where $\boldsymbol{F}$ is a second order tensor defined by $\mathrm{F_{iM}e_i \otimes E_M}$, sometimes called a two point tensor. Equation (2.3) describes how an arbitrary line segment $d\boldsymbol{X}$ at $\boldsymbol{X}$ transforms under deformation (i.e. change of shape and size) to a line segment $d\boldsymbol{x}$ (consisting of the same material as $d\boldsymbol{X}$) at point $\boldsymbol{x}$ in the deformed configuration. For rigid body movement $d\boldsymbol{x} = d\boldsymbol{X}$. Whereas,

$$\boldsymbol{F} = \frac{\partial \boldsymbol{x}}{\partial \boldsymbol{X}} = Grad\, \boldsymbol{x} = \boldsymbol{x} \otimes \nabla = \frac{\partial x_i}{\partial X_M} \boldsymbol{e}_i \otimes \boldsymbol{E}_M \tag{2.4}$$

$$= F_{iM} \boldsymbol{e}_i \otimes \boldsymbol{E}_M = F_{iM} \mu_i^N \boldsymbol{E}_N \otimes \boldsymbol{E}_M = F_{NM} \boldsymbol{E}_N \otimes \boldsymbol{E}_M$$

where $\otimes$ represents tensor multiplication, μ_i^N is a shifter such that $\mu_i^N \mathbf{E}_N = \mathbf{e}_i$ where N represent the co-ordinates X,Y,Z. With $J = \det \boldsymbol{F}$ and $0 \le J < \infty$, equation (2.4) represents the deformation gradient relative to the reference configuration. The condition of $J = 0$ refers to a state where the particles of a body tend to move towards its centre of gravity. Due to this, no deformation occurs. Whereas, the condition of $J \to \infty$ refers to a state where particles of a body tend to escape from its boundaries. That is, the body undergoes a state of disintegration.

The change in length of the segment dX is taken as the difference between the length of a line segment in the deformed configuration and the reference configuration, and is given in Dym and Shames (1973) and Ogden (1984) as

$$dx^2 - dX^2 = dx \cdot dx - dX \cdot dX \tag{2.5}$$

Substituting equation (2.3) into equation (2.5) yields the change in length as

$$dx^2 - dX^2 = dX \cdot \left(\boldsymbol{F}^T \boldsymbol{F} - \boldsymbol{I}\right) dX = 2dX \cdot \boldsymbol{E} dX \tag{2.6}$$

where $\boldsymbol{I} \equiv \boldsymbol{E}_M \otimes \boldsymbol{E}_M \equiv \boldsymbol{e}_i \otimes \boldsymbol{e}_i = \delta_{ij} \boldsymbol{e}_i \otimes \boldsymbol{e}_j$ represents the Gibbs identity tensor, j the co-ordinates (x, y, z) and δ_{ij} the Kroneker delta with the property $\delta_{ij} = 1$ for $i = j$ and $\delta_{ij} = 0$ for $i \neq j$. The tensor $\boldsymbol{F}^T \boldsymbol{F} - \boldsymbol{I}$ is regarded as a strain tensor in that it provides a measure of the change in length of an arbitrary line segment of the material. This leads to the definition of the Green strain tensor given by Ogden (1984) as

$$\begin{aligned} \boldsymbol{E} &= \tfrac{1}{2}\left[\boldsymbol{F}^T \boldsymbol{F} - \boldsymbol{I}\right] = \tfrac{1}{2}\left[F_{iM} \boldsymbol{E}_M \otimes \boldsymbol{e}_i F_{jN} \boldsymbol{e}_j \otimes \boldsymbol{E}_N - \boldsymbol{I}\right] \\ &= \tfrac{1}{2}\left[F_{iM} F_{jN} - \delta_{ij}\right] \boldsymbol{E}_M \otimes \boldsymbol{E}_N = E_{MN} \boldsymbol{E}_M \otimes \boldsymbol{E}_N \end{aligned} \tag{2.7}$$

The second-order tensors in Lagrangian co-ordinates are given as $\frac{1}{m}\left[\boldsymbol{U}^m - \boldsymbol{I}\right]$ for $m \neq 0$ and $\ln \boldsymbol{U}$ for $m = 0$, where $\boldsymbol{U}$ is the right stretching tensor $\boldsymbol{F} = \boldsymbol{R}\boldsymbol{U}$. It turns out that the Green $(m = 2)$, Biot $m = 1$ and Henky $m = 0$ strain tensors are of central importance in applications to elasticity (Ogden, 1984).

Considering equation (2.2), the displacement gradient is given, in the Lagrangian co-ordinates, as

$$\boldsymbol{H} = \frac{\partial \boldsymbol{u}}{\partial \boldsymbol{X}} = Grad\ \boldsymbol{u} = \frac{\partial \{\boldsymbol{x} - \boldsymbol{X}\}}{\partial \boldsymbol{X}} = \boldsymbol{F} - \boldsymbol{I} = \frac{\partial u_{\mathrm{M}}}{\partial X_{\mathrm{N}}} \boldsymbol{E}_M \otimes \boldsymbol{E}_N \tag{2.8}$$

Substituting equation (2.8) into equation (2.7) yields the Green strain tensor as

$$\boldsymbol{E} = \tfrac{1}{2}\left[\boldsymbol{H} + \boldsymbol{H}^T + \boldsymbol{H}^T \boldsymbol{H}\right] \tag{2.9}$$

or, in a full tensorial form as

$$\boldsymbol{E} = \tfrac{1}{2}\left[\frac{\partial u_M}{\partial X_N} + \frac{\partial u_N}{\partial X_M} + \frac{\partial u_I}{\partial X_M}\frac{\partial u_I}{\partial X_N}\right]\boldsymbol{E}_M \otimes \boldsymbol{E}_N = E_{MN}\boldsymbol{E}_M \otimes \boldsymbol{E}_N = \varepsilon_{MN}\boldsymbol{E}_M \otimes \boldsymbol{E}_N$$

where the symbol ε represents strains, in engineering applications (Ogden, 1984). Dym and Shames (1973) and Timoshenko (1959) arrived at the same by using a different approach.

2.4 Constitutive equations

For the structure embedded with piezoelectric sensor(s) and actuator(s), the frame of reference coincides with the orthogonal axes of the material. The structure undergoing the action of external forces is assumed to be perfectly elastic and orthotropic in behaviour. The structure is also assumed to be homogeneous, both mechanically and electrically, over its volume so that the smallest element cut from the composite possesses the same specific properties as the main structure. The deformations are assumed to take place under isothermal conditions. The constitutive relations of the form

$$\frac{\partial U}{\partial \varepsilon_{ij}} = \sigma_{ij} \tag{2.10}$$

is adopted (Dym and Shames, 1973), where U is the work density function including material properties. For elastic behaviour this work density function is called the strain energy function. In the following derivations, summation is assumed over the subscripts a,b,h,i,j,k,l,m. However no summation is implied over p and c.

2.4.1 Linear elastic behaviour

The expression for the work density function for an elastic material is given in Dym and Shames (1973) as

$$U = \tfrac{1}{2} C_{ijkl}\, \varepsilon_{ij}\, \varepsilon_{kl} \qquad i,j,k,l = 1,2,3 \qquad (2.11)$$

By using equation (2.10) the resulting constitutive equation, which is Hooke's law, is

$$\sigma_{ij} = C_{ijkl}\, \varepsilon_{kl} \qquad (2.12)$$

where σ_{ij} represents components of the stress tensor, ε_{ij} the strain tensor and C_{ijkl} the elastic constants. Also, C_{ijkl} must have the symmetry property $C_{ijkl} = C_{klij}$. Since σ_{ij} is symmetric, C_{ijkl} must also be symmetric in ij. And since ε_{kl} is symmetric, C_{ijkl} must also be symmetric in kl without violating equation (2.12). By taking advantage of the given symmetry conditions, and for the purpose of numerical simulation, equation (2.12) can be written as

$$\sigma_a = C_{ab}\, \varepsilon_b \qquad a,b = 1,2,\ldots,6 \qquad (2.13)$$

This is given in matrix form as

$$\{\sigma\} = [C]\{\varepsilon\} \qquad (2.14)$$

The expanded form for the orthotropic material is given as

$$\begin{Bmatrix} \sigma_{11} \\ \sigma_{22} \\ \sigma_{33} \\ \tau_{23} \\ \tau_{13} \\ \tau_{12} \end{Bmatrix} = \begin{bmatrix} C_{11} & C_{12} & C_{13} & 0 & 0 & 0 \\ C_{21} & C_{22} & C_{23} & 0 & 0 & 0 \\ C_{31} & C_{32} & C_{33} & 0 & 0 & 0 \\ 0 & 0 & 0 & C_{44} & 0 & 0 \\ 0 & 0 & 0 & 0 & C_{55} & 0 \\ 0 & 0 & 0 & 0 & 0 & C_{66} \end{bmatrix} \begin{Bmatrix} \varepsilon_{11} \\ \varepsilon_{22} \\ \varepsilon_{33} \\ \gamma_{23} \\ \gamma_{13} \\ \gamma_{12} \end{Bmatrix}$$

The full tensor can be reconstructed from the above equation using symmetry conditions. By assuming perfect bonding between the laminates, the reference surface deflections,

curvatures and twists are all identical at any given point in the structure. Thus, the constitutive equation for a typical lamina n $(n=1,2,...,K)$ is represented as

$$\{\sigma^{(n)}\}=[C^{(n)}]\{\varepsilon\} \tag{2.15}$$

It is, therefore, implied in the notation of equation (2.14) that

$$\{\sigma\}=\sum_{n=1}^{K}\{\sigma^{(n)}\}=\sum_{n=1}^{K}[C^{(n)}]\{\varepsilon\} \tag{2.16}$$

where K represents the total number of laminae (Herakovich, 1998; Jones, 1975).

2.4.2 *Linear elastic, dielectric and piezoelectric behaviour*

The work density function for a piezo-elastic material is given in Cady (1946) as

$$U=\tfrac{1}{2}C_{ijkl}\,\varepsilon_{ij}\,\varepsilon_{kl}-e_{hij}\,E_h\,\varepsilon_{ij}-\tfrac{1}{2}g_{hm}\,E_h\,E_m \qquad h,m=1,2,3 \tag{2.17}$$

where $\boldsymbol{C}$ represents the elasticity matrix, ε the strain, $\boldsymbol{g}$ the dielectric permittivity, $\boldsymbol{E}$ the gradient of the electric potential ϕ and $\boldsymbol{e}$ the piezoelectric matrix at constant mechanical strain. Using the approach of Dym and Shames (1973), i.e. equation (2.10), gives the constitutive equation describing the effect of additional stress induced by the electric field $\boldsymbol{E}$ as

$$\sigma_{ij}=\frac{\partial U}{\partial \varepsilon_{ij}}=C_{ijkl}\,\varepsilon_{kl}-e_{hij}\,E_h \tag{2.18}$$

Similarly, by taking advantage of the stress-strain symmetry conditions, and for the purpose of numerical simulation, this equation can be written as

$$\sigma_a=C_{ab}\,\varepsilon_b-e_{ha}\,E_h$$

This is given in matrix form as

$$\{\sigma\}=[C]\{\varepsilon\}-[e]\{E\} \tag{2.19}$$

The expanded form for the orthotropic material is given as

$$\begin{Bmatrix}\sigma_{11}\\ \sigma_{22}\\ \sigma_{33}\\ \tau_{23}\\ \tau_{13}\\ \tau_{12}\end{Bmatrix}=\begin{bmatrix}C_{11} & C_{12} & C_{13} & 0 & 0 & 0\\ C_{21} & C_{22} & C_{23} & 0 & 0 & 0\\ C_{31} & C_{32} & C_{33} & 0 & 0 & 0\\ 0 & 0 & 0 & C_{44} & 0 & 0\\ 0 & 0 & 0 & 0 & C_{55} & 0\\ 0 & 0 & 0 & 0 & 0 & C_{66}\end{bmatrix}\begin{Bmatrix}\varepsilon_{11}\\ \varepsilon_{22}\\ \varepsilon_{33}\\ \gamma_{23}\\ \gamma_{13}\\ \gamma_{12}\end{Bmatrix}-\begin{bmatrix}0 & 0 & e_{13}\\ 0 & 0 & e_{23}\\ 0 & 0 & e_{33}\\ 0 & e_{42} & 0\\ e_{51} & 0 & 0\\ 0 & 0 & 0\end{bmatrix}\begin{Bmatrix}E_1\\ E_2\\ E_3\end{Bmatrix}$$

The constitutive equation describing the effect of elastic strain on the electric displacement $\boldsymbol{D}$ is given as

$$D_h=\frac{\partial U}{\partial E_h}=e_{hij}\,\varepsilon_{ij}+g_{hm}E_m \tag{2.20}$$

Taking advantage of the stress-strain symmetry conditions, and for the purpose of numerical simulation, this equation can be written as

$$D_h=e_{ha}\,\varepsilon_a+g_{hm}\,E_m$$

and in matrix form as

$$\{\boldsymbol{D}\}=[\boldsymbol{e}]^{\mathrm{T}}\{\boldsymbol{\varepsilon}\}+[\boldsymbol{g}]\{\boldsymbol{E}\} \tag{2.21}$$

The expanded form is given as

$$\begin{Bmatrix}D_1\\ D_2\\ D_3\end{Bmatrix}=\begin{bmatrix}0 & 0 & 0 & 0 & e_{51} & 0\\ 0 & 0 & 0 & e_{42} & 0 & 0\\ e_{13} & e_{23} & e_{33} & 0 & 0 & 0\end{bmatrix}\begin{Bmatrix}\varepsilon_{11}\\ \varepsilon_{22}\\ \varepsilon_{33}\\ \gamma_{23}\\ \gamma_{12}\\ \gamma_{12}\end{Bmatrix}+\begin{bmatrix}g_{11} & 0 & 0\\ 0 & g_{22} & 0\\ 0 & 0 & g_{33}\end{bmatrix}\begin{Bmatrix}E_1\\ E_2\\ E_3\end{Bmatrix}$$

2.5 Transformation of material properties

Frequently, laminates are constructed in such a manner that the fibre angles of each layer θ_n, $(n=1,2,...,K)$, do not coincide with the co-ordinate system of the structure, namely the natural co-ordinate system, as shown in Figure 2.2 (see for instance Jones, 1975; Gürdal *et*

al, 1999; Adali *et al*, 1996; Walker, 2000 and Walker *et al* (1996 & 1997)). The aim here is to determine material properties, elastic and piezoelectric, in the co-ordinate system of the structure when those in the material co-ordinate system are known. This transformation of material properties is conducted by taking

$$e_{ij} = [T_1] = \begin{bmatrix} \cos\theta & \sin\theta & 0 \\ -\sin\theta & \cos\theta & 0 \\ 0 & 0 & 1 \end{bmatrix}$$

$$e_{im} \otimes e_{jn} = [T_2] = \begin{bmatrix} \cos^2\theta & \sin^2\theta & 0 & 0 & 0 & 2\cos\theta\cdot\sin\theta \\ \sin^2\theta & \cos^2\theta & 0 & 0 & 0 & -2\cos\theta\cdot\sin\theta \\ 0 & 0 & 1 & 0 & 0 & 0 \\ 0 & 0 & 0 & \cos\theta & -\sin\theta & 0 \\ 0 & 0 & 0 & \sin\theta & \cos\theta & 0 \\ -\cos\theta\cdot\sin\theta & \cos\theta\cdot\sin\theta & 0 & 0 & 0 & \cos^2\theta - \sin^2\theta \end{bmatrix}$$

as first and second order tensor transformation matrices, respectively (Jones, 1975 and Ogden, 1984). Since tensors can be transformed using these transformations, to transform engineering strains Jones (1975) introduced a matrix $[R]$, such that

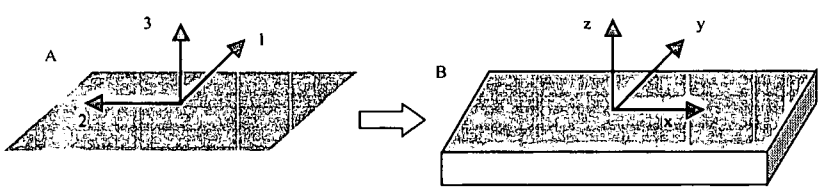

Figure 2.2 *Transformation of material properties from material (A) to natural (B) co-ordinate system.*

$$[R]\begin{Bmatrix} \varepsilon_{11} \\ \varepsilon_{22} \\ \varepsilon_{33} \\ \frac{1}{2}\gamma_{23} \\ \frac{1}{2}\gamma_{13} \\ \frac{1}{2}\gamma_{12} \end{Bmatrix}^{I'} = \begin{Bmatrix} \varepsilon_{11} \\ \varepsilon_{22} \\ \varepsilon_{33} \\ \gamma_{23} \\ \gamma_{13} \\ \gamma_{12} \end{Bmatrix}^{I'} ; \quad [R]\begin{Bmatrix} \varepsilon_{xx} \\ \varepsilon_{yy} \\ \varepsilon_{zz} \\ \frac{1}{2}\gamma_{yz} \\ \frac{1}{2}\gamma_{xz} \\ \frac{1}{2}\gamma_{xy} \end{Bmatrix} = \begin{Bmatrix} \varepsilon_{xx} \\ \varepsilon_{yy} \\ \varepsilon_{zz} \\ \gamma_{yz} \\ \gamma_{xz} \\ \gamma_{xy} \end{Bmatrix} = \{\varepsilon\} \quad \text{where } [R] = \begin{bmatrix} 1 & 0 & 0 & 0 & 0 & 0 \\ 0 & 1 & 0 & 0 & 0 & 0 \\ 0 & 0 & 1 & 0 & 0 & 0 \\ 0 & 0 & 0 & 2 & 0 & 0 \\ 0 & 0 & 0 & 0 & 2 & 0 \\ 0 & 0 & 0 & 0 & 0 & 2 \end{bmatrix}$$

where p, in this instance, represents the material co-ordinate system. The numeric and alphabetic subscripts represent components in material and natural co-ordinate axes, respectively. The strain transformation equations are (Jones, 1975)

$$\begin{aligned} &[R]^{-1}\{\varepsilon^{p}\}=[T_2][R]^{-1}\{\varepsilon\} \\ &\Rightarrow \{\varepsilon^{p}\}=[R][T_2][R]^{-1}\{\varepsilon\} \end{aligned} \tag{2.22}$$

The stress transformation equations are (Jones, 1975)

$$\{\sigma^{p}\}=\begin{Bmatrix}\sigma_{11}\\ \sigma_{22}\\ \tau_{23}\\ \tau_{13}\\ \tau_{12}\end{Bmatrix}=[T_2]\begin{Bmatrix}\sigma_{xx}\\ \sigma_{yy}\\ \tau_{yz}\\ \tau_{xz}\\ \tau_{xy}\end{Bmatrix}=[T_2]\{\sigma\} \tag{2.23}$$

The transformation for the electric potential gradient and the electric displacement, respectively, is carried out a using first order tensor transformation matrix and takes the form

$$\{E^{p}\}=\begin{Bmatrix}E_1\\ E_2\\ E_3\end{Bmatrix}=[T_1]\begin{Bmatrix}E_x\\ E_y\\ E_z\end{Bmatrix}=[T_1]\{E\} \tag{2.24}$$

$$\{D^{p}\}=\begin{Bmatrix}D_1\\ D_2\\ D_3\end{Bmatrix}=[T_1]\begin{Bmatrix}D_x\\ D_y\\ D_z\end{Bmatrix}=[T_1]\{D\} \tag{2.25}$$

Variations of the electric displacements in material co-ordinate system, i.e. equation (2.21), may be transformed to variations in the natural co-ordinate system through

$$[T_1]\{D\}=[e]^{T}[R][T_2][R]^{-1}\{\varepsilon\}+[g][T_1]\{E\} \tag{2.26}$$

Through matrix multiplication, it can be shown that $[R][T_2][R]^{-1}=[T_2]^{-T}$. The electric

displacement may then be computed using

$$\{D\} = [T_1]^{-1}[e][T_2]^{-T}\{\varepsilon\} + [T_1]^{-1}[g][T_1]\{E\} \tag{2.27}$$

Taking $[\bar{e}]^T = [T_1]^{-1}[e]^T[T_2]^{-T}$ and $[\bar{g}] = [T_1]^{-1}[g][T_1]$, the electric displacement is represented in compact form as

$$\{D\} = [\bar{e}]^T\{\varepsilon\} + [\bar{g}]\{E\} \tag{2.28}$$

The stress resultants in material co-ordinate system, i.e. equation (2.19), are transformed to the natural co-ordinate system through

$$[T_2]\{\sigma\} = [C][R][T_2][R]^{-1}\{\varepsilon\} - [e]^T[T_1]\{E\} \tag{2.29}$$

Consequent to $[R][T_2][R]^{-1} = [T_2]^{-T}$, the stress resultants represented in compact form given $[\bar{C}] = [T_2]^{-1}[C][T_2]^{-T}$ and $[\bar{e}] = [T_2]^{-1}[e][T_1]$ as

$$\{\sigma\} = [\bar{C}]\{\varepsilon\} - [\bar{e}]\{E\} \tag{2.30}$$

2.6 Piezo-elastic dynamics: a variational formulation

The equations of motion of a piezo-elastic structure are derived using the Hamilton's variational principle (Dym and Shames, 1973)[1]

$$\int_t \delta(T + W)dt = 0 \tag{2.31}$$

where T represents the kinetic energy and W the work functions. The kinetic energy (T) of the body occupying the domain Ω is defined as

---

[1] *Henceforth, the brackets $[\cdot]$ and braces $\{\cdot\}$ will be omitted, for convenience, but implied in the notation. All products will be taken as matrix multiplication except where explicit notation is indicated.*

$$T = \frac{1}{2}\int_{\Omega} \dot{\boldsymbol{u}}^T \rho \dot{\boldsymbol{u}} d\Omega \tag{2.32}$$

where ρ represent the mass density and $\dot{\boldsymbol{u}}$ the velocity vector. The work functions (W), which includes the piezo-elastic work density function (Cady, 1946) and external forces, are given as

$$W = \frac{1}{2}\int_{\Omega}\left(\overbrace{-\boldsymbol{\varepsilon}^T \overline{\boldsymbol{C}} \boldsymbol{\varepsilon}}^{strain} + \overbrace{2\boldsymbol{\varepsilon}^T \overline{\boldsymbol{e}} \boldsymbol{E}}^{piezoelectric} + \overbrace{\boldsymbol{E}^T \overline{\boldsymbol{g}} \boldsymbol{E}}^{dielectric} \right) d\Omega + \sum_{i=1}^{N} \overbrace{\boldsymbol{u}_i^T \boldsymbol{f}_i}^{ext.forces} \tag{2.33}$$

Considering mechanical and electrical forces, the work done by external forces is given in Tzou and Tseng (1990) as

$$\sum_{i=1}^{N} \boldsymbol{u}_i^T \boldsymbol{f}_i = \overbrace{\int_{\Omega} \boldsymbol{u}^T \boldsymbol{P}_b d\Omega}^{body\ force} + \overbrace{\int_{\Gamma_u} \boldsymbol{u}^T \boldsymbol{P}_s d\Gamma_u}^{surfaceload} + \overbrace{\boldsymbol{u}^T \boldsymbol{P}_c}^{pointload} - \overbrace{\int_{\Gamma_\phi} \phi Q d\Gamma_\phi}^{chargeload} \tag{2.34}$$

Where ϕ represent the electric potential, Q the electric charge, Γ_u and Γ_ϕ are the surfaces where the forces and electric charge are applied, respectively. The statement of Hamilton's variational principle, i.e. equation (2.31), states that:

Given $\boldsymbol{P}_h \in \Omega \times]0,T[$, *find* $\boldsymbol{u}(\boldsymbol{x},t)$ *and* $\phi(\boldsymbol{x},t)$ *such that for all* $\delta\boldsymbol{u}$ *and* $\delta\phi$

$$\int_{t}\left(\int_{\Omega} \left(\delta\boldsymbol{u}^T \rho \ddot{\boldsymbol{u}} + \delta\boldsymbol{\varepsilon}^T \overline{\boldsymbol{C}} \boldsymbol{\varepsilon} - \delta\boldsymbol{\varepsilon}^T \overline{\boldsymbol{e}} \boldsymbol{E} - \delta\boldsymbol{E}^T \overline{\boldsymbol{e}}^T \boldsymbol{\varepsilon} - \delta\boldsymbol{E}^T \overline{\boldsymbol{g}} \boldsymbol{E} - \delta\boldsymbol{u}^T \boldsymbol{P}_h \right) d\Omega + \int_{\Gamma_\phi} \delta(\phi Q) d\Gamma_\phi \right) dt = 0 \tag{2.35}$$

subject to initial conditions

$$\boldsymbol{u}(\boldsymbol{x},0) = \boldsymbol{u}_0,\ \dot{\boldsymbol{u}}(\boldsymbol{x},0) = \dot{\boldsymbol{u}}_0 \ \text{on}\ \boldsymbol{x} \in \Omega \tag{2.36}$$

where $\boldsymbol{x} \in \Omega$. By representing the strains as $\boldsymbol{\varepsilon} = \boldsymbol{L}\boldsymbol{u}$, the gradient of the potential as $\boldsymbol{E} = -\nabla\phi$ and separating the variations of the spatial and electric variables, Hamilton's

principle requires that

$$\int_t \left(\int_\Omega \left(\delta \boldsymbol{u}^T \rho \ddot{\boldsymbol{u}} + [\boldsymbol{L}\delta \boldsymbol{u}]^T \bar{\boldsymbol{C}} \boldsymbol{L}\boldsymbol{u} + [\boldsymbol{L}\delta \boldsymbol{u}]^T \bar{\boldsymbol{e}} \nabla \phi - \delta \boldsymbol{u}^T \boldsymbol{P}_b \right) d\Omega \right) dt = 0 \tag{2.37}$$

$$\int_t \left(\int_\Omega \left(\{\nabla \delta \phi\}^T \bar{\boldsymbol{e}}^T \boldsymbol{L}\boldsymbol{u} - \{\nabla \delta \phi\}^T \bar{\boldsymbol{g}} \nabla \phi \right) d\Omega + \int_{\Gamma_\phi} \delta(\phi Q) d\Gamma_\phi \right) dt = 0 \tag{2.38}$$

where the linear strains are given as:

$$\varepsilon = \begin{bmatrix} \frac{\partial}{\partial x} & 0 & 0 \\ 0 & \frac{\partial}{\partial y} & 0 \\ 0 & 0 & \frac{\partial}{\partial z} \\ 0 & \frac{\partial}{\partial z} & \frac{\partial}{\partial y} \\ \frac{\partial}{\partial z} & 0 & \frac{\partial}{\partial x} \\ \frac{\partial}{\partial y} & \frac{\partial}{\partial x} & 0 \end{bmatrix} \begin{Bmatrix} u \\ v \\ w \end{Bmatrix} = \boldsymbol{L}\boldsymbol{u} \tag{2.39}$$

Equation (2.37) and (2.38) represent the general formulation for a geometrical linear vibrating an-isotropic structure with piezoelectric effect. Analytical solutions for equation (2.37) and (2.38) are restricted to relatively simple geometry and boundary conditions. When the geometry and/or boundary conditions become relatively complicated, difficulties occur with both theoretical and experimental models. Thus, the finite element method becomes an important tool in modelling and analysis of such geometry.

2.7 References

1. ADALI S, WALKER M AND VERIJENKO V E [1996], Multiobjective optimization of laminated plates for maximum prebuckling, buckling and postbuckling strength using continuous and discrete ply angles, *Composite Stuctures*, **35**, 117-130.
2. CADY W G [1946], *Piezoelectricity*, pub. McGraw-Hill.
3. DYM C L AND SHAMES I H [1973], *Solid Mechanics: A Variational Approach*, pub. McGraw-Hill.

4. GÜRDAL Z, HAFTKA R T AND HAJELA P [1999], *Design and Optimisation of Laminated Composite Materials*, pub. John Wiley & Sons.
5. HERAKOVICH C T [1998], *Mechanics of Fibrous Composites*, pub. John Wiley and Sons.
6. JONES R M [1975], *Mechanics of Composite Materials*, pub. McGraw-Hill.
7. OGDEN R W [1984], *Non-linear Elastic Deformation*, pub. Ellis Horwood.
8. TZOU H S AND TSENG C I [1990], Distributed piezoelectric sensor/actuator design for dynamic measurement/control of distributed parameter systems: A piezoelectric finite element approach, *Journal of Sound and Vibration*, **138**, no. 1, 17-34.
9. WALKER M [2000], A method for optimally designing laminated plates subject to fatigue loads for minimum weight using a cumulative damage constraint, *Composite Structures*, **48**, 213-218.
10. WALKER M, ADALI S AND VERIJENKO V [1996], Optimization of symmetric laminates for maximum buckling load including the effects of bending-twisting coupling, *Computers & Structures*, **58**, no. 2, 313-319.
11. WALKER M, REISS T AND ADALI S [1997], Optimal design of symmetrically laminated plates for minimum deflection and weight, *Composite Structures*, **39**, 337-346.

3 FE and control of piezo-elastic structures

3.1 Introduction

The finite element method is a numerical method for obtaining approximate solutions to a wide variety of problems described by differential or integral equations. A given domain, like a structure, is represented as a collection of a number of geometrically simple sub-domains, called finite elements, which are connected at points called the nodes. This domain can be represented by more than one type of element. A typical element is isolated from the collection. A variational problem is then formulated, in terms of the unknown nodal values of the element, for arbitrary boundary conditions. The formulation requires piecewise continuous polynomials called interpolation functions. The global model is obtained by fitting elements together. Using nodal values at the boundaries between elements enforces the inter-element continuity. The solution is generally obtained with the aid of a computer. The finite element method coupled with the advent of the digital computer has resulted in the ability of analysing a variety of complex engineering problems (Hinton and Owen, 1997; Owen and Hinton, 1980; Cook *et al*, 1989; Bathe, 1996 and Hughes, 1987).

In this chapter, the framework of the finite element method is presented. This is then used to demonstrate the classical finite element formulation of piezo-elastic equations of motion. The main focus are studies in which the finite element method was used to solve the piezo-elastic equations of motion. These studies were conducted by Tzou and Tseng (1990 & 1991), Hwang and Park (1993), Mitchell and Reddy (1995), Detwiler and Venkayya (1995), Wang *et al* (1997) and Chandrashekhara and Donthireddy (1997) amongst others.

3.2 Approximation of variables

This section presents a framework which is used in finite element analysis to approximate solutions to problems described by governing equations. A class of functions, i.e. a functional space, in which the solution field belongs, is chosen. Thereafter, its properties are used to approximate the continuous solution field by a discrete one. In view of equation (2.37) and (2.38), the solution field belongs to a class of square integrable functions; viz. the Hilbert collection of functions.

Denote by $L_2(\Omega)$ the Hilbert collection (i.e. space) of square integrable functions and by $\boldsymbol{H}^1(\Omega)$ the Sobolev collection of functions which are square integrable up to their first derivative. This collection satisfies equation (2.37) and (2.38), since it consists of first derivatives of the displacement and potential functions. Denote by V the collection of *trial solutions* in $\boldsymbol{H}^1(\Omega)$ which takes the value of $\boldsymbol{g}$ at the boundary Γ of the domain Ω occupied by the body, i.e.

$$V = \left\{ \boldsymbol{u} \,\middle|\, \boldsymbol{u} \in \boldsymbol{H}^1, \boldsymbol{u} = \boldsymbol{g} \text{ on } \Gamma \right\} \tag{3.1}$$

For the moment, no physical attribute is attached to $\boldsymbol{u}$ except that it represents the collection of trial solutions, be it the displacement field or the potential field. Denote by $\boldsymbol{U}$ the collection of *weighting functions* or *variations* which satisfy the homogeneous essential boundary condition given as

$$\boldsymbol{U} = \left\{ \delta\boldsymbol{u} \,\middle|\, \delta\boldsymbol{u} \in \boldsymbol{H}^1, \delta\boldsymbol{u} = \boldsymbol{0} \text{ on } \Gamma \right\} \tag{3.2}$$

Denote by V^h and $\boldsymbol{U}^h$ finite-dimensional approximations of V and $\boldsymbol{U}$, respectively. The superscript h refers to the association of V^h and $\boldsymbol{U}^h$ with the mesh, or discretisation, of the

domain Ω. Each member of V^h admits the representation

$$u^h = v^h + g^h \tag{3.3}$$

where $v^h \in U^h$ and g^h satisfy the prescribed boundary condition $u = g$ on Γ. Let U^h consist of all linear combinations of functions denoted by N_i - referred to as shape, basis or interpolation functions - where $i \in [1, n]$. That is, given $v^h \in U^h$ then there exist constants q_i such that

$$v^h = \sum_{i=1}^{n} N_i q_i \tag{3.4}$$

These constants in the finite element context are the solutions, or unknowns, of the problem to be solved. The interpolation functions are chosen according to the order of interpolation required to satisfy continuity. Commonly used orders of interpolation are linear and quadratic functions.

Viewing a domain as discretised into non-overlapping finite elements (see Figure 3.1), a typical $u^h \in V^h$ may be represented as

$$u^h = \sum_{i \in \eta - \eta_u} N_i q_i + \sum_{i \in \eta_u} N_i g_i$$

$$= \sum_{i \in \eta} N_i \left(q_i|_{i \in \eta - \eta_u} + g_i|_{i \in \eta_u} \right)$$

$$u^h = N_i \tilde{u}_i \tag{3.5}$$

where η represents a set of global node numbers and $\eta_u \subset \eta$ a set of nodes at which $u = g$ is prescribed. N_i has the property

$$N_i(x_j) = \begin{cases} 1 & i = j \\ 0 & i \neq j \end{cases} \tag{3.6}$$

where $j \in [1, n]$. This allows for the continuous solution given by equation (3.1) to be approximated by the discrete one given in equation (3.5). This is the finite element method.

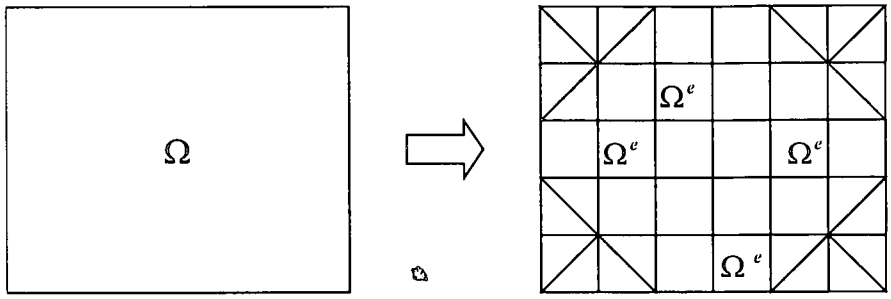

Figure 3.1 *Spatial domain* Ω *discretised into non-overlapping elements* Ω^e.

3.2.1 Electric potential

The study of piezo-elastic structures leads to the determination of the displacement field and the potential field. The displacement field is well understood in the study of structures. Hence, only an overview of the potential is given. This is approached by using the principle of work done.

Whenever the work done on a body undergoing a displacement can be represented in terms of a potential energy function, the corresponding force is said to be conservative. If the potential energy U has the value U_a at point a and the value U_b at point b, then the work $W_{a \to b}$ done by the force during any displacement from a to b, along any path, is given by

$$W_{a \to b} = U_a - U_b \tag{3.7}$$

Similarly, the force on a charged particle q' during a displacement along a radial line from a to b is a conservative force field (see Figure 3.2). The magnitude of this force on q' is

given by Coulomb's law. The work done by this force on q' as it moves from r_a to r_b is given by

$$W_{a\to b} = \int_{r_a}^{r_b} F dr \tag{3.8}$$

For a detailed derivation of this law, see Sears, Zemansky and Young (1982). Thus, the work for this particular path depends only on the endpoints.

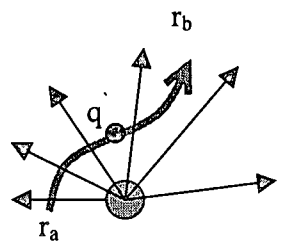

Figure 3.2 *The displacement of a particle of charge in an electric field.*

Instead of dealing directly with the potential energy of a charged particle, a concept of potential energy per unit charge is introduced. This quantity is called the potential and is represented by ϕ. Thus

$$\phi = \frac{U}{q'} = \frac{1}{4\pi\varepsilon}\sum\frac{q_i}{r_i} \tag{3.9}$$

The potential energy and charge are both scalars, so the potential is a scalar quantity. For brevity, a potential of 1 JC^{-1} is called 1 volt (V), where J is joules and C is coulombs. The potential due to a collection of point charges is obtained by use of equation (3.9), but where the electric field $\boldsymbol{E}$ is known it is obtained as

$$\phi = \phi_a - \phi_b = \oint_l \boldsymbol{E}\cdot d\boldsymbol{l} \tag{3.10}$$

The integral is called the line integral of $\boldsymbol{E}$. The instrument used to measure the potential difference between the points to which its terminals are connected is called the voltmeter.

Further consideration of the potential is given in section 4.2.

The phenomena of piezoelectric material described in section 1.2 leads to the quantification of the potential as an indication of dynamic strains induced in a vibrating structure. In the study of finite element modelling of piezo-elastic structures conducted by Tzou *et al* (Ibid.), this continuous potential field is spatially discretised using the procedure given in equation (3.5). The discrete potentials are given as

$$\phi(x,y,z,t) \approx \phi^h(x,y,z,t) = N_i(z)\widetilde{\phi}_i(x,y,t) \tag{3.11}$$

where ϕ represents the continuous potential field, ϕ^h the approximate potential field, $\widetilde{\phi}_i$ the discrete potentials, N_i the interpolation functions in the thickness direction and h the association of the approximate potential with the mesh. This corresponds to modelling the variation of the potential through the thickness of the piezoelectric film with one-dimensional finite elements. In general, i.e. three-dimensional, the approximation is given as

$$\phi \approx \phi^h = N_i(x,y,z)\widetilde{\phi}_i(t) \tag{3.12}$$

where N_i now represents the three-dimensional interpolation functions.

3.2.2 Displacement field

In the same study (Tzou *et al*, Ibid.), the displacement field is discretised using the procedure given by equation (3.5). The discrete displacements are given, in general, as

$$\boldsymbol{u}(x,y,z,t) \approx \boldsymbol{u}^h(x,y,z,t) = N_i(x,y,z)\widetilde{u}_i(t) \tag{3.13}$$

where $\boldsymbol{u}$ represents the continuous displacement field, $\boldsymbol{u}^h$ the approximate displacement field, $\widetilde{u}_i$ the discrete displacements, N_i the interpolation functions and h the association of the approximate displacements with the mesh. The discrete displacements and potentials

were used to approximate the continuous fields, respectively, used in the equations of motion, thus enabling the equation of motion to be represented in discrete form.

3.3 Finite element formulation

The discrete potentials and displacements derived previously are used in this section to present the variational statement of the continuous field in the discrete form, i.e. finite element form.

The finite element form is based on the variational statement given by equation (2.37) and (2.38), rewritten here for convenience as

$$\int_t \left(\int_\Omega \left(\delta \boldsymbol{u}^T \rho \ddot{\boldsymbol{u}} + [\boldsymbol{L}\delta \boldsymbol{u}]^T \bar{\boldsymbol{C}} \boldsymbol{L}\boldsymbol{u} + [\boldsymbol{L}\delta \boldsymbol{u}]^T \bar{\boldsymbol{e}} \nabla \phi - \delta \boldsymbol{u}^T \boldsymbol{P}_h \right) d\Omega \right) dt = 0 \qquad (3.14)$$

$$\int_t \left(\int_\Omega \left(\{\nabla \delta \phi\}^T \bar{\boldsymbol{e}}^T \boldsymbol{L}\boldsymbol{u} - \{\nabla \delta \phi\}^T \bar{\boldsymbol{g}} \nabla \phi \right) d\Omega + \int_{\Gamma_\phi} \delta(\phi Q) d\Gamma_\phi \right) dt = 0 \qquad (3.15)$$

Upon substituting equation (3.12) and (3.13) into the variational statement of equation (3.14) and (3.15), the statement of the finite element approximation states that:

Given $\boldsymbol{P}_h$ *find* $\tilde{\boldsymbol{u}}$ *and* $\tilde{\phi}$ *such that for all* $\delta\tilde{\boldsymbol{u}} \in \boldsymbol{U}^h$ *and* $\delta\tilde{\phi} \in \boldsymbol{U}^h$:

$$\int_t \int_\Omega \left(\delta \tilde{\boldsymbol{u}}^T \boldsymbol{N}_u \rho \boldsymbol{N}_u \ddot{\tilde{\boldsymbol{u}}} + \delta \tilde{\boldsymbol{u}}^T [\boldsymbol{L}\boldsymbol{N}_u]^T \bar{\boldsymbol{C}} \boldsymbol{L}\boldsymbol{N}_u \tilde{\boldsymbol{u}} + \delta \tilde{\boldsymbol{u}}^T [\boldsymbol{L}\boldsymbol{N}_u]^T \bar{\boldsymbol{e}} \nabla \boldsymbol{N}_\phi \tilde{\phi} - \delta \tilde{\boldsymbol{u}}^T \boldsymbol{N}_u^T \boldsymbol{P}_h \right) d\Omega dt = 0$$

..... (3.16)

$$\int_t \left(\int_\Omega \left(\delta \tilde{\phi}^T [\nabla \boldsymbol{N}_\phi]^T \bar{\boldsymbol{e}}^T \boldsymbol{L}\boldsymbol{N}_u \tilde{\boldsymbol{u}} - \delta \tilde{\phi}^T [\nabla \boldsymbol{N}_\phi]^T \bar{\boldsymbol{g}} \nabla \boldsymbol{N}_\phi \tilde{\phi} \right) d\Omega + \int_\Gamma \delta \tilde{\phi}^T \boldsymbol{N}_\phi^T Q d\Gamma \right) dt = 0$$

..... (3.17)

where $\boldsymbol{N}_u$ represents the interpolation functions for the displacement field and $\boldsymbol{N}_\phi$ the

interpolation functions for the potential field. Thus, interpolation functions for the displacement field may be chosen to be different to that of the potential field. In equation (3.17), the last term was obtained by assuming that the electric charge Q was constant. Adopting the representation $\boldsymbol{B}_u = \boldsymbol{L}\boldsymbol{N}_u$ and $\boldsymbol{B}_\phi = \nabla \boldsymbol{N}_\phi$, where $\boldsymbol{L}$ is given by equation (2.39), the finite element statement is written as

$$\int_t \int_\Omega \left(\delta\tilde{\boldsymbol{u}}^T \boldsymbol{N}_u^T \rho \boldsymbol{N}_u \ddot{\tilde{\boldsymbol{u}}} + \delta\tilde{\boldsymbol{u}}^T \boldsymbol{B}_u^T \bar{\boldsymbol{C}} \boldsymbol{B}_u \tilde{\boldsymbol{u}} + \delta\tilde{\boldsymbol{u}}^T \boldsymbol{B}_u^T \bar{\boldsymbol{e}} \boldsymbol{B}_\phi \tilde{\phi} \right) d\Omega dt = \int_t \int_\Omega \delta\tilde{\boldsymbol{u}}^T \boldsymbol{N}_u^T \boldsymbol{P}_b d\Omega dt$$

..... (3.18)

$$\int_t \left(\int_\Omega \left(\delta\tilde{\phi}^T \boldsymbol{B}_\phi^T \bar{\boldsymbol{e}}^T \boldsymbol{B}_u \tilde{\boldsymbol{u}} - \delta\tilde{\phi}^T \boldsymbol{B}_\phi^T \bar{\boldsymbol{g}} \boldsymbol{B}_\phi \tilde{\phi} \right) d\Omega \right) dt = -\int_t \int_\Gamma \delta\tilde{\phi}^T \boldsymbol{N}_\phi^T Q d\Gamma dt \qquad (3.19)$$

Equations (3.18) and (3.19) indicate that the variation in the total internal energy, i.e. kinetic, potential, piezoelectric and dielectric energy, is equal to the variation of the external energy, mechanical and electrical. Since for non-trivial solutions it is required that $\delta\tilde{\boldsymbol{u}} \neq \boldsymbol{0}$ and $\delta\tilde{\phi} \neq \boldsymbol{0}$, the dynamic and sensor equations were given in Tzou *et al* (Ibid.), respectively, as

$$\int_\Omega \left(\boldsymbol{N}_u^T \rho \boldsymbol{N}_u \ddot{\tilde{\boldsymbol{u}}} + \boldsymbol{B}_u^T \bar{\boldsymbol{C}} \boldsymbol{B}_u \tilde{\boldsymbol{u}} + \boldsymbol{B}_u^T \bar{\boldsymbol{e}} \boldsymbol{B}_\phi \tilde{\phi} \right) d\Omega = \int_\Omega \boldsymbol{N}_u^T \boldsymbol{P}_b d\Omega \qquad (3.20)$$

$$\int_\Omega \left(\boldsymbol{B}_\phi^T \bar{\boldsymbol{e}}^T \boldsymbol{B}_u \tilde{\boldsymbol{u}} - \boldsymbol{B}_\phi^T \bar{\boldsymbol{g}} \boldsymbol{B}_\phi \tilde{\phi} \right) d\Omega = -\int_\Gamma \boldsymbol{N}_\phi^T Q d\Gamma \qquad (3.21)$$

These equations are represented in short form as

$$\boldsymbol{M}_{uu} \ddot{\tilde{\boldsymbol{u}}} + \boldsymbol{K}_{uu} \tilde{\boldsymbol{u}} + \boldsymbol{K}_{u\phi} \tilde{\phi} = \tilde{\boldsymbol{F}} \qquad (3.22)$$

$$\boldsymbol{K}_{\phi u} \tilde{\boldsymbol{u}} - \boldsymbol{K}_{\phi\phi} \tilde{\phi} = -\tilde{\boldsymbol{G}} \qquad (3.23)$$

where

$$\boldsymbol{K}_{uu} = \int_\Omega \boldsymbol{B}_u^T \bar{\boldsymbol{C}} \boldsymbol{B}_u d\Omega \qquad (3.24)$$

represents the mechanical stiffness matrix,

$$\boldsymbol{K}_{u\phi} = \int_{\Omega} \boldsymbol{B}_u^T \bar{\boldsymbol{e}} \boldsymbol{B}_\phi d\Omega = \boldsymbol{K}_{\phi u}^T \tag{3.25}$$

the coupled mechanical-electrical stiffness matrix,

$$\boldsymbol{K}_{\phi\phi} = \int_{\Omega} \boldsymbol{B}_\phi^T \bar{\boldsymbol{g}} \boldsymbol{B}_\phi d\Omega \tag{3.26}$$

the electrical stiffness matrix,

$$\boldsymbol{M}_{uu} = \int_{\Omega} \boldsymbol{N}_u^T \rho \boldsymbol{N}_u d\Omega \tag{3.27}$$

the mass matrix,

$$\tilde{\boldsymbol{F}} = \int_{\Omega} \boldsymbol{N}_u^T \boldsymbol{P}_b d\Omega \tag{3.28}$$

the externally applied forces due to body load and

$$\tilde{\boldsymbol{G}} = \int_{\Gamma} \boldsymbol{N}_\phi^T Q d\Gamma \tag{3.29}$$

the applied electric charge. Equations (3.22) and (3.23) were then used to model the dynamic measurement and control of piezo-elastic structures.

By definition, $\delta\tilde{\phi} = \boldsymbol{0}$ at the boundary and arbitrary elsewhere in the domain occupied by the body (refer to equation (3.2)). Thus equation (3.23) is not a logical result of equation (3.19); also the order of the integral on the LHS is not the same as that of the RHS. Before the condition $\delta\tilde{\phi} = \boldsymbol{0}$ is enforced, either the surface integral on the RHS must be converted to the volume integral by using Gauss' theorem or vice versa. Further discussion on this topic is presented in sections 4.2.3 and 5.2.

3.4 Vibration measurement and control

Among materials with adaptable properties piezoelectric materials can be used both as sensors and actuators. Thus, the structure considered is a laminated composite with one piezoelectric layer serving as a distributed sensor and the other layer serving as a distributed actuator. The direct effect is used in distributed sensing and the converse effect is used in distributed active vibration suppression and control of the structure. Thus, the sensing layer detects the oscillations of the structure and the actuator layer controls the vibration of the system. The modelling of these actions as used in computational simulation follows.

3.4.1 Active measurement

The coupled finite element statement given by equation (3.22) is uncoupled to give the dynamic equation in terms of displacements only. The uncoupling process results in two sets of equations; viz. the dynamic equation and the sensor potential. These are given, respectively, as

$$\boldsymbol{M}_{uu}\ddot{\tilde{\boldsymbol{u}}} + \boldsymbol{K}_{uu}\tilde{\boldsymbol{u}} + \boldsymbol{K}_{u\phi}\boldsymbol{K}_{\phi\phi}^{-1}\boldsymbol{K}_{\phi u}\tilde{\boldsymbol{u}} = \tilde{\boldsymbol{F}} - \boldsymbol{K}_{u\phi}\boldsymbol{K}_{\phi\phi}^{-1}\tilde{\boldsymbol{G}} \tag{3.30}$$

$$\tilde{\boldsymbol{\phi}} = \boldsymbol{K}_{\phi\phi}^{-1}\left[\tilde{\boldsymbol{G}} + \boldsymbol{K}_{\phi u}\tilde{\boldsymbol{u}}\right] \tag{3.31}$$

The sensor output in equation (3.31) is composed of two components, namely the applied charge $\tilde{\boldsymbol{G}}$ and the displacements $\tilde{\boldsymbol{u}}$. Based on the assumption that there is no externally applied charge to the sensor layer, the feedback component is set to zero. As a result of this assumption, the sensor potential, contributed to by mechanical displacements only, is estimated by

$$\tilde{\boldsymbol{\phi}} = \boldsymbol{K}_{\phi\phi}^{-1}\boldsymbol{K}_{\phi u}\tilde{\boldsymbol{u}} \tag{3.32}$$

This potential is regarded as the output signal from the piezoelectric sensor layer and can be processed further to provide feedback to the piezoelectric actuators for active vibration control.

To determine the potential when the charge is applied and when there is no charge applied on the sensor layer, equation (3.31) and (3.32) is used, respectively - although the application of equation (3.31) has not been implemented in the aforementioned literature.

3.4.2 Active control model - ACF1

The right hand side of equation (3.30) contains two force terms, i.e. mechanical forces and electrical forces, respectively. The latter are given as

$$\widetilde{\boldsymbol{F}}_f = \boldsymbol{K}_{u\phi}\boldsymbol{K}_{\phi\phi}^{-1}\widetilde{\boldsymbol{G}} \tag{3.33}$$

In active vibration control, these electrical forces are regarded as feedback control forces. It should be noted (see section 3.6) that a more relevant expression for the electrical forces will be the last term on the LHS of equation (3.30). This argument is based on the assumption of constant Q which was implemented in the formulation of equation (3.17), where this constant includes zero as well.

Later, $\widetilde{\boldsymbol{G}}$ is taken as a function of the feedback potential in terms of the output from the sensor layer – contrary to the initial assumption which led to equation (3.16). Hence, the feedback forces are given by Tzou *et al* (Ibid.) as

$$\widetilde{\boldsymbol{F}}_f = \boldsymbol{K}_{u\phi}\boldsymbol{K}_{\phi\phi}^{-1}\left(A_u + A_{\dot{u}}\frac{d}{dt}\right)\widetilde{\phi} \tag{3.34}$$

where A_u represents the proportional feedback gain and $A_{\dot{u}}$ the derivative feedback gain (see also section 5.4). In vibration suppression, A_u is generally assumed to be zero.

Substituting equation (3.32) into equation (3.34), the feedback forces associated with the velocities are given as

$$\tilde{F}_f = K_{u\phi} K_{\phi\phi}^{-1} A_{\dot{u}} K_{\phi\phi}^{-1} K_{\phi u} \dot{\tilde{u}} \tag{3.35}$$

The equation of motion representing the existing active control formulation (ACF1) for a piezo-elastic structure is obtained by substituting the expression for electrical forces given in equation (3.35) into equation (3.30). The equation of motion takes the following form

$$M_{uu} \ddot{\tilde{u}} + K_{u\phi} K_{\phi\phi}^{-1} A_{\dot{u}} K_{\phi\phi}^{-1} K_{\phi u} \dot{\tilde{u}} + K_{uu} \tilde{u} + K_{u\phi} K_{\phi\phi}^{-1} K_{\phi u} \tilde{u} = \tilde{F} \tag{3.36}$$

The first term represents the contribution of the mass to the inertial forces. The magnitude of this mass depends on the density of the materials used. Once the piezo-elastic structure has been constructed, its mass cannot be varied during operation. The third term represents the contribution of the stiffness of the piezo-elastic structure. This also cannot be varied during the operation of the structure. The second term is responsible for damping out the transient vibrations of the structure. The magnitude of this damping can be varied during operation by the feedback gain $A_{\dot{u}}$. Thus, the damping depends on the piezoelectric and dielectric properties which are fixed for every piezoelectric material and the feedback potential which is variable during operation.

By decomposing the force on the RHS to $F = F_m + F_d + F_s + F_a$, where m, d and s represent mass, damping and stiffness, respectively, indicates that

$$F_a = {}^{A}K_{u\phi} \, {}^{S}K_{\phi\phi}^{-1} \, {}^{S}K_{\phi u} u \tag{3.37}$$

where the superscripts A and S represent material properties associated with the actuator and the sensor layers, respectively. This force suggests that there is a direct link/connection

between the sensor layer and the actuator layer over and above that which is associated with the feedback gain A_{ii}. As a result it takes part in feedback control since the potential from the sensor layer is fed to the actuator layer through it. This is represented by system (A) in Figure 3.3. The ideal system is represented by (B) in the same figure.

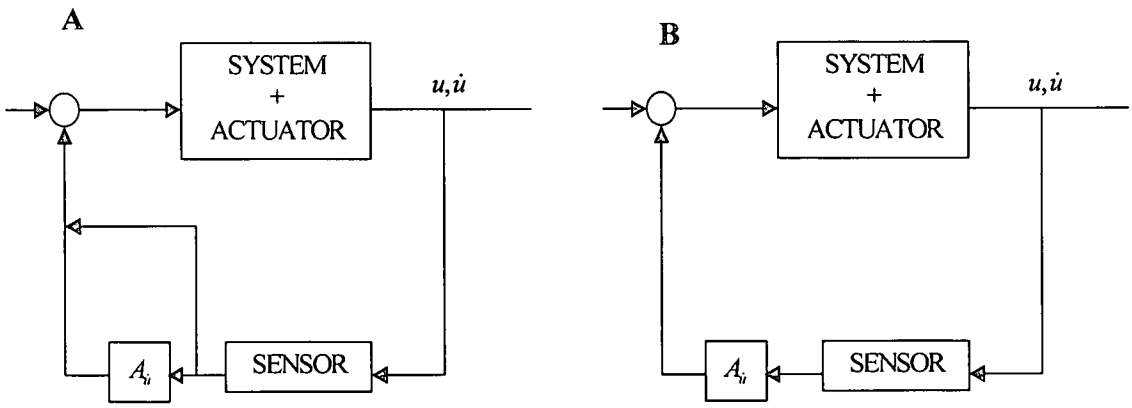

Figure 3.3 *Flowchart showing (A) the undesired and (B) the desired closed loop system.*

To determine the feedback control forces, equation (3.35) is used. However, the role of the additional force F_a in feedback control is not mentioned in Tzou *et al* (Ibid.). Therefore, stability analysis will be conducted to determine the role of this term in feedback control.

3.5 Stability analysis

The stability of a linear time-invariant system, represented by equation (3.30), is expressed by the condition that the output response must be bounded when the input is bounded. This requires all eigenvalues to have negative real parts. This implies that the transient terms decrease with time and the output response approaches a particular solution which is determined by the input. An alternate way of expressing stability uses Lyapunov's second method (D'Azzo and Houpis, 1995).

The second method of Lyapunov provides a means for determining the stability of a system without explicitly solving for the eigenvalues. The procedure requires the selection of a scalar functional $V(q)$, where $q \in \{u, \phi\}$, which is tested for conditions that indicate stability. When $V(q)$ meets these conditions, it is called a Lyapunov functional. According to Lyapunov, a system is asymptotically stable if there is only one equilibrium point and there exist an energy functional such that

$V(q)$ *is continuous and has first derivatives*

$V(q) > 0$ *for* $q \neq 0$

$V(0) = 0$

$V(q) \to \infty$ *as* $\|q\| \to \infty$

$\dot{V}(q) < 0$ *for* $q \neq 0$

This is a sufficient and not a necessary condition for stability. This functional will be chosen to be representative of the mechanical energy of the piezo-elastic structure.

3.5.1 *Lyapunov energy functional*

The energy flux is obtained from the equation of motion by pre-multiplying equation (3.36) by $\dot{u}$ and integrating with respect to time. That is

$$\int_t \dot{\tilde{u}}^T \left\{ M_{uu}\ddot{\tilde{u}} + K_{u\phi}K_{\phi\phi}^{-1}A_{\dot{u}}K_{\phi\phi}^{-1}K_{\phi u}\dot{\tilde{u}} + K_{uu}\tilde{u} + K_{u\phi}K_{\phi\phi}^{-1}K_{\phi u}\tilde{u} \right\} dt = \int_t \dot{\tilde{u}}^T F dt \qquad (3.38)$$

The external forces will be omitted since they are considered to be bounded. Thus,

$$\int_t \dot{\tilde{u}}^T F dt < \infty \qquad (3.39)$$

In light of $d\tilde{u} = \dot{\tilde{u}}dt$ and $d\dot{\tilde{u}} = \ddot{\tilde{u}}dt$, equation (3.38) suggests that the Lyapunov's functional V may be taken as

$$\int_{\dot{u}} \dot{\tilde{u}}^T M_{uu} d\dot{\tilde{u}} + \int_{u} \tilde{u}^T K_{uu} d\tilde{u} = -\int_{t} \dot{\tilde{u}}^T K_{u\phi} K_{\phi\phi}^{-1} A_{\dot{u}} K_{\phi\phi}^{-1} K_{\phi u} \dot{\tilde{u}} dt - \int_{t} \dot{\tilde{u}}^T K_{u\phi} K_{\phi\phi}^{-1} K_{\phi u} \tilde{u} dt \tag{3.40}$$

In equation (3.40), the mass matrix M_{uu} is positive definite. Also, the stiffness matrix for linear problems – as is the case in hand – is always positive definite; however in the case of physical and geometrical non-linearity there are some turning points where $|K_{uu}| = 0$ or $|K_{uu}| = \infty$. Thus the stiffness matrix K_{uu} is positive definite. When $\dot{\tilde{u}} \neq 0$ and $\tilde{u} \neq 0$, the LHS of V is positive definite. Since the LHS is equal to the RHS, the RHS is positive definite. However, asymptotic stability is guaranteed when the time derivative of equation (3.40) is negative definite: i.e. when

$$\dot{V} < 0 \tag{3.41}$$

where

$$\dot{V} = -\dot{\tilde{u}}^T K_{u\phi} K_{\phi\phi}^{-1} A_{\dot{u}} K_{\phi\phi}^{-1} K_{\phi u} \dot{\tilde{u}} - \dot{\tilde{u}}^T K_{u\phi} K_{\phi\phi}^{-1} K_{\phi u} \tilde{u} \tag{3.42}$$

The validity of expression (3.41) as a sufficient condition for asymptotic stability is supported through physical insight. Since the Lyapunov functional is based on the energy of the piezo-elastic structure, equation (3.42) represents the energy flux of the piezo-elastic structure. Thus, when the gain is set to zero, it is required that there should be no energy loss through the piezoelectric influence. The dissipative forces such as structural damping, inter-laminae friction and non-ideal boundary constraints ensure that the system energy flux of the passive structure is still negative-definite. As long as the active piezoelectric elements do not add energy to the structure, then asymptotic stability is ensured.

3.5.2 *Stability criteria*

Sufficient conditions for the actuator control inputs to ensure stability follows from expression (3.41) and (3.42). Introducing the relation $\tilde{u} \approx \dot{\tilde{u}}\Delta t$ from $d\tilde{u} = \dot{\tilde{u}}dt$, equation (3.42) can be written as

$$\dot{V} = -\dot{\tilde{u}}^{T} K_{u\phi} K_{\phi\phi}^{-1}\left[A_{u} K_{\phi\phi}^{-1} + \Delta t I\right] K_{\phi u}\dot{\tilde{u}} \tag{3.43}$$

Since the stiffness matrices are positive-definite, then equation (3.43) can be negative-definite if $A_{u} K_{\phi\phi}^{-1} + \Delta t I > 0$. This implies that the gain condition $A_{u} I > -K_{\phi\phi}\Delta t$ must be satisfied.

For the (amplifier) gain $0 < A_{u} < 1$ the potential to the actuator is less than the sensor potential in magnitude. For $A_{u} = 1$, the sensor potential is the same as the actuator potential. For $A_{u} > 1$ the actuator potential is greater than the sensor potential. The condition $A_{u} = 0$ describes a zero actuator potential. Equation (3.43) suggests that the energy will be dissipated through the piezoelectric effect when $A_{u} = 0$. Generally, it is required that there should be no energy dissipation through the piezoelectric film when the gain is set to zero. It is evident, however, that the condition $A_{u} I > -K_{\phi\phi}\Delta t$ must be satisfied for asymptotic stability to exist.

Based on equation (3.36), the second term on the LHS represents accessible feedback control elements. The fourth term represents inaccessible feedback control elements. In order to achieve the full benefit of the feedback system, all control states must be accessible. Although this requirement may not be satisfied generally, the design procedure represented

by equation (3.36) may still be valid. That is, the required feedback gain may be computed based on the accessible control states to achieve the desired response of the structure. In view of this, a new active control strategy will be developed to satisfy the condition of no piezoelectric effects when the gain is set to zero.

3.6 A new active control model - ACF2

In the direct piezoelectric effect, the potential observed across the piezoelectric layer is proportional to the deformation (as shown in equation (3.32)). That is

$$\tilde{\phi} \propto \tilde{u} \tag{3.44}$$

In the absence of feedback control, the potential will be observed on the layer identified as the sensor as well as the layer identified as the actuator. The potential observed across the actuator layer may be represented as

$$\tilde{\phi}_S^A \propto \tilde{u}$$

During feedback control, the potential observed across the actuator layer, ϕ_S^A, and the feedback potential, ϕ_f, occur at the same (measuring) points; so that the effective feedback voltage is given as

$$\phi_{eff} = \phi_f - \phi_S^A$$

The feedback potential may be represented in terms of the output from the sensor layer, through the derivative gain. Hence,

$$\phi_f = A_u \dot{\phi}_S = \phi_{eff} + \phi_S^A \tag{3.45}$$

Later it will be shown that $\tilde{\mathbf{G}}$ in equation (3.23) has no contribution in the direct and converse piezoelectric effects (see section 5.2). In view of equation (3.32), the feedback forces associated with the velocities are given as

$$\tilde{F}_f = K_{u\phi} A_{\ddot{u}} K_{\phi\phi}^{-1} K_{\phi u} \ddot{\tilde{u}} \tag{3.46}$$

Upon substituting the expression for electrical forces given in equation (3.46) into equation (3.22), the equation of motion representing the new active control formulation (ACF2) for piezo-elastic structures is represented as

$$M_{uu} \ddot{\tilde{u}} + K_{u\phi} A_{\ddot{u}} K_{\phi\phi}^{-1} K_{\phi u} \dot{\tilde{u}} + K_{uu} \tilde{u} = \tilde{F} \tag{3.47}$$

Omitting the external forces, this suggests that the Lyapunov functional V may be taken as

$$\int_{\ddot{u}} \dot{\tilde{u}}^T M_{uu} d\dot{\tilde{u}} + \int_{u} \tilde{u}^T K_{uu} d\tilde{u} = -\int_{t} \dot{\tilde{u}}^T K_{u\phi} A_{\ddot{u}} K_{\phi\phi}^{-1} K_{\phi u} \dot{\tilde{u}} dt \tag{3.48}$$

When $\dot{\tilde{u}} \neq \mathbf{0}$ and $\tilde{u} \neq \mathbf{0}$, the LHS of V is positive definite. Since the LHS is equal to the RHS, the RHS is positive definite. Considering the RHS

$$\dot{V} = -\dot{\tilde{u}}^T K_{u\phi} A_{\ddot{u}} K_{\phi\phi}^{-1} K_{\phi u} \dot{\tilde{u}} \tag{3.49}$$

With $A_{\ddot{u}} > 0$, $\dot{V}$ is negative definite. This implies that equation (3.48) is a proper Lyapunov functional. Thus, the system represented by it is asymptotically stable. It is evident that the control approach represented by equation (3.47) requires less computational effort when compared to that of equation (3.36).

3.7 References

1. BATHE K [1996] *Finite Element Procedures*, pub. Prentice Hall.
2. CHANDRASHEKHARA K AND DONTHIREDDY [1997], Vibration suppression of composite beams with piezoelectric devices using a higher order theory, *Eur. J. Mech., A/Solids*, **16**, no. 4, 709-721.
3. COOK R D, MALKUS D S AND PLESHA M E [1989], *Concepts and Application of Finite Element Analysis*, 3rd ed., John Wiley & Sons.
4. D'AZZO J J AND HOUPIS C H [1995], *Linear Control System Analysis and Design: Conventional and Modern*, 4th Ed., pub. McGraw-Hill.
5. DETWILER D T, SHEN M H H AND VENKAYYA [1995], Finite element analysis of laminated composite structures containing distributed piezoelectric actuators and sensors, *Finite Elements in Analysis and Design*, **20**, 87-100.

6. HINTON E AND OWEN D J R [1977] *Finite Element Programming*, pub. Academic Press Inc.
7. HUGHES T J R [1987], *The Finite Element Method: Linear Static and Dynamic Finite Element Analysis*, pub. Prentice-Hall.
8. HWANG W S AND PARK H C [1993], Finite Element Modeling of Piezoelectric Sensor and Actuators, *AIAA Journal,* **31**, no. 5, 930-937.
9. MITCHELL J A AND REDDY J N [1995], A refined hybrid plate theory for composite laminates with piezoelectric laminae, *Int. J. Solids Structures*, **32**, no 16, 2345-2367.
10. OWEN D R J AND HINTON E [1980], *Finite Elements in Plasticity*, pub. Pineridge Press.
11. SARAVANOS D A AND HEYLINGER P R, HOPKINS D A [1997], Layerwise Mechanics and Finite Element for the Dynamic Analysis of Piezoelectric Composites Plates, *Int. J. Solids Structures*, **34**, no 3, 359-378.
12. SEARS F W, ZEMANSKY M W AND YOUNG H D [1982], *University Physics*, pub. Addison-Wesley.
13. TZOU H S AND TSENG C I [1990], Distributed piezoelectric sensor/actuator design for dynamic measurement/control of distributed parameter systems: a piezoelectric finite element approach, *Journal of Sound and Vibration*, **138**, no. 1, 17-34.
14. TZOU H S AND TSENG C I [1991], Distributed vibration control and identification of coupled elastic/piezoelectric systems: finite element formulation and applications, *Mechanical Systems and Signal Processing*, **5**, no. 3, 215-231.
15. WANG Z, CHEN S AND HAN W [1997], The static shape control for intelligent structures, *Finite Elements in Analysis and Design*, **26**, 303-314.

4 Spatial discretisation

4.1 Introduction

The design and analysis of large complicated structures with integrated piezoelectric materials requires the development and implementation of finite element methods. Several of these finite element methods have been developed for laminated composite structures with integrated piezoelectric layers (Tzou and Tseng, 1990 & 1991; Saravanos *et al*, 1997; Mitchell and Reddy, 1995; Hwang and Park, 1993; Detwiler and Venkayya, 1995; Wang, Chen and Han, 1997 and Chandrashekara and Donthireddy, 1997). These methods used three-dimensional hexahedron (brick) elements, two-dimensional (plate) elements as well as one-dimensional (beam) elements.

What is common in Tzou *et al* (Ibid.) is that the continuous potential and displacement fields are discretised to give discrete potentials and displacements. This report presents a modelling approach whereby the continuous potential is modelled as the difference in potential measured between the electrodes separated by a dielectric. That is, finite element discretisation is not performed on the potential field. The displacement field is discretised using the finite element method. This then allows for mixed modelling of the piezo-elastic equations of motion using the active control formulation ACF2 whereby no approximation is introduced for the potential field and the displacement field is discretised using the finite element method. It is envisaged that this will overcome some inaccuracies associated with the finite element method such as the locking phenomenon.

4.2 Approximation of variables

4.2.1 *Electric potential*

Consider a laminated composite structure hosting piezoelectric films for sensing and actuating purposes as shown in Figure 4.1. These piezoelectric films are, generally, constructed out of two electrodes sandwiching a dielectric material (see Figure 4.2). Upon straining, an electric field $\mathbb{E}$ is developed, i.e. a difference in potential is observed between the electrodes.

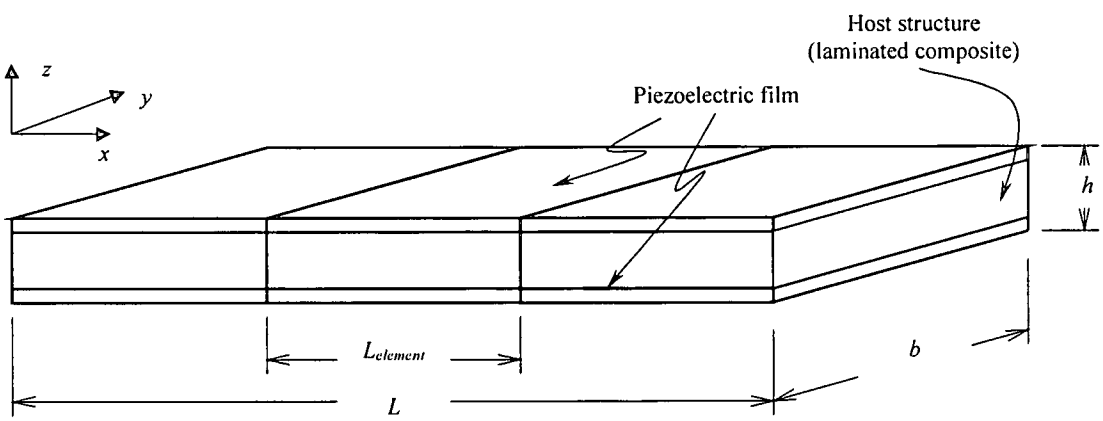

Figure 4.1 *The discretised laminated composite structure hosting piezoelectric films.*

Tzou *et al* (Ibid.) modelled this potential using finite element approximations as

$$\phi(x,y,z,t) = N_i(z)\tilde{\phi}_i(x,y,t) \tag{4.1}$$

where $N_i(z)$ represents the interpolation functions and $\tilde{\phi}_i(x,y,t)$ the nodal values. In this approach, the potential was assumed to vary linearly across the dielectric. Based on this assumption, linear interpolation functions were used. Considering the dimensions of the potential element, it is noted that the element length $= (h_n - h_{n-1})$, width $= b$, and thickness $= L_{element}$.

When using the finite element method to model beams/plates/shells, it is assumed that the thickness is very small when compared to the length. That is

$$L >> h \tag{4.2}$$

This assumption also holds at the element level (Kekana and Badur, 2000). That is

$$L_{element} >> h \tag{4.3}$$

It follows, therefore, that the aspect ratio for the potential element becomes

$$\frac{thickness}{length} = \frac{L_{element}}{h_n - h_{n-1}} >> 1 \tag{4.4}$$

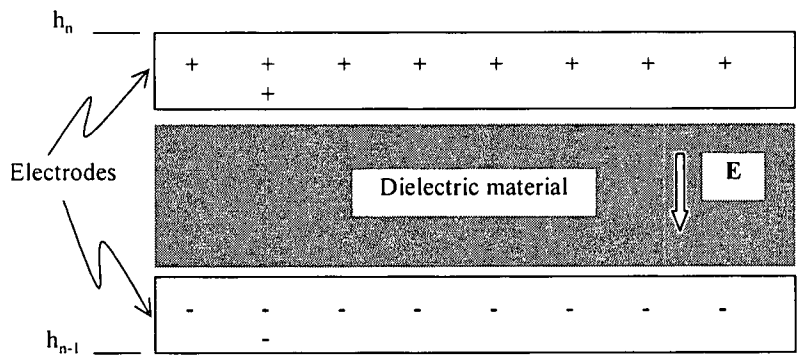

Figure 4.2 *Piezoelectric construction model showing the electric field across the electrodes.*

It has been shown that upon using finite element approximations to model the assumed displacement field, integration in the width and thickness direction is exact for beams. However, in the direction of the length, analytical results have been obtained numerically by calculating the stiffness matrix, using reduced integration for thin beams, i.e. $\frac{1}{100} \le \frac{h}{L} \le \frac{1}{16}$, and full integration for thick beams, i.e. $\frac{1}{16} \le \frac{h}{L} \le \frac{1}{10}$. For $\frac{h}{L} \to 1$ three-dimensional effects dominate both the finite element and analytical results. It was also found that in introducing mesh refinement, there was a limit case for convergence. This is governed by the aspect

ratio, as just described (Kekana and Badur, 2000).

With this in mind and using the finite element approximation to model the potential, one cannot choose *a priori* full/reduced integration scheme with confidence knowing the aspect ratio of the potential element. Also, to optimise the accuracy of the finite element solution, mesh refinement is introduced generally (Kekana, 1996; Mahomed and Kekana, 1996a & b, 1998; Kekana and Badur, 2000). This will lead to $h_n - h_{n-1} \to 0$ for the potential elements. The resulting aspect ratio becomes $\frac{L_{element}}{h_n - h_{n-1}} \to \infty$.

Meanwhile the effect on accuracy in using these ranges of aspect ratios is not known, and thus this approach must be treated with discretion. Moreover, the literature reviewed does not touch on the subject. Based on the current findings, it follows that the solution of the potential obtained using finite element approximation will be ill defined and requires treatment.

4.2.2 Treatment of the electrical potential

Practically, the electric potential is measured between the electrodes using a voltmeter. In this application, i.e. piezo-elastic structures, of importance is the difference in potential between the electrodes rather than the potential field across the dielectric. Thus, it is proposed that the continuous potential be monitored at a discrete point rather than being discretised using finite element approximation. That is

$$\phi = \phi_n - \phi_{n-1} \tag{4.5}$$

Based on Figure 4.2, this implies the potential at h_n with respect to h_{n-1}. Often, in

measuring the potential, ϕ_{n-1} is connected to ground, which is taken to be at zero potential.

Modelling the potential using this approach is computationally efficient, in comparison to (4.1), since it reduces memory requirements and computational time drastically. Also, it is a practical representation of measuring the potential. Since no approximation is made regarding the potential, the solution obtained will be accurate (exact). Even though the electric potential depends on other variables, the solution obtained will be an exact representation of them.

4.2.3 Treatment of the electric charge

In Tzou *et al* (Ibid.), the variation of the work done by electrical forces has been given as

$$\int_{\Gamma} \delta\phi Q d\Gamma \tag{4.6}$$

Q has been taken to be a constant; and a constant includes zero as well. It is well known that the potential ϕ, between two oppositely charged plates, is related to the charge Q (Sears, Zemansky and Young; 1982). This relation is given by

$$Q = C\phi \tag{4.7}$$

where C represent the capacitance. That is, the ratio of the charge and the potential is constant and depends on the dielectric material between two charged plates. Therefore, the variation of the electrical forces as presented in the literature is not adopted in this report. Consequently, the variation of the work done by electrical forces is taken as

$$\int_{\Gamma} \delta(\phi Q) d\Gamma \tag{4.8}$$

4.2.4 *Displacement field*

The continuous displacement field is approximated by a discrete one using the finite element approximation. This was given in equation (3.13) as

$$\boldsymbol{u}(\mathrm{x},\mathrm{y},\mathrm{z},\mathrm{t}) = N_i(\mathrm{x},\mathrm{y},\mathrm{z})\widetilde{u}_i(\mathrm{t}) = \boldsymbol{N}\widetilde{\boldsymbol{u}} \tag{4.9}$$

where N_i represents the interpolation functions and $\widetilde{u}_i$ the discrete displacements.

4.3 Finite element 3-D formulation

Integrating by parts the terms having the variations of the gradients of the potential in equation (2.38) results in

$$\int_t \left(\int_\Omega \left(-\delta\phi \nabla^T \bar{\boldsymbol{e}}^T \boldsymbol{L}\boldsymbol{u} + \delta\phi \nabla^T \bar{\boldsymbol{g}} \nabla\phi \right) d\Omega + \int_{\Gamma_\phi} \delta(\phi Q) d\Gamma_\phi \right) dt = 0 \tag{4.10}$$

subject to boundary conditions

$$\int_t \left(\int_\Gamma \delta\phi\, \bar{\boldsymbol{e}}^T \boldsymbol{L}\boldsymbol{u} d\Gamma - \int_\Gamma \delta\phi \bar{\boldsymbol{g}} \nabla\phi d\Gamma \right) dt = \boldsymbol{0} \tag{4.11}$$

Rearranging this equation yields

$$\int_t \int_\Gamma \delta\phi \left\{ \boldsymbol{e}^T \boldsymbol{L}\boldsymbol{u} - \bar{\boldsymbol{g}} \nabla\phi \right\} d\Gamma dt = \boldsymbol{0} \tag{4.12}$$

It follows that either the potential ϕ is specified or the electric displacement $\boldsymbol{D}$ is set to zero. Setting the latter to zero gives rise to the displacement-potential relationship

$$\boldsymbol{e}^T \boldsymbol{L}\boldsymbol{u} - \bar{\boldsymbol{g}} \nabla\phi = \boldsymbol{0} \tag{4.13}$$

Consider equation (2.37) and (4.10). Upon substituting equation (4.9), the FE statement states that

Given $\boldsymbol{P}_h$ *find* $\tilde{\boldsymbol{u}}$ *and* ϕ *such that for all* $\delta\tilde{\boldsymbol{u}} \in \boldsymbol{U}^h$ *and* $\delta\phi \in \boldsymbol{U}$ *:*

$$\int_t \left(\int_\Omega \left(\delta\tilde{\boldsymbol{u}}^T \boldsymbol{N}_u^T \rho \boldsymbol{N}_u \ddot{\tilde{\boldsymbol{u}}} + \delta\tilde{\boldsymbol{u}}^T \boldsymbol{B}_u^T \overline{\boldsymbol{C}} \boldsymbol{B}_u \tilde{\boldsymbol{u}} + \delta\tilde{\boldsymbol{u}}^T \boldsymbol{B}_u^T \overline{\boldsymbol{e}} \nabla\phi - \delta\tilde{\boldsymbol{u}}^T \boldsymbol{N}_u^T \boldsymbol{P}_h \right) d\Omega \right) dt = 0 \qquad (4.14)$$

$$\int_t \left(\int_\Omega \left(-\delta\phi \nabla^T \overline{\boldsymbol{e}}^T \boldsymbol{B}_u \tilde{\boldsymbol{u}} + \delta\phi \nabla^T \overline{\boldsymbol{g}} \nabla\phi \right) d\Omega + \int_{\Gamma_\phi} \delta(\phi Q) d\Gamma_\phi \right) dt = 0 \qquad (4.15)$$

For non-trivial solutions of equation (4.14), $\delta\tilde{\mathbf{u}} \neq \mathbf{0}$ is chosen. This gives the equation of motion as

$$\int_\Omega \left\{ \boldsymbol{N}_u^T \rho \boldsymbol{N}_u \ddot{\tilde{\boldsymbol{u}}} - \boldsymbol{B}_u^T \overline{\boldsymbol{C}} \boldsymbol{B}_u \tilde{\boldsymbol{u}} + \boldsymbol{B}_u^T \overline{\boldsymbol{e}} \nabla\phi \right\} d\Omega = \int_\Omega \boldsymbol{N}_u^T \boldsymbol{P}_h d\Omega \qquad (4.16)$$

The above equation may be written in short form as

$$\boldsymbol{M}_{uu} \ddot{\tilde{\boldsymbol{u}}} - \boldsymbol{K}_{uu} \tilde{\boldsymbol{u}} + \boldsymbol{K}_{u\nabla} \phi = \tilde{\boldsymbol{F}} \qquad (4.17)$$

where the mass and stiffness matrices are defined respectively as

$$\boldsymbol{M}_{uu} = \int_\Omega \boldsymbol{N}_u^T \rho \boldsymbol{N}_u d\Omega \qquad (4.18)$$

$$\boldsymbol{K}_{uu} = \int_\Omega \boldsymbol{B}_u^T \overline{\boldsymbol{C}} \boldsymbol{B}_u d\Omega \qquad (4.19)$$

$$\boldsymbol{K}_{u\nabla} = \int_\Omega \left[\boldsymbol{B}_u^T \overline{\boldsymbol{e}} \nabla \right] d\Omega \qquad (4.20)$$

For non-trivial solutions of equation (4.15), $\delta\phi \neq 0$ is chosen. The results of enforcing this condition will be used to de-couple the equation of motion represented by equation (4.16), thus enabling for the equation of motion to be given in terms of displacements only. Further development and results obtained by enforcing the condition $\delta\phi \neq 0$ in equation (4.15) are considered in the next chapter.

4.4 References

1. CHANDRASHEKHARA K AND DONTHIREDDY [1997], Vibration suppression of composite beams with piezoelectric devices using a higher order theory, *Eur. J. Mech., A/Solids*, **16**, no. 4, 709-721.
2. DETWILER D T, SHEN M H H AND VENKAYYA [1995], Finite element analysis of laminated composite structures containing distributed piezoelectric actuators and sensors, *Finite Elements in Analysis and Design*, **20**, 87-100.
3. HWANG W S AND PARK H C [1993], Finite element modeling of piezoelectric sensor and actuators, *AIAA Journal*, **31**, no. 5, 930-937.
4. KEKANA M [1996], *An Adaptive Mesh Generation Technique for non-Newtonian Flow*, MDip Dissertation, Peninsula Technikon, South Africa.
5. KEKANA M AND BADUR J [2000], Modelling of beams using the reduced integration technique: statics and free vibrations, *R & D Journal*, **16**, no. 1, 9-15.
6. MAHOMED N AND KEKANA M [1996], A new error estimator for adaptive mesh refinement analysis based on strain energy equalisation, *31st Solid Mechanics Conference*, Polish Academy of Sciences, Poland
7. MAHOMED N AND KEKANA M [1996], Adaptive mesh refinement analysis for non-Newtonian Stokes flow, *1st South African Conference on Applied Mechanics*, South Africa.
8. MAHOMED N AND KEKANA M [1998], An error estimator for adaptive mesh refinement analysis based on strain energy equalisation, *Computational Mechanics*, **22**, 355-366.
9. MITCHELL J A AND REDDY J N [1995], A refined hybrid plate theory for composite laminates with piezoelectric laminae, *Int. J. Solids Structures*, **32**, no 16, 2345-2367.
10. SARAVANOS D A AND HEYLINGER P R, HOPKINS D A [1997], Layerwise mechanics and finite element for the dynamic analysis of piezoelectric composites plates, *Int. J. Solids Structures*, **34**, no 3, 359-378.
11. SEARS F W, ZEMANSKY M W AND YOUNG H D [1982], *University Physics*, pub. Addison-Wesly.
12. TZOU H S AND TSENG C I [1990], Distributed piezoelectric sensor/actuator design for dynamic measurement/control of distributed parameter systems: a piezoelectric finite element approach, *Journal of Sound and Vibration*, **138**, no. 1, 17-34.
13. TZOU H S AND TSENG C I [1991], Distributed vibration control and identification of coupled elastic/piezoelectric systems: finite element formulation and applications, *Mechanical Systems and Signal Processing*, **5**, no. 3, 215-231.
14. WANG Z, CHEN S AND HAN W [1997], The static shape control for intelligent structures, *Finite Elements in Analysis and Design*, **26**, 303-314.

5 Measurement and control

5.1 Introduction

The basic configuration of a piezo-elastic structure is shown in Figure 5.1. This consists of a composite structure (beam, plate or shell) sandwiched between two thin piezoelectric layers acting as a distributed sensor and actuator, respectively. The distributed sensor generates a signal ϕ_s when the structure oscillates. This signal is then used to determine the feedback ϕ_f to be fed onto the actuator. The actuator, in turn, produces a force counteracting the motion of the structure. The advantage of incorporating the piezoelectric layers in the structure is that the sensing and actuating mechanism becomes part of the structure. Furthermore, sensing and actuating take place in real-time.

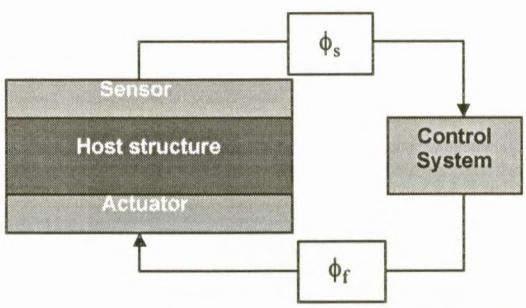

Figure 5.1 *Schematic showing the signal flow from sensor layer to the actuator layer.*

5.2 Dynamic measurement

One phenomenological characteristic of piezoelectric materials is that application of pressure σ leads to electric polarisation $\boldsymbol{D}$. By virtue of polarisation charges, an electric field $\boldsymbol{E}$ exists. This field can then be used to measure the vibration of the piezo-elastic structure, and

may be further processed to provide feedback control.

Two approaches in vibration measurement using piezoelectric sensors have been adopted. Both are based on equation (2.21). One approach assumes the signal from the sensor to be the electric current I (Hwang and Park, 1993; Chandrashekara and Donthireddy, 1997) and vibration measurement takes the form:

$$\boldsymbol{D} = e\varepsilon$$

$$\Rightarrow I = \frac{d}{dt}Q = \frac{d}{dt}\int_A e\varepsilon \, dA$$

The other approach assumes the signal from the sensor to be the potential ϕ for beam/plate applications (Tzou and Tseng, 1990 & 1991; Mitchell and Reddy, 1995; Detwiler, Shen and Venkayya, 1995; Saravanos, Heyliger and Hopkins, 1997; Wang, Cheng and Han, 1997) as well as shell applications (Tzou, 1991; Tzou, Zhong and Natori, 1993; Tzou and Zhong, 1993) and vibration measurement takes the form[2]:

$$\bar{g}\nabla\phi = -e\varepsilon$$

$$\Rightarrow \phi = -\int_l \bar{g}^{-1}\bar{e}\varepsilon \, dl$$

It is not intended to solicit the reader on which approach is appropriate, i.e. the potential or the current. This might require, perhaps, the understanding of piezoelectric phenomena at a micro-level. Rather, the appropriate signal will be determined using the variational formulation developed thus far.

[2] *It is noted that finite element approximation was not used in the above shell applications.*

Denote by $\phi_s = \phi_s(x,y,z,t)$ and $\phi_f = \phi_f(x,y,z,t)$ the internally generated (sensor) and externally applied (feedback) potential, respectively. With this in mind, the variational statement given in equation (4.10) may be rewritten as

$$\int_t \int_\Omega \delta\phi_s \left(\nabla^T \bar{\mathbf{g}} \nabla \phi_s - \nabla^T \bar{\mathbf{e}}^T \varepsilon\right) d\Omega dt = -\int_t \int_\Gamma \delta(\phi_f Q) d\Gamma dt \tag{5.1}$$

The LHS considers variations in Ω whereas the RHS considers variations in Γ. For uniformity, Gauss' theorem is applied to the RHS to associate the variations with Ω. Thus,

$$\int_t \int_\Omega \nabla(\phi_f \delta Q + Q \delta\phi_f) d\Omega dt \tag{5.2}$$

Expanding by use of the chain rule leads to

$$\int_t \int_\Omega (\delta\phi_f \nabla Q + \delta Q \nabla \phi_f + \phi_f \nabla \delta Q + Q \nabla \delta\phi_f) d\Omega dt \tag{5.3}$$

Integrating by parts gradients of the variation and grouping like terms results in

$$\int_t \int_\Gamma (Q \delta\phi_f|_\Gamma + \phi_f \delta Q|_\Gamma) d\Gamma dt \tag{5.4}$$

In equation (5.4), two boundary conditions are obtained as a result of the variational process. These are the potential and charge boundary conditions. Thus on Γ it is required that:

Either $Q = 0$ or ϕ_f is prescribed

Either $\phi_f = 0$ or Q is prescribed

The only condition that can satisfy these boundary conditions simultaneously is $Q = \phi_f = 0$. Enforcing the boundary conditions, equation (5.1) becomes

$$\int_t \int_\Omega \delta\phi_s \left(\nabla^T \bar{\mathbf{g}} \nabla \phi_s - \nabla^T \bar{\mathbf{e}} \varepsilon\right) d\Omega dt = 0 \tag{5.5}$$

Omitting the time integral, equation (5.5) may be written as

$$\int_{\Omega} \nabla^T \left(\bar{\boldsymbol{g}} \nabla \phi - \bar{\boldsymbol{e}} \boldsymbol{\varepsilon} \right) d\Omega = \int_{\Omega} \nabla^T \boldsymbol{D} d\Omega = 0 \tag{5.6}$$

This integral describes the divergence of the electric displacement in Ω. To determine the flux of the electric displacement out of the enclosing surface, Gauss' theorem may be used.

$$\int_{\Gamma} \boldsymbol{D} d\Gamma = 0 \tag{5.7}$$

As shown in equation (5.6), the electric displacement is divergence free. It follows, from equation (5.7), that the flux of the electric displacement across any surface Γ is zero. That is, the net amount of charge to flow into Ω will be zero. Thus, as much charge flows into Ω as flows out, in unit time. Subsequently, the displacement-potential relationship may be given as

$$-\bar{\boldsymbol{e}}^T \boldsymbol{\varepsilon} + \bar{\boldsymbol{g}} \nabla \phi_s = \boldsymbol{0} \tag{5.8}$$

Equation (5.8) shows that there is no electro-mechanical hysterisis, which is consistent with the assumptions introduced in section 2.4. That is, the assumed piezoelectric properties have no electrical or mechanical dissipation; the result which was arrived at earlier using a different argument (see equation (4.13)).

Since the variables in equation (5.8) are the potential and displacement, it follows that the signal obtained from the piezoelectric sensor is the potential. Thus the gradient of the potential may be computed from

$$\nabla \phi_s = \bar{\boldsymbol{g}}^{-1} \bar{\boldsymbol{e}}^T \boldsymbol{\varepsilon} \tag{5.9}$$

Equation (5.9) demonstrates the direct piezoelectric effect, i.e. potential produced as a result of strains. Using the finite element method to approximate the strains, the expression for the sensor is given as

$$\nabla \phi_s = \bar{\boldsymbol{g}}^{-1} \bar{\boldsymbol{e}}^T \boldsymbol{B}_u \tilde{\boldsymbol{u}} = \boldsymbol{K}_{\phi\nabla} \tilde{\boldsymbol{u}} \tag{5.10}$$

where $\boldsymbol{B}_u = \boldsymbol{L}\boldsymbol{N}_u$ and $\boldsymbol{L}$ is given by equation (2.39).

In view of equation (5.1), equation (5.8) shows that the piezoelectric sensor/actuator does not accumulate charge when subjected to an external potential – the accumulation of charge is a phenomenon characteristic of dielectric materials where $\boldsymbol{D} = \bar{\boldsymbol{g}}\boldsymbol{E}$. However, Tzou *et al* asserted the contrary (see equation (3.31)). It may be deduced that the work density function given in equation (2.17) leads to the statement of equation (5.8). It follows then that the feedback potential does not affect the sensor relationship of the piezoelectric material as proposed in equation (3.31).

Looking at the effect of the feedback potential from a different perspective, equation (3.46) asserts that the piezoelectric material subjected to external potential subjects a force per unit area on the host structure. This force is derived from the fact that the piezoelectric material is bonded onto the host structure. Subsequently, any tendency of the piezoelectric material to deform will lead to action-reaction forces developing between the piezoelectric material and the host structure. As a result, the forces constraining the deformation of the piezoelectric material subject the host to the same but opposite in direction. Hence, the converse effect is explained.

In this section, it has been demonstrated that the sensor potential may be determined by following the variational process. Two homogeneous boundary conditions were obtained as a result. These indicated that the feedback potential has no effect on the displacement-potential relationship of the piezoelectric sensor/actuator. Thus the assumption of no feedback potential applied on the piezoelectric sensor is obsolete. The effect of the feedback potential is to be found in equation (3.46). Furthermore, the confusion that may arise over the choice of the signal, i.e. potential or current, has been cleared. This may be extended to say that the work

density function given in equation (2.17) leads to the potential as the sensor signal. The signal type is obtained given equation (2.38) and following the procedure in equation (4.10) through (4.13). Hence, the variational process has brought about erudition in the modelling of the sensor potential that engineers could use to tackle problems.

5.3 Which direction to poll the potential?

In modelling the potential, it was taken that the major dimensions of the beam/plate coincide with the $x-y$ axes of the Cartesian plane (Tzou *et al*, Ibid.). Hence, the z-axis is used for polling. It is intended to determine the direction for polling the potential when the structure is oriented arbitrarily given that the potential is constant across the surface of the piezoelectric film. The problem is posed as:

Find the direction of polling given that the potential $\phi(\boldsymbol{x}) = c$.

The given, $\phi(\boldsymbol{x}) = c$ where $\boldsymbol{x} = (x, y, z)$, defines a level surface (Figure 5.2) of value c at the point $\boldsymbol{x}$ of the domain Ω. That is $\{\boldsymbol{x} \in \Omega \,|\, \phi(\boldsymbol{x}) = c\}$. Considering a position vector $\boldsymbol{r} = \boldsymbol{i}x + \boldsymbol{j}y + \boldsymbol{k}z$, then a small displacement in this surface may be represented by a vector $d\boldsymbol{r} = \boldsymbol{i}dx + \boldsymbol{j}dy + \boldsymbol{k}dz$ as shown in Figure 5.2. Along the surface, the change in potential is given by $d\phi = 0$. Also,

$$d\phi = \frac{\partial \phi}{\partial x}dx + \frac{\partial \phi}{\partial y}dy + \frac{\partial \phi}{\partial z}dz = \nabla\phi \cdot d\boldsymbol{r}$$

$$\Rightarrow \nabla\phi \cdot d\mathbf{r} = 0 \tag{5.11}$$

for all such small displacements $d\boldsymbol{r}$ in the surface. Since

$$\nabla\phi \cdot d\mathbf{r} = \|\nabla\phi\|\|d\mathbf{r}\| cos\theta = 0$$

$$\therefore \theta = \frac{\pi}{2} \tag{5.12}$$

Hence $\nabla\phi$ is a vector perpendicular to dr. That is, $\nabla\phi$ is a vector perpendicular to the surface at any point on the surface. For structures oriented arbitrarily, the polling direction is therefore the same as that of $\nabla\phi$. From this it suggests then, as a special case, that for beams and plates lying in the x-y plane,

$$\nabla\phi \equiv \boldsymbol{k}\frac{\partial\phi}{\partial z} \tag{5.13}$$

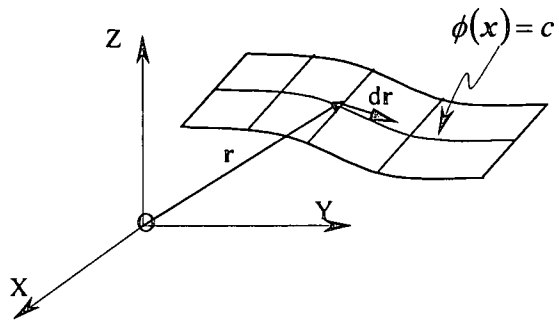

Figure 5.2 *A surface (S) in space representing* $\phi(x,y,z)=$ *constant*.

5.4 Feedback Control

When the transient response of a feedback system must be improved, it is necessary to reshape the root locus so that it is moved farther to the left of the imaginary axis. The actuating signal ϕ_f can be operated on to produce a signal that is proportional to both the magnitude and the derivative of the sensor signal ϕ_s (D'Azzo and Houpis, 1995). Physically, the effect can be described as introducing anticipation into the structure. The structure reacts not only to the magnitude of the sensor signal but also to its rate of change. The feedback signal is related to the sensor signal through the proportional plus derivative controller as

$$\phi_f = \left(A_u + A_{\dot{u}}\frac{d}{dt}\right)\phi_s \tag{5.14}$$

where A_u represents the proportional or attenuation coefficient and $A_{\dot{u}}$ the derivative or damping coefficient. If the sensor signal is changing then the actuator signal will be large and the system settles faster.

5.4.1 *Proportional control*

The sensor-actuator relationship of a proportional controller, i.e. displacement driven control, may be given as

$$\phi_f = A_u \phi_s \tag{5.15}$$

where A_u represents the proportional amplification factor. With this in mind, the last term on the LHS of equation (4.17) may be expressed as

$$\widetilde{F} = \boldsymbol{K}_{u\nabla}\phi_f = \boldsymbol{K}_{u\nabla} A_u \phi_s \tag{5.16}$$

Substituting equation (5.10) into (5.16) gives the piezoelectric feedback force responsible for signal attenuation. That is, this force will act in such a manner that it changes the stiffness of the piezo-elastic structure consequently changing its natural frequency. This force is given by

$$\widetilde{\boldsymbol{F}}_p = \boldsymbol{K}_{u\nabla} A_u \boldsymbol{K}_{\phi\nabla} \widetilde{\boldsymbol{u}} = \boldsymbol{K}_p \widetilde{\boldsymbol{u}} \tag{5.17}$$

where $\boldsymbol{K}_p$ represents the piezoelectric stiffness. The compensated equation of motion becomes

$$\boldsymbol{M}_{uu}\ddot{\widetilde{\boldsymbol{u}}} + \left[\boldsymbol{K}_{uu} + \boldsymbol{K}_{u\nabla} A_u \boldsymbol{K}_{\phi\nabla}\right]\widetilde{\boldsymbol{u}} = \widetilde{\boldsymbol{F}} \tag{5.18}$$

5.4.2 *Derivative control*

In natural structures undergoing oscillatory motion, it is observed that energy is dissipated during this process. In modelling, this is usually taken into account by introducing velocity-dependent damping forces. For structural damping this dissipation is represented by a Rayleigh damping matrix

$$\boldsymbol{C}_R = \frac{\partial \Phi}{\left\{\partial \dot{\tilde{\boldsymbol{u}}}\right\}^T \partial \dot{\tilde{\boldsymbol{u}}}}$$

where $\Phi(\dot{\boldsymbol{u}})$ is the Rayleigh dissipation function. Usually, the structural-damping matrix $\boldsymbol{C}_R$ is defined in terms of a linear combination of the mass matrix $\boldsymbol{M}$ and stiffness matrix $\boldsymbol{K}$.

To introduce damping due to the piezoelectric effect, a derivative controller is used. The sensor-actuator relationship for this controller, i.e. velocity-driven control, may be taken as

$$\phi_f = A_{ii}\dot{\phi}_s \tag{5.19}$$

where A_{ii} represents the derivative amplification factor. With this in mind, the last term on the LHS of equation (4.17) may be expressed as

$$\tilde{\boldsymbol{F}} = \boldsymbol{K}_{u\nabla}\phi_f = \boldsymbol{K}_{u\nabla}A_{ii}\dot{\phi}_s \tag{5.20}$$

Substituting equation (5.10) into (5.20) gives the piezoelectric feedback force responsible for signal damping. That is, this force will act in such a manner that it changes the damping of the piezo-elastic structure, consequently changing its settling time. This force is given by

$$\tilde{\boldsymbol{F}}_p = \boldsymbol{K}_{u\nabla}A_{ii}\boldsymbol{K}_{\phi\nabla}\dot{\tilde{\boldsymbol{u}}} = \boldsymbol{C}_p\dot{\tilde{\boldsymbol{u}}} \tag{5.21}$$

where $\boldsymbol{C}_p$ represents the piezoelectric stiffness. The compensated equation of motion becomes

$$M_{uu}\ddot{\tilde{u}} + \left[C_R + K_{u\nabla}A_{\dot{u}}K_{\phi\nabla}\right]\dot{\tilde{u}} + K_{uu}\tilde{u} = \tilde{F} \tag{5.22}$$

5.4.3 *Proportional plus derivative control*

The sensor-actuator relationship of a proportional plus derivative controller is given in equation (5.14). Thus, the last term on the LHS of equation (4.17) may be expressed as

$$\tilde{F} = K_{u\nabla}\phi_f = K_{u\nabla}\left(A_u + A_{\dot{u}}\frac{d}{dt}\right)\phi_s \tag{5.23}$$

Substituting equation (5.10) into (5.23) gives the piezoelectric feedback force responsible for signal attenuation as well as damping; that is, this force will act in such a manner that it changes the natural frequency as well as the settling time. This force is given by

$$\tilde{F}_p = K_{u\nabla}A_u K_{\phi\nabla}\tilde{u} + K_{u\nabla}A_{\dot{u}}K_{\phi\nabla}\dot{\tilde{u}} = K_p\tilde{u} + C_p\dot{\tilde{u}} \tag{5.24}$$

The compensated equation of motion thus becomes

$$M_{uu}\ddot{\tilde{u}} + \left[C_R + K_{u\nabla}A_{\dot{u}}K_{\phi\nabla}\right]\dot{\tilde{u}} + \left[K_{uu} + K_{u\nabla}A_u K_{\phi\nabla}\right]\tilde{u} = \tilde{F} \tag{5.25}$$

This equation may be written in compact form as

$$M_{uu}\ddot{\tilde{u}} + \left[C_R + C_p\right]\dot{\tilde{u}} + \left[K_{uu} + K_p\right]\tilde{u} = \tilde{F}$$

Omitting structural damping, equation (5.25) is similar to the active control formulation (ACF2) given in equation (3.47) except that in ACF2 both the displacement and the potential fields are discretised whereas in equation (5.25) only the displacement field is discretised.

5.5 Stability analysis

The purpose of this exercise is to determine whether the system of equations developed above is asymptotically stable or not. Consider the dynamic equation (5.25) after dropping the tilde (~) for convenience. Pre-multiplying by $\dot{u}^T$ and integrating with respect to the time, the

energy flux is given as

$$\int_t \dot{\boldsymbol{u}}^T \boldsymbol{M}_{uu} \ddot{\boldsymbol{u}} dt + \int_t \dot{\boldsymbol{u}}^T \left[\boldsymbol{C}_R + \boldsymbol{C}_p\right] \dot{\boldsymbol{u}} dt + \int_t \dot{\boldsymbol{u}}^T \left[\boldsymbol{K}_{uu} + \boldsymbol{K}_p\right] \boldsymbol{u} dt = \int_t \dot{\boldsymbol{u}}^T \boldsymbol{F} dt \tag{5.26}$$

The external forces will be omitted since they are bounded, that is $\int_t \dot{\boldsymbol{u}}^T \boldsymbol{F} dt < \infty$. Equation (5.26) suggests that the Lyapunov function V may be taken as

$$\int_{\dot{\boldsymbol{u}}} \boldsymbol{M}_{uu} \dot{\boldsymbol{u}} d\dot{\boldsymbol{u}} + \int_{\boldsymbol{u}} \left[\boldsymbol{K}_{uu} + \boldsymbol{K}_p\right] \boldsymbol{u} d\boldsymbol{u} = -\int_t \dot{\boldsymbol{u}}^T \left[\boldsymbol{C}_R + \boldsymbol{C}_p\right] \dot{\boldsymbol{u}} dt \tag{5.27}$$

In equation (5.27), the mass matrix $\boldsymbol{M}_{uu}$ is positive definite and the stiffness matrix $\boldsymbol{K}_{uu}$ is positive definite. For the additional piezoelectric stiffness matrix, $\boldsymbol{K}_p = \boldsymbol{K}_{u\phi} A_u \boldsymbol{K}_{\phi\nabla}$, to be positive definite, the gain condition $A_u > 0$ must be satisfied. For the gain condition $A_u \geq 0$ the piezoelectric stiffness $\boldsymbol{K}_p$ will be positive semi-definite. Therefore, when $A_u \geq 0$, $\boldsymbol{u} \neq \boldsymbol{0}$ and $\dot{\boldsymbol{u}} \neq \boldsymbol{0}$ the LHS of V is positive definite. Since the LHS is equal to the RHS, the RHS is positive definite. Considering the RHS,

$$\dot{V} = \frac{d}{dt}\left(-\int_t \dot{\boldsymbol{u}}^T \left[\boldsymbol{C}_R + \boldsymbol{C}_p\right] \dot{\boldsymbol{u}} dt \right) = -\dot{\boldsymbol{u}}^T \left[\boldsymbol{C}_R + \boldsymbol{C}_p\right] \dot{\boldsymbol{u}} \tag{5.28}$$

In equation (5.28), the Rayleigh damping matrix $\boldsymbol{C}_R$ is positive definite. For the piezoelectric damping matrix $\boldsymbol{C}_p = \boldsymbol{K}_{u\phi} A_{\dot{u}} \boldsymbol{K}_{\phi\nabla}$ to be positive definite, the gain condition $A_{\dot{u}} > 0$ must be satisfied. For the gain condition $A_{\dot{u}} \geq 0$ the piezoelectric damping matrix $\boldsymbol{C}_p$ will be positive semi-definite. Equation (5.25) suggests that energy dissipation will occur through Rayleigh damping when $A_{\dot{u}} = 0$. This is in contrast to ACF1 in equation (3.36) where energy dissipation will still occur through the piezoelectric effect when the feedback gain is set to

zero. When $\dot{\boldsymbol{u}} \neq \mathbf{0}$ and $A_{\dot{u}} > 0$ equation (5.28) is negative definite. This implies that V in (5.27) is a proper Lyapunov function which means that the system represented by it is asymptotically stable (D'azzo and Houpis, 1995). Actually, this conclusion can be extended to mean that all systems represented by equations developed using Hamilton's principle are stable.

Therefore, asymptotic stability exists when $A_{\dot{u}} > 0$ and $A_u \geq 0$ are both satisfied. Otherwise, the response of the system will be unstable. That is, the amplitude of vibration will increase in time without bound. By setting $A_{\dot{u}} = A_u = 0$, the response is reduced to that of a vibrating structure without piezoelectric feedback effects; yet, structural vibration can still be monitored through the use of equation (5.10).

5.6 Summary of active control formulations

Active control formulations presented in this thesis are brought together to give a clear perspective of the text. These are:

ACF1 [eqn (3.36)] $$\widetilde{\boldsymbol{F}} = \boldsymbol{M}_{uu}\ddot{\widetilde{\boldsymbol{u}}} + \boldsymbol{K}_{u\phi}\boldsymbol{K}_{\phi\phi}^{-1}\boldsymbol{A}_{\dot{u}}\boldsymbol{K}_{\phi\phi}^{-1}\boldsymbol{K}_{\phi u}\dot{\widetilde{\boldsymbol{u}}} + \boldsymbol{K}_{uu}\widetilde{\boldsymbol{u}} + \boldsymbol{K}_{u\phi}\boldsymbol{K}_{\phi\phi}^{-1}\boldsymbol{K}_{\phi u}\widetilde{\boldsymbol{u}}$$

ACF2 [eqn (3.47)] $$\widetilde{\boldsymbol{F}} = \boldsymbol{M}_{uu}\ddot{\widetilde{\boldsymbol{u}}} + \boldsymbol{K}_{u\phi}\boldsymbol{A}_{\dot{u}}\boldsymbol{K}_{\phi\phi}^{-1}\boldsymbol{K}_{\phi u}\dot{\widetilde{\boldsymbol{u}}} + \boldsymbol{K}_{uu}\widetilde{\boldsymbol{u}}$$

ACF2 mixed [eqn (5.22)] $$\widetilde{\boldsymbol{F}} = \boldsymbol{M}_{uu}\ddot{\widetilde{\boldsymbol{u}}} + \boldsymbol{K}_{u\nabla}\boldsymbol{A}_{\dot{u}}\boldsymbol{K}_{\phi\nabla}\dot{\widetilde{\boldsymbol{u}}} + \boldsymbol{K}_{uu}\widetilde{\boldsymbol{u}}$$

5.7 References

1. CHANDRASHEKHARA K AND DONTHIREDDY P [1997], Vibration suppresion of composite beams with piezoelectric devices using a higher order theory, *Eur. J. Mech. A/Solids*, **16**, no. 4, 709-721.

2. D'AZZO J J AND HOUPIS C H [1995], *Linear Control System Analysis and Design: Conventional and Modern*, 4th Ed., pub. McGraw-Hill.
3. DETWILER D T, SHEN M H H AND VENKAYA V B [1995], Finite element analysis of laminated composite structures containing distributed piezoelectric actuators and sensors, *Finite Elements in Analysis and Design*, **20**, 87-100.
4. HWANG W S AND PARK H C [1993], Finite element modeling of piezoelectric sensors and actuators, *AIAA Journal*, **31**, no. 5, 930-937.
5. MITCHELL J A AND REDDY JN [1995], A refined hybrid plate theory for composite laminates with piezoelectric laminae, *Int. J. Solids Structures*, **32**, no 16, 2345-2367.
6. SARAVANOS D A, HEYLIGER P R AND HOPKINS D A [1997], Layerwise mechanics and finite element for the dynamic analysis of piezoelectric composite plates, *Int. J. Solids Structures*, **34**, no. 3, 359-378.
7. TZOU H S [1991], Distributed vibration control and identification of coupled elastic/piezoelectric shells: theory and experiment, *Mechanical Systems and signal processing*, **5**, no. 3, 199-214.
8. TZOU H S AND TSENG C I [1990], Distributed sensor/actuator design for dynamic measurement/control of distributed parameter systems: a piezoelectric finite element approach, *Journal of Sound and Vibration*, **138**, no. 1, 17-34.
9. TZOU H S AND TSENG I [1991], Distributed vibration control and identification of coupled elastic/piezoelectric systems: finite element formulation and applications, *Mechanical Systems and Signal Processing*, **5**, no. 3, 215-231.
10. TZOU H S AND ZHONG J P [1993], Electromechanics and vibrations of piezoelectric shell distributed systems, *Journal of Vibration and Acoustics*, **115**, 506-517.
11. TZOU H S, ZHONG J P AND NATORI M [1993], Sensor mechanics of distributed shell convolving sensors applied to flexible rings, *Journal of Vibration and acoustics*, **115**, 40-46.
12. WANG Z, CHEN S AND HAN W [1997], The static shape control for intelligent structures, *Finite Elements in Analysis and Design*, **26**, 303-314.

6 Time discretisation

6.1 Introduction

The semi-discrete equations of motion describing the behaviour of a piezo-elastic structure are given by equation (5.25). These equations represent second order ordinary differential equations in time. Methods of dynamic analysis, i.e. modal and direct integration methods, focus on how to solve these equations. Modal methods attempt to uncouple these equations, each of which can then be solved independent of the others. Direct integration methods discretise equation (5.25) in time to obtain a sequence of simultaneous algebraic equations. Instead of trying to satisfy the equation of motion at any time t, it is then aimed to satisfy such only at discrete intervals Δt apart. Also, a variation of the displacements, velocities and accelerations within each time interval Δt is assumed. The form of the assumption of the displacement, velocities and accelerations within each time interval determines the accuracy and stability of the solution procedure. These concepts, which have been developed for passive structures, will be investigated in light of the piezo-elastic structure. This report considers a time integration scheme using the method of Newmark (1959) primarily because of its popularity (Bathe, 1996; Cook, Malkus and Plesha, 1989; Hughes, 1987; Owen and Hinton, 1980, Weaver, Timoshenko and Young, 1990; Woods, 1990). Also, recent integration methods use the method of Newmark as a benchmark (Kaunda, 1994; Crisfield and Shi, 1994).

6.2 Time response scheme

Consider the semi-discrete equation (5.25), after dropping the tilde (~), re-written as

$$\boldsymbol{F} - \boldsymbol{M}\ddot{\boldsymbol{u}} - \boldsymbol{C}\dot{\boldsymbol{u}} - \boldsymbol{K}\boldsymbol{u} = \boldsymbol{0} \tag{6.1}$$

where $\boldsymbol{M} = \boldsymbol{M}_{uu}$ represents the mass matrix, $\boldsymbol{C} = \boldsymbol{C}_R + \boldsymbol{K}_{u\phi}\boldsymbol{A}_{\dot{u}}\boldsymbol{K}_{\phi\nabla}$ the damping matrix, $\boldsymbol{K} = \boldsymbol{K}_{uu} + \boldsymbol{K}_{u\phi}\boldsymbol{A}_{u}\boldsymbol{K}_{\phi\nabla}$ the stiffness matrix, $\boldsymbol{F}$ the vector of mechanically applied forces and $\boldsymbol{u}(t)$, $\dot{\boldsymbol{u}}(t)$ and $\ddot{\boldsymbol{u}}(t)$ are the displacement, velocity and acceleration vectors, respectively. $\boldsymbol{M}$ is taken to be symmetric and positive definite whereas $\boldsymbol{C}$ and $\boldsymbol{K}$ are taken to be symmetric and positive semi-definite.

The residual "forces" (Owen and Hinton, 1980; Woods, 1990; Kaunda, 1994, 1996, 1997 & 1998) at the beginning of the time step is defined as

$$\Psi_n = \Psi(t_n, \boldsymbol{u}_n, \dot{\boldsymbol{u}}_n, \ddot{\boldsymbol{u}}_n) = \boldsymbol{F}_n - \boldsymbol{M}\ddot{\boldsymbol{u}}_n - \boldsymbol{C}\dot{\boldsymbol{u}}_n - \boldsymbol{K}\boldsymbol{u}_n \tag{6.2}$$

where $\boldsymbol{u}_n, \dot{\boldsymbol{u}}_n, \ddot{\boldsymbol{u}}_n$ are solutions to (6.2), and $n \in [1, \infty]$ is the current time-step. For the next time step $t + \Delta t$, the problem to be solved can be posed as,

$$\begin{aligned} &\textit{given } \boldsymbol{F}_{n+1} = \boldsymbol{F}(t + \Delta t), \textit{find } \{\boldsymbol{u}_{n+1}, \dot{\boldsymbol{u}}_{n+1}, \ddot{\boldsymbol{u}}_{n+1}\} \textit{ such that} \\ &\Psi(t_{n+1}, \boldsymbol{u}_{n+1}, \dot{\boldsymbol{u}}_{n+1}, \ddot{\boldsymbol{u}}_{n+1}) = \boldsymbol{0} \end{aligned} \tag{6.3}$$

subject to initial conditions of displacement and velocity. Using the notation $\Delta\boldsymbol{u}_n = \boldsymbol{u}_{n+1} - \boldsymbol{u}_n$, represent the residual "forces" at the end of the time step as

$$\Psi(t_{n+1}, \boldsymbol{u}_{n+1}, \dot{\boldsymbol{u}}_{n+1}, \ddot{\boldsymbol{u}}_{n+1}) = \Psi(t + \Delta t_n, \boldsymbol{u}_n + \Delta\boldsymbol{u}_n, \dot{\boldsymbol{u}}_n + \Delta\dot{\boldsymbol{u}}_n, \ddot{\boldsymbol{u}}_n + \Delta\ddot{\boldsymbol{u}}_n) \tag{6.4}$$

Expanding the residual "forces" using the Taylor series

$$\Psi_{n+1} = \Psi_n + \tfrac{1}{m!}\left\{\Delta t\frac{\partial}{\partial t} + \Delta x_n \frac{\partial}{\partial x} + \Delta \dot{x}_n \frac{\partial}{\partial \dot{x}} + \Delta \ddot{x}_n \frac{\partial}{\partial \ddot{x}}\right\}^m \Psi_n + O\left(\Psi_n^{m+1}\right) \tag{6.5}$$

gives rise to

$$\Psi_{n+1} = \Psi_n + \Delta F - M\Delta \ddot{u}_n - C\Delta \dot{u}_n - K\Delta u_n \tag{6.6}$$

for constant time step, where $\Delta F = F(\Delta t) = F(t+\Delta t) - F(t)$. For variable time step Δt is taken as Δt_n. Equation (6.6) is discretised in time implicitly using the following equations

$$u_{n+1} = u_n + \Delta t\dot{u}_n + \left(\tfrac{1}{2} - \beta\right)\Delta t^2 \ddot{u}_n + \beta\Delta t^2 \ddot{u}_{n+1} \tag{6.7}$$

$$\dot{u}_{n+1} = \dot{u}_n + (1-\gamma)\Delta t\ddot{u}_n + \gamma\Delta t\ddot{u}_{n+1} \tag{6.8}$$

These equations represent the prominent method of Newmark (1959) for a direct time integration scheme, where $0 \le \beta \le 1$ and $0 \le \gamma \le 1$ are Newmark's parameters. These parameters determine the stability and accuracy characteristics of time integration scheme. Rewriting equations (6.7) and (6.8) in terms of change of displacement and velocity, respectively, gives

$$\begin{aligned} \Delta u_n &= \Delta t\dot{u}_n + \tfrac{1}{2}\Delta t^2 \ddot{u}_n + \beta\Delta t^2 \Delta\ddot{u}_n \\ \Delta \dot{u}_n &= \Delta t\ddot{u}_n + \gamma\Delta t\Delta\ddot{u}_n \end{aligned} \tag{6.9}$$

Substituting equation (6.9) into equation (6.6), yields

$$\Psi_{n+1} = \Psi_n - \Delta F - \left[M + \gamma\Delta tC + \beta\Delta t^2 K\right]\Delta\ddot{u}_n - C\left\{\Delta t\ddot{u}\right\} - K\left\{\Delta t\dot{u}_n + \tfrac{1}{2}\Delta t^2 \ddot{u}_n\right\}$$

..... (6.10)

By substituting equation (6.2), which is equivalent to adding a zero force Ψ_n into equation (6.10), the expression for the residual is given as

$$\begin{aligned} \Psi_{n+1} = -\left[M + \gamma\Delta tC + \beta\Delta t^2 K\right]\Delta\ddot{u}_n + F_{n+1} - M\ddot{u}_n - \\ C\left\{\dot{u}_n + \Delta t\ddot{u}_n\right\} - K\left\{u_n + \Delta t\dot{u}_n + \tfrac{1}{2}\Delta t^2 \ddot{u}_n\right\} \end{aligned} \tag{6.11}$$

Alternatively, equation (6.11) can be written as

$$\Psi_{n+1} = -\left[M + \gamma\Delta tC + \beta\Delta t^2 K\right]\Delta\ddot{u}_n + F_{n+1} - M\ddot{\overline{u}}_n - C\dot{\overline{u}}_n - K\overline{u}_n \tag{6.12}$$

or in short form as

$$\Psi_{n+1} = -J\Delta\ddot{u}_n + \overline{F}_{n+1} \tag{6.13}$$

where the effective load is given by

$$\overline{F}_{n+1} = F_{n+1} - M\ddot{\overline{u}}_n - C\dot{\overline{u}}_n - K\overline{u}_n \tag{6.14}$$

and the Jacobian matrix, which has to exist and be invertible, is given by

$$J = M + \gamma\Delta tC + \beta\Delta t^2 K \tag{6.15}$$

By enforcing the condition given in (6.3), equation (6.11) represents the well-known Newton-Raphson method used in conjunction with Newmark's method. Hence, Newmark's method is implemented in predictor-corrector form. The predictors are given by

$$\begin{aligned}
\overline{u}_{n+1} &= u_n + \Delta t\dot{u}_n + \tfrac{1}{2}\Delta t^2\ddot{u}_n \\
\dot{\overline{u}}_{n+1} &= \dot{u}_n + \Delta t\ddot{u}_n \\
\ddot{\overline{u}}_{n+1} &= \ddot{u}_n
\end{aligned} \tag{6.16}$$

Subsequent to equation (6.11), the corrector values are calculated as

$$\begin{aligned}
u_{n+1} &= \overline{u}_{n+1} + \beta\Delta t^2\Delta\ddot{u}_n \\
\dot{u}_{n+1} &= \dot{\overline{u}}_n + \gamma\Delta t\Delta\ddot{u}_n \\
\ddot{u}_{n+1} &= \ddot{\overline{u}}_n + \Delta\ddot{u}_n
\end{aligned} \tag{6.17}$$

Thus completing the calculations for the $(n+1)^{th}$ time step.

6.3 Convergence of the algorithm

Using the predictor-corrector approach, it may be necessary to test if the solution obtained satisfies equation (6.13). Also, it helps in deciding if the results produced by a computer purporting the solution of (6.13) are to be accepted. To indicate that convergence may occur

in subsequent iteration $i+1$ within the time interval Δt, equation (6.13) is written for the use of the Newton-Raphson method as

$$\ddot{\boldsymbol{u}}^{i+1} = \ddot{\boldsymbol{u}}^{i} + \boldsymbol{J}^{-1}\overline{\boldsymbol{F}}^{i} \tag{6.18}$$

where i is the number of iterations required to satisfy the condition given in equation (6.3). From here it is seen that as $\{\boldsymbol{u}, \dot{\boldsymbol{u}}, \ddot{\boldsymbol{u}}\}^{i+1} \rightarrow \{\boldsymbol{u}, \dot{\boldsymbol{u}}, \ddot{\boldsymbol{u}}\}$, i.e. as the approximate solution converges, the residual $\Psi_{n+1}^{i+1} \rightarrow \boldsymbol{0}$.

To satisfy the condition in (6.3) on the level of forces, the test for convergence may require that

$$\left\|\Psi^{i+1}\right\| < \varepsilon_a \tag{6.19}$$

where ε_a is a predefined tolerance expressing the level of accuracy and $\| \ \|$ is any vector norm. It may as well be necessary to satisfy condition (6.3) at the level of independent variables $q \in \{\boldsymbol{u}, \dot{\boldsymbol{u}}, \ddot{\boldsymbol{u}}\}$. Thus, it may be required that

$$\left\|q^{i+1} - q^{i}\right\| < \delta_a \tag{6.20}$$

where δ_a is a predefined tolerance (Woodford,1992). Equation (6.19) and (6.20) expresses absolute accuracy. It may be more attractive to measure relative accuracy rather than absolute accuracy (Bathe *et al*, Ibid.). For solutions with large absolute values, relative accuracy, which may be regarded as percentage accuracy, is a more meaningful measure. Thus, the force and independent variables may be required to satisfy, respectively,

$$\left\|\Psi^{i+1}\right\| \div \left\|\boldsymbol{F}_{n+1}\right\| < \varepsilon_r \tag{6.21}$$

$$\left\|q^{i+1} - q^{i}\right\| \div \left\|q^{i+1}\right\| < \delta_r \tag{6.22}$$

To give an indication of when both the forces and independent variables have converged, the amount of work done by the out-of-balance forces on the displacement increments may be considered (Bathe, 1996). This is interpreted as satisfying static equilibrium, by requiring that

$$\left|\left\{\boldsymbol{u}^{i+1}-\boldsymbol{u}^{i}\right\}^{T}\Psi^{i+1}\right|=\left|\left\{\Delta\boldsymbol{u}^{i}\right\}^{T}\Psi^{i+1}\right|<c \tag{6.23}$$

where c is a predefined tolerance. However, Crisfield (1991) believes that as the limit point is approached, the amount of work done by the out-of-balance forces can be small and yet the solution procedure may not have converged at all. Since $\Delta\ddot{\boldsymbol{u}}$ is readily available, equation (6.23) may be given as

$$\left|\beta\,\Delta t^{2}\left\{\Delta\ddot{\boldsymbol{u}}^{i}\right\}^{T}\Psi^{i+1}\right|<c \tag{6.24}$$

Assuming that the solution converges for a given interval Δt_1, a smaller interval Δt_2 will yield a smaller amount of work done by the out-of-balance force. An interval $\Delta t_n<\ldots<\Delta t_2<\Delta t_1$ will yield an even smaller amount of work done that can satisfy the criterion for convergence. Hence, the iteration procedure will terminate before the solution converges to an acceptable accuracy.

The criteria for convergence used in this thesis follows from equation (6.12), after enforcing the requirement given in (6.3), rewritten here as

$$\boldsymbol{J}\;\Delta\ddot{\boldsymbol{u}}^{i}=\boldsymbol{F}_{n+1}-\boldsymbol{M}\ddot{\overline{\boldsymbol{u}}}^{i}-\boldsymbol{C}\dot{\overline{\boldsymbol{u}}}^{i}-\boldsymbol{K}\overline{\boldsymbol{u}}^{i} \tag{6.25}$$

where $\ddot{\overline{\boldsymbol{u}}},\dot{\overline{\boldsymbol{u}}},\overline{\boldsymbol{u}}$ are predictors given in equation (6.16). Upon solving for the increment $\Delta\ddot{\boldsymbol{u}}^{i}$ in this equation, the correctors are calculated as shown in equation (6.17), thus satisfying

$$\boldsymbol{0}=\boldsymbol{F}_{n+1}-\boldsymbol{M}\ddot{\boldsymbol{u}}_{n+1}-\boldsymbol{C}\dot{\boldsymbol{u}}_{n+1}-\boldsymbol{K}\boldsymbol{u}_{n+1} \tag{6.26}$$

Subtracting the RHS of equation (6.26) from the RHS of equation (6.25) gives

$$\boldsymbol{M}\Delta\ddot{\boldsymbol{u}}^i + \boldsymbol{C}\Delta\dot{\boldsymbol{u}}^i + \boldsymbol{K}\Delta\boldsymbol{u}^i \tag{6.27}$$

where $\Delta\boldsymbol{u}^i = \boldsymbol{u}^{i+1} - \boldsymbol{u}^i$. Expression (6.27) gives the increment required on the RHS of equation (6.25) to satisfy equation (6.26). Hence convergence requires that

$$\boldsymbol{M}\Delta\ddot{\boldsymbol{u}}^i + \boldsymbol{C}\Delta\dot{\boldsymbol{u}}^i + \boldsymbol{K}\Delta\boldsymbol{u}^i \to \boldsymbol{0} \tag{6.28}$$

That is, the solution procedure checks for any increment (6.27) that can be added to the RHS of equation (6.25). If there is no such increment, it implies that the independent variables at i are the same as those obtained at the subsequent iteration $i+1$. Hence the solution can be assumed to have converged, i.e. equation (6.26) holds. For the application in hand, characteristic of linear analysis, convergence i.e. expression (6.28), is achieved on the first iteration.

6.4 Predictor-corrector algorithm

1. *Specify* γ, β *and* J.
2. *Specify time, the number of time steps, that is* $n = n+1$, *and set* $i = 0$.
3. *For each time step.*
4. *Compute predictors* $\overline{\boldsymbol{u}}^i_{n+1}, \overline{\dot{\boldsymbol{u}}}^i_{n+1}, \overline{\ddot{\boldsymbol{u}}}^i_{n+1}$.
5. *Compute* $\overline{\boldsymbol{F}}^i_{n+1}$.
6. *Solve for* $\Delta\ddot{\boldsymbol{u}}^i_n$.
7. *Compute correctors* $\boldsymbol{u}^i_{n+1}, \dot{\boldsymbol{u}}^i_{n+1}, \ddot{\boldsymbol{u}}^i_{n+1}$.
8. *Check for convergence:*
   a) *if satisfied terminate iteration; else*
   b) *if* $i+1 > \max$ *iterations exit the program; else*
   c) *set* $i = i+1$ *and go to step 5.*
9. *Check for time limit:*
   a) *if* $n+1 > \max(\textit{time steps})$, *stop; else*
   b) *if* $n+1 \le \max$ *time steps, go to step 2.*

6.5 Consistency of the algorithm

Here, it is required to measure how closely the solution of the differential equation (6.1) satisfies the difference scheme (6.11), following the approach to the concept of consistency given in Woods (1990).

The residual is defined as $\Psi_{n+1}^{i+1} = O\left(\Delta t^{\rho}\right)$ as $\Delta t \to 0$, for all sufficiently smooth classical solutions of the differential equation (6.1). It follows that if the residual tends to zero as the time step tends to zero, the algorithm is called consistent. Thus here consistency requires that $\rho \geq 1$. Setting $\Delta t = 0$ in (6.11) satisfies this requirement, thus $\Psi_{n}^{i+1} = O\left(\Delta t^{2}\right)$.

6.6 Stability analysis

In the literature, the subject of stability analysis of time-stepping schemes used in conjunction with piezo-elastic equations of motion has not been encountered. It is recognised that it might exist somewhere else but not within the media accessible to the author. Therefore, the stability analysis that is presented here follows closely the works of Woods (1990), conducted for dynamic systems with symmetric mass and stiffness matrices, and Kaunda (1994, 1996, 1997 and 1998), for elasto-plastic dynamics. The purpose of this exercise is to determine the stability criteria based on the energy method for equation (6.2) when used in conjunction with Newmark's scheme. The approach presented here is suitable for symmetric as well as unsymmetric mass and stiffness matrices.

Consider equation (6.2). Multiplying by $-\dot{\boldsymbol{u}}^{T}$ and integrating with respect to time (Woods, 1990), yields

$$V = \int \dot{u}^T \{-F + M\ddot{u} + C\dot{u} + Ku\} dt \tag{6.29}$$

Expanding equation (6.29) using Taylor series defines the increment as

$$\Delta V = \Delta u^T \{-\mathbf{M}\ddot{\mathbf{u}} - \mathbf{K}u\} + \Delta\dot{\mathbf{u}}^T \mathbf{M}\{\dot{\mathbf{u}} + 0.5\Delta\dot{\mathbf{u}}\} + \Delta u^T \mathbf{K}\{u + 0.5\Delta u\} + \Delta\dot{\mathbf{u}}^T \mathbf{C}\{u + \Delta u\} \tag{6.30}$$

Introducing implicit time integration using Newmark's scheme, equation (6.7) becomes

$$\Delta\dot{u} = \Delta t\{\ddot{u} + \gamma\Delta\ddot{u}\} \tag{6.31}$$

$$\Delta t\dot{u} = \Delta u - \Delta t^2\{0.5\ddot{u} + \beta\Delta\ddot{u}\} \tag{6.32}$$

Then substituting (6.31) and (6.32) into (6.30) yields

$$\Delta V = \Delta u^T \{-M\ddot{u} - Ku\} + \Delta u^T K\{u + 0.5\Delta u\} + \Delta t\{\ddot{u} + \gamma\Delta\ddot{u}\}^T C\{u + \Delta u\} + \{\ddot{u} + \gamma\Delta\ddot{u}\}^T M\{\Delta u - \Delta t^2(\beta - 0.5\gamma)\Delta\ddot{u}\} \tag{6.33}$$

After rearranging, the following is obtained

$$\Delta V = -(\beta - 0.5\gamma)\Delta t^2 \Delta\ddot{u}^T \mathbf{M}\{\ddot{u} + \gamma\Delta\ddot{u}\} + \gamma\Delta u^T \mathbf{M}\Delta\ddot{u} + 0.5\Delta u^T \mathbf{K}\Delta u + \Delta t\{\ddot{u} + \gamma\Delta\ddot{u}\}\mathbf{C}\{u + \Delta u\} \tag{6.34}$$

Using the collocation of the differential equation (6.2), with $n = [j, j+1]$, and noting that

$$M\Delta\ddot{u} = \Delta F - C\Delta\dot{u} - K\Delta u \tag{6.35}$$

results in

$$\Delta V = -(\beta - 0.5\gamma)\Delta t^2 \Delta\ddot{u}^T M\{\ddot{u} + \gamma\Delta\ddot{\mathbf{u}}\} - (\gamma - 0.5)\Delta u^T K\Delta u + \gamma\Delta u\{\Delta F - C\Delta\dot{u}\} + \Delta t\{\ddot{u} + \gamma\Delta\ddot{u}\}C\{u + \Delta u\} \tag{6.36}$$

It remains now to reconstruct the energy that results in this incremental. Let

$$F = \tfrac{1}{2}(\beta - 0.5\gamma)(2\gamma)\Delta t^2 \ddot{u}^T M\ddot{u} \tag{6.37}$$

which must be positive semi-definite. Then

$$\Delta F = (\beta - 0.5\gamma)\Delta t^2 \Delta\ddot{u}^T M\{2\gamma\,\ddot{u} + \gamma\,\Delta\ddot{u}\} \tag{6.38}$$

Summing up and rearranging with the aid of (6.31) gives rise to

$$\Delta V + \Delta F = (\gamma - 0.5)\{2(\beta - 0.5\gamma)\Delta t^2 \Delta \ddot{\boldsymbol{u}}^T \boldsymbol{M}\ddot{\boldsymbol{u}} - \Delta \boldsymbol{u}^T \boldsymbol{K}\Delta \boldsymbol{u}\} + \gamma \Delta \boldsymbol{u}^T \Delta \boldsymbol{F} + \{\boldsymbol{u} + (1-\gamma)\Delta \boldsymbol{u}\}^T \boldsymbol{C}\Delta \dot{\boldsymbol{u}} \tag{6.39}$$

Omitting the forcing function as it is bounded, $\gamma - 0.5 = 0$ and $A_{\ddot{u}} \geq 0$ in $\boldsymbol{C} = \boldsymbol{C}_R + \boldsymbol{K}_{u\phi} A_{\ddot{u}} \boldsymbol{K}_{\phi\nabla}$ implies that energy change in the system is due to positive damping. Equation (6.39) suggests that the energy norm (or Lyapunov function) may be taken as

$$E = \tfrac{1}{2}\dot{\boldsymbol{u}}^T \boldsymbol{M}\dot{\boldsymbol{u}} + \tfrac{1}{2}\boldsymbol{u}^T \boldsymbol{K}\boldsymbol{u} + \tfrac{1}{2}(\beta - 0.5\gamma)(2\gamma)\Delta t^2 \ddot{\boldsymbol{u}}^T \boldsymbol{M}\ddot{\boldsymbol{u}} \tag{6.40}$$

$$= \tfrac{1}{2}\dot{\boldsymbol{u}}^T \boldsymbol{M}_{uu}\dot{\boldsymbol{u}} + \tfrac{1}{2}\boldsymbol{u}^T [\boldsymbol{K}_{uu} + \boldsymbol{K}_p]\boldsymbol{u} + \tfrac{1}{2}(\beta - 0.5\gamma)(2\gamma)\Delta t^2 \ddot{\boldsymbol{u}}^T \boldsymbol{M}_{uu}\ddot{\boldsymbol{u}}$$

Expression (6.40) is legitimate for a norm if $\beta - 0.5\gamma \geq 0$ and $A_u \geq 0$, in $\boldsymbol{K}_p = \boldsymbol{K}_{u\phi} A_u \boldsymbol{K}_{\phi\nabla}$, so that the matrices $(\beta - 0.5\gamma)\boldsymbol{M}$ and $\boldsymbol{K}_p$ are positive semi-definite. With $\beta - 0.5\gamma = 0$ and $A_u = 0$, equation (6.40) represents the standard energy norm. The condition $\gamma - 0.5 \geq 0$ in equation (6.39) implies that the energy norm is either constant or decreasing, which is required for the scheme to be stable. For unconditional stability of Newmark's numerical algorithm, the condition $\gamma - 0.5 = 0$ and $\beta - 0.5\gamma = 0$ is applied. Using equation (6.36)

$$E^{i+1} = E^i + \gamma \Delta \boldsymbol{u}^T \{\Delta \boldsymbol{F}(t) - \boldsymbol{C}\Delta \dot{\boldsymbol{u}}\} + \Delta t\{\ddot{\boldsymbol{u}} + \gamma \Delta \ddot{\boldsymbol{u}}\}\boldsymbol{C}\{\boldsymbol{u} + \Delta \boldsymbol{u}\} \tag{6.41}$$

Therefore, it follows that the conditions $\beta - 0.5\gamma \geq 0$, $\gamma - 0.5 = 0$, $A_{\ddot{u}} > 0$ and $A_u \geq 0$ must be satisfied for unconditional stability to exist in the time-stepping scheme.

6.7 Accuracy analysis

The accuracy of the iterative equations given by equation (6.7) and (6.8) will be determined simply by estimating the discretisation or truncation error (Kaunda, 1994). The incremental

equation (6.8) may be expanded as follows:

$$\dot{\boldsymbol{u}}_{n+1} = \dot{\boldsymbol{u}}_n + (1-\gamma)\Delta t\ddot{\boldsymbol{u}}_n + \gamma\Delta t\left\{\ddot{\boldsymbol{u}}_n + \frac{\Delta t^k}{k!}\boldsymbol{u}_n^{(k+2)}\right\} \tag{6.42}$$

Comparing this equation with that of a (corresponding) complete Taylor series expansion $\dot{\boldsymbol{u}}_{n+1} = \dot{\boldsymbol{u}}_n + \frac{\Delta t^k}{k!}\boldsymbol{u}_n^{(k+1)}$ gives a truncation error $O(\Delta t^3)$ for $\gamma = 0.5$ and a truncation error $O(\Delta t^2)$ for $\gamma \neq 0.5$. Similarly, the iterative equation (6.7) may be expanded as follows:

$$\boldsymbol{u}_{n+1} = \boldsymbol{u}_n + \Delta t\dot{\boldsymbol{u}}_n + \left(\tfrac{1}{2}-\beta\right)\Delta t^2\ddot{\boldsymbol{u}}_n + \beta\Delta t^2\left\{\ddot{\boldsymbol{u}}_n + \frac{\Delta t^k}{k!}\boldsymbol{u}_n^{(k+2)}\right\} \tag{6.43}$$

Comparing this equation with that of a (corresponding) complete Taylor series expansion $\boldsymbol{u}_{n+1} = \boldsymbol{u}_n + \frac{\Delta t^k}{k!}\boldsymbol{u}_n^{(k)}$ gives a truncation error $O(\Delta t^3)$.

6.8 References

1. BATHE K [1996] *Finite element procedures*, pub. Prentice Hall.
2. COOK R D, MALKUS D S AND PLESHA M E [1989], *Concepts and Application of Finite Element Analysis*, 3rd ed., pub. John Wiley & Sons.
3. CRISFIELD M A [1991], *Non-linear Finite Element Analysis of Solids and Structures: Volume 1*, pub. John Wiley & Sons.
4. CRIESFIELD M A AND SHI J [1994], A co-rotational element/time-integration strategy for non-linear dynamics, *International Journal for Numerical Methods in Engineering*, **37**, 18971913.
5. HUGHES T J R [1987], *The Finite Element Method: Linear Static and Dynamic Finite Element Analysis*, pub. Prentice-Hall.
6. KAUNDA M A E [1994], *Finite Element Algorithms for the Static and Dynamic Analysis of Time-Dependent and Time-Independent Plastic Bodies*, PhD Thesis, University of Cape Town, South Africa.
7. KAUNDA M A E [1997], A generalised Newton-Raphson scheme for elastoplastic dynamic, *Computational Plasticity: Fundamentals and Applications, Proc. 5th Int. Conf. on Computational Plasticity (Spain)*, **1**, 447-450.
8. KAUNDA M A E [1998], A forward-backward difference scheme for elastoplastic dynamics: Lyapunov asymptotic stability, *Proc. 2nd South African Conference on Applied Mechanics*, **1**, 547-558.

9. KAUNDA M A E AND MARTIN J B [1996], A forward-backward difference scheme for elastoplastic dynamics: control of amplitude and phase-shift errors, *Proc. 1st South African Conference on Applied Mechanics*, **2**, 42-53.
10. NEWMARK N M [1959], A method of computation for structural dynamics, *Journal of Engineering Mechanics Division,* 67-94, July.
11. OWEN D R J AND HINTON E [1980], *Finite Elements in Plasticity: Theory and Practice*, pub. Pineridge Press.
12. WEAVER W JR., TIMOSHENKO S P AND YOUNG D H [1990], *Vibration Problems in Engineering*, 5th ed., pub. John Wiley & Sons.
13. WOODFORD C [1992], *Solving Linear and Non-linear Equations*, pub. Ellis Horwood.
14. WOODS W L [1990], *Practical Time-stepping Schemes*, pub. Claredon Press, Oxford.

7 Numerical implementation

7.1 Introduction

Numerical results demonstrating the behaviour of the piezo-elastic structure using the active control formulations are presented. An in-house finite element program was developed for this purpose. An integrity test of this program was performed using an isotropic material without piezoelectric effects. Numerical results for statics and eigen-problems (Kekana and Badur, 2000) obtained were compared with analytical results found in Weaver, Timoshenko and Young (1990). Also, results for the transient response using Newmark's scheme were obtained. Effects of the numerical integration schemes – reduced and full – in modelling statics, eigen-problems and forced vibration are reviewed. These results are presented in section 7.2. In section 7.3, the eigen-problem and time response results demonstrating the behaviour of the piezo-elastic structure are presented. The eigen-problem was solved with the aid of the subroutine *jacobi* presented by Bathe (1996).

7.2 Verification of the program

7.2.1 Stiffness matrix

By omitting the dynamic contribution in equation (A.1) given in the Appendix, the static behaviour of the beam was modelled using simply supported boundary conditions. Material properties of this beam are given in Table 7.1. Numerical results showing deflections of the beam at different positions across the length are shown in Table 7.2. They were obtained

using one-dimensional three-noded elements with full (3-Gauss points) and reduced (2-Gauss points) integration schemes.

Property	Value
Plexiglas	A1 T-6061
Young's Modulus (GPa)	70
Density (kg/m^3)	2710
Poisson's ratio	0.25
Length (m)	0.4572
Width (m)	0.0254
Thickness (m)	0.008

Table 7.1 *Material properties and dimensions.*

The full integration scheme (FIS) underestimated the deflections of the beam relative to the analytical solution. This shows that FIS introduced fictitious stiffness into the beam thus making it appear stiffer. Such phenomenon is attributed to locking. For the reduced integration scheme (RIS), values compared favourably with analytical results. From a physical point of view, RIS modified the assumed displacement field at a numerical level by introducing the assumption that a straight segment normal to the neutral axis before deformation stays normal and straight after deformation. Of course, looking at the beam aspect ratio qualifies this assumption.

x-coord.	FEM				Analytical	
[m]	2-elements [$m\times10^{-6}$]		4-elements [$m\times10^{-6}$]		[$m\times10^{-6}$]	
	3-Gauss points	2-Gauss points	3-Gauss points	2-Gauss points	Thick beam	Thin beam
0.0	0.0	0.0	0.0	0.0	0.0	0.0
0.1143	-4.5175	-5.2539	-5.0857	-5.3477	-5.3477	-5.3435
0.2286	-6.0323	-7.5052	-7.1559	-7.5052	-7.5052	-7.4997
0.3429	-4.5175	-5.2539	-5.0857	-5.3477	-5.3477	-5.3435
0.4572	0.0	0.0	0.0	0.0	0.0	0.0

Table 7.2 *Deflection results of a simply supported beam,* h/L = 1/57.1.

For the beam aspect ratios $1/100 \le h/L \le 1$ the following were observed: as the beam aspect

ratio $h/L \rightarrow 1/10$, the full integration scheme modelled the deflection curve favourably compared to reduced integration (see Table 7.3). For the case where $h/L \rightarrow 1$ both schemes produced results which were three-times greater when compared to the analytical results, which meant that three-dimensional effects dominated in both numerical and analytical approaches.

		FEM		**Analytical**	
		4-elements $[m \times 10^{-6}]$		$[m \times 10^{-6}]$	
	Aspect ratio	3-Gauss points	2-Gauss points	Thick beam	Thin beam
Thin beam	h=L/100	38.226	40.188	40.208	40.179
	h=L/50	4.7980	5.0271	5.0260	5.0223
	h=L/30	1.0449	1.0877	1.0856	1.0848
	h=L/20	0.3133	0.3234	0.3217	0.3213
	h=L/18	0.2293	0.2361	0.2345	0.2343
	h=L/16	0.1619	0.1661	0.1647	0.1646
Thick beam	h=L/14	0.1091	0.1116	0.1103	0.1102
	h=L/12	0.0693	0.0706	0.0695	0.0694
	h=L/10	0.04056	0.04114	0.04021	0.04018
3-D effects	h=L/1	1.3660×10^{-4}	1.3661×10^{-4}	4.021×10^{-5}	4.018×10^{-5}

Table 7.3 *Maximum deflections at different beam aspect ratios.*

Furthermore, as the number of elements was increased, it was observed that RIS converged rapidly towards the analytical solution (see Figure 7.1). On the other hand, slow convergence was observed with the FIS up to a point where both schemes converged no more but diverged with a further increase in the number of elements. This divergence is attributed to dominance of three-dimensional effects where the aspect ratios for the elements are approaching unity.

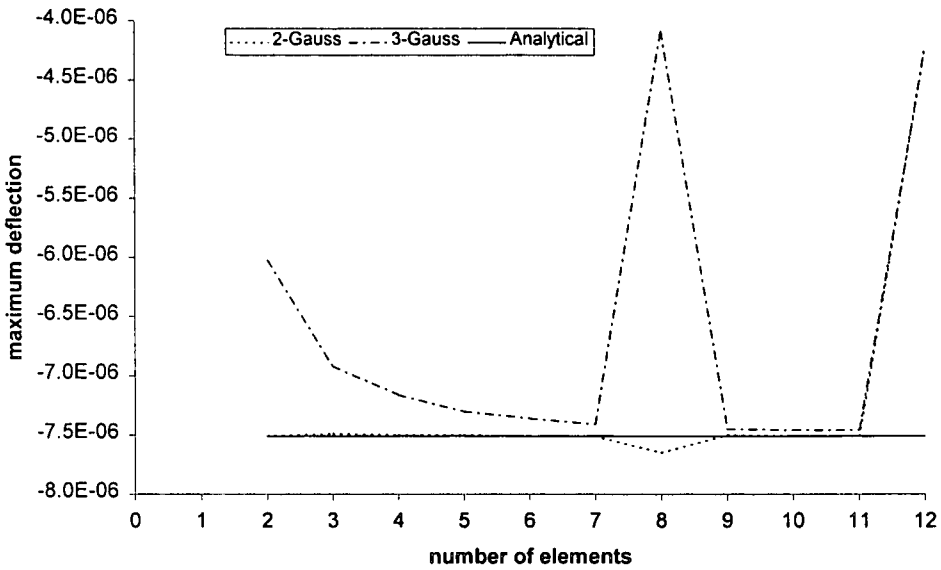

Figure 7.1 *Maximum deflection vs. number of elements.*

7.2.2 Mass matrix

The eigenvalue problem was solved using the finite element stiffness and mass matrices. The prescribed conditions were enforced by introducing a large value, in the stiffness matrix, on the corresponding diagonal of the nodes. FIS was employed for the mass matrix together with full and reduced integration schemes for the stiffness matrix.

The natural frequencies obtained using FIS were pronounced when compared to both the analytical solution and RIS (Table 7.4). This phenomenon is accredited to the fictitious stiffness introduced by this scheme. That is, the stiffer the beam, the higher the frequency. However, a deviation from the analytical results was observed when using the RIS for frequencies above the natural frequency. This deviation became pronounced at higher frequencies. This is due to fewer elements used in the calculation of the natural frequencies. To improve these results, more elements may be used while observing the aspect ratios.

	FEM [2-Gauss points]		Analytical		FEM [3-Gauss points]	
ω_n^2	2-elements	4-elements	Thick beam[1]	Thin beam[1]	2-elements	4-elements
ω_1^2	3.134×10^5	3.073×10^5	3.068×10^5	3.071×10^5	3.765×10^5	3.219×10^5
ω_2^2	6.025×10^6	5.006×10^6	4.894×10^6	4.914×10^6	6.025×10^6	5.943×10^6
ω_3^2	9.118×10^7	2.731×10^7	2.465×10^7	2.487×10^7	2.368×10^9	3.723×10^7
ω_4^2	2.97×10^{10}	9.508×10^7	7.738×10^7	7.862×10^7	1.61×10^{12}	9.508×10^7

Table 7.4 *Natural frequencies of a simply supported,* h/L = 1/57.1.

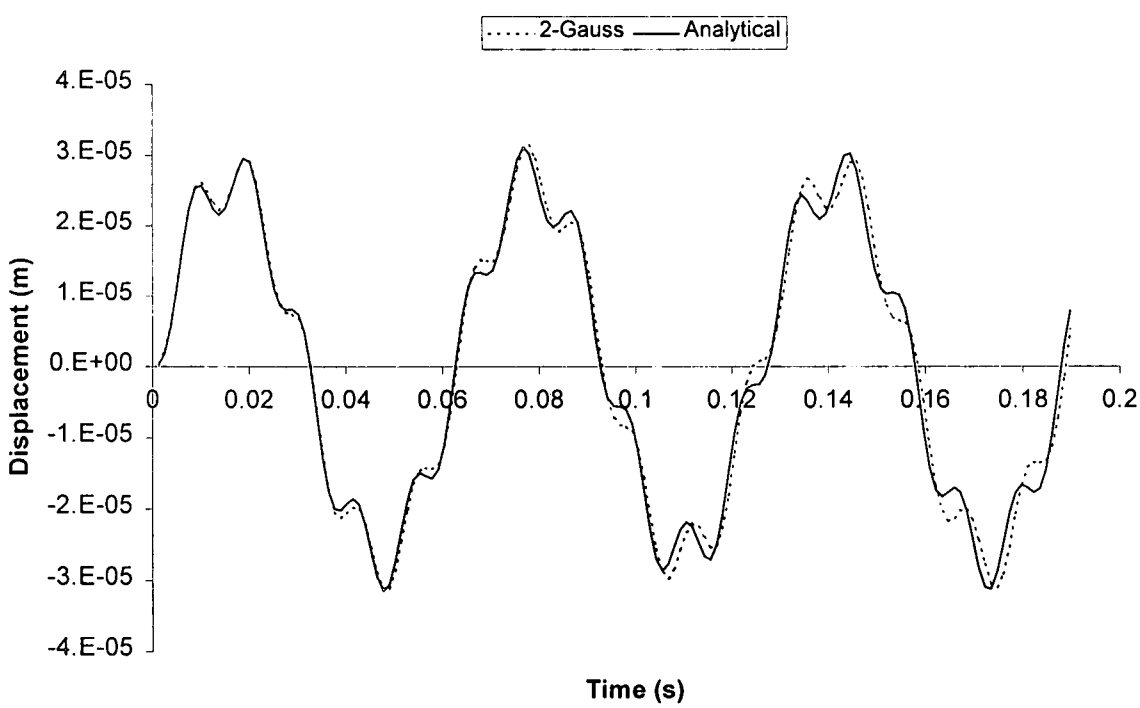

Figure 7.2 *Displacement vs. time plot using reduced integration scheme.*

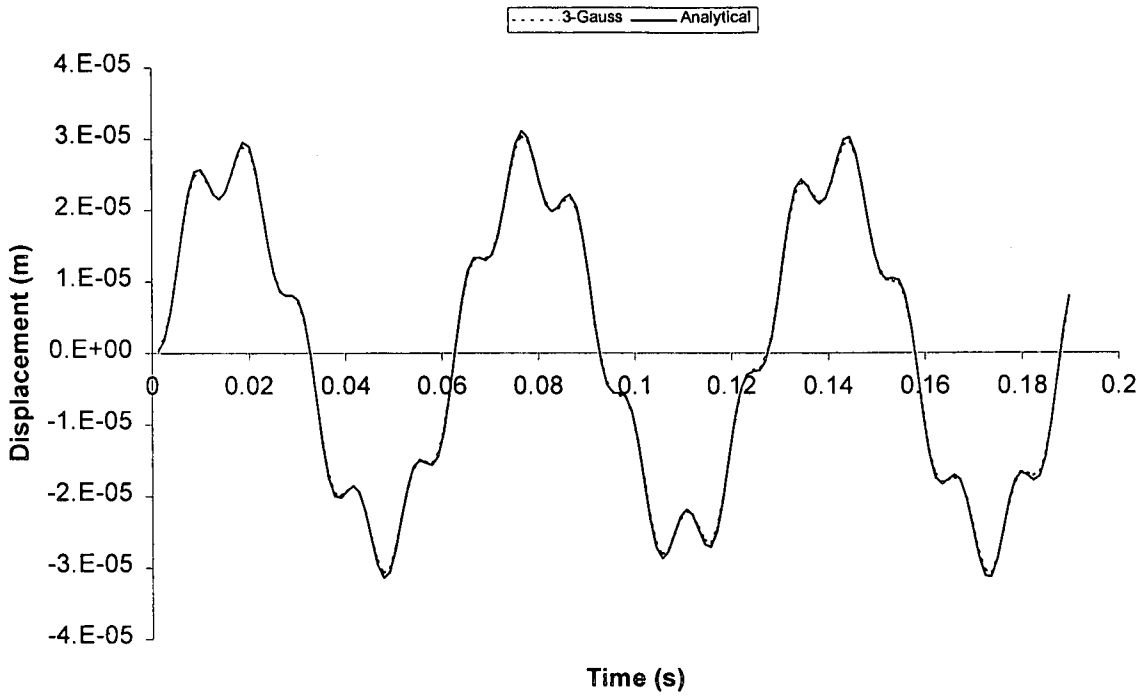

Figure 7.3 *Displacement vs. time plot using full integration scheme.*

7.2.3 Time stepping scheme

The transient response was solved using a sinusoidal forcing function with the maximum amplitude of unity. The frequency was set to 100 radians per second. Integration parameters were set at $\gamma = 2\beta = 0.5$. The time step was obtained using the frequency of the forcing function. For RIS, period errors were not observed (see Figure 7.2). However, slight amplitude increase was observed. This slight deviation manifested itself as a phase delay, which became pronounced in instances were there was a change from acceleration to deceleration and visa-versa. A push-pull effect occurred in these regions.

It can be seen in Figure 7.3 that FIS is accurate.

7.3 Active control effects

Damping effects due to piezoelectricity using the active control formulations ACF1, ACF2 and ACF2-mixed, here onwards represented as ACF2M, given in section 5.6 are presented. Properties of the piezoelectric and Graphite/Epoxy lamina are shown in Table 7.5. The structure was modelled as a cantilever beam subjected to a uniformly distributed unit step load, i.e. $f(x,t)=1$ Newton/metre. Zero initial conditions for the displacement and velocity were assumed. The piezo-elastic structure was discretised into six elements (see Figure 4.1). Quadratic interpolation functions were used for the discrete displacements and linear interpolation functions were used for the discrete potentials. The piezoelectric sensor(s) and actuator(s) where assumed to be collocated. Piezoelectric damping was effected by assuming zero proportional gain, i.e. $A_u = 0$. The time step was determined using the fundamental frequency at zero feedback gain, i.e. at $A_u = A_{ii} = 0$. The results that follow show the response at the tip of the cantilever.

Property	Graphite/Epoxy	Piezoelectric
E_{11} (Pa)	0.980E+11	0.200E+10
E_{22} (Pa)	0.790E+10	0.200E+10
G_{23} (Pa)	0.317E+10	0.775E+10
G_{13} (Pa)	0.317E+10	0.775E+10
G_{12} (Pa)	0.560E+10	0.775E+09
Density (kg/m^3)	0.152E+4	0.180E+4
E_{31}		46.0E-3
e_{32}		46.0E-3
e_{33}		46.0E-3
g_{11}		0.1062E-9
g_{22}		0.1062E-9
g_{33}		0.1062E-9
Width (m)	0.005	0.005
Thickness (m)	0.0005	0.00005
Length (m)	0.1	0.1

Table 7.5 *Material properties for a piezoelectric and composite material.*

7.3.1 Time response

Figure 7.4 and Figure 7.5 show the deflection/rotation vs. time plots obtained using the ACF1 model. Figure 7.6 and Figure 7.7 shows the same using ACF2 model. Figure 7.8 to Figure 7.11 shows the same using ACF2-mixed model.

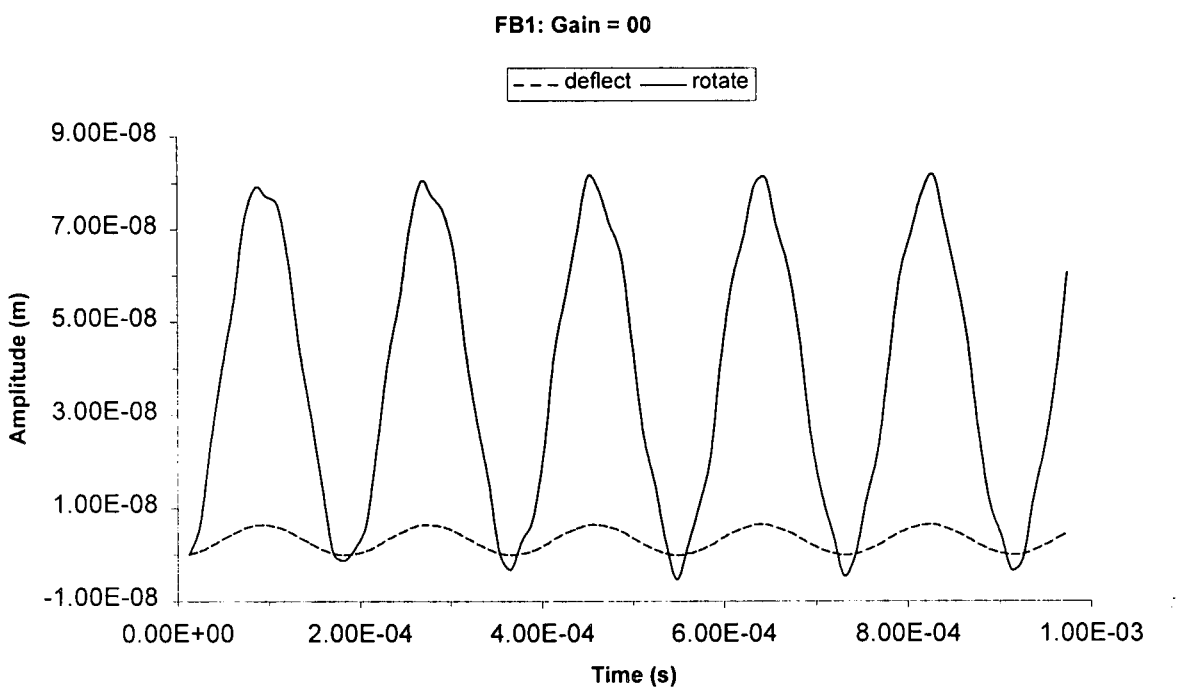

Figure 7.4 *Deflection/rotation vs. time plot for ACF1 at* $A_u = A_{\dot{u}} = 0$.

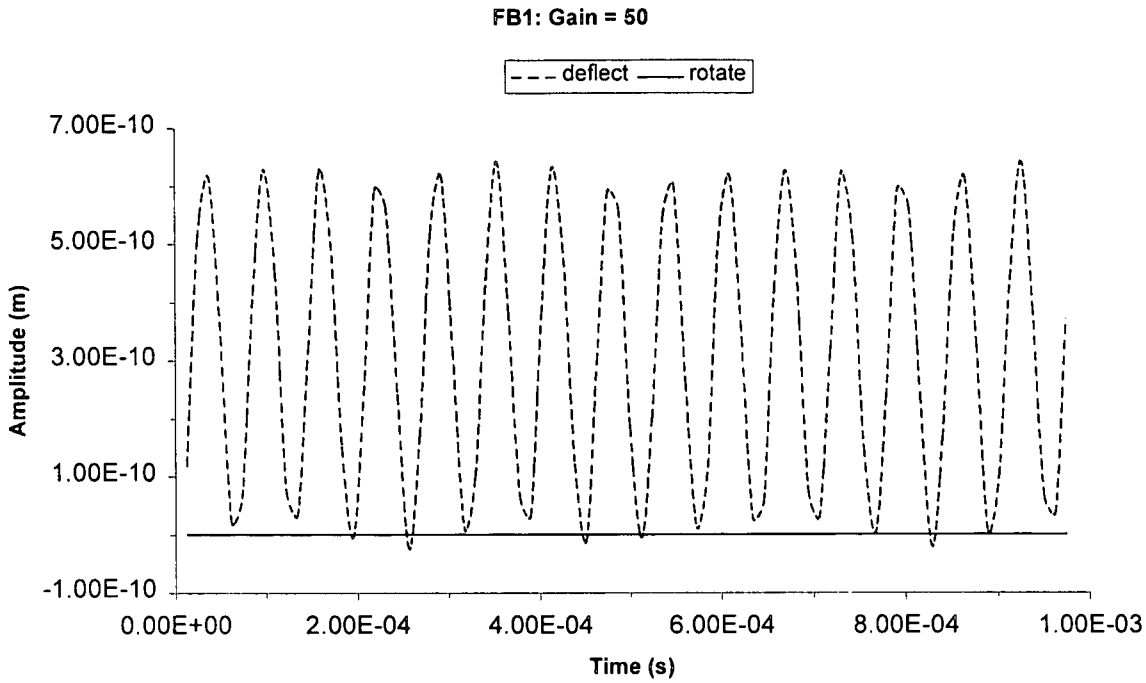

Figure 7.5 *Deflection/rotation vs. time plot for ACF1 at* $A_u = 0,\ A_{\dot{u}} = 50$.

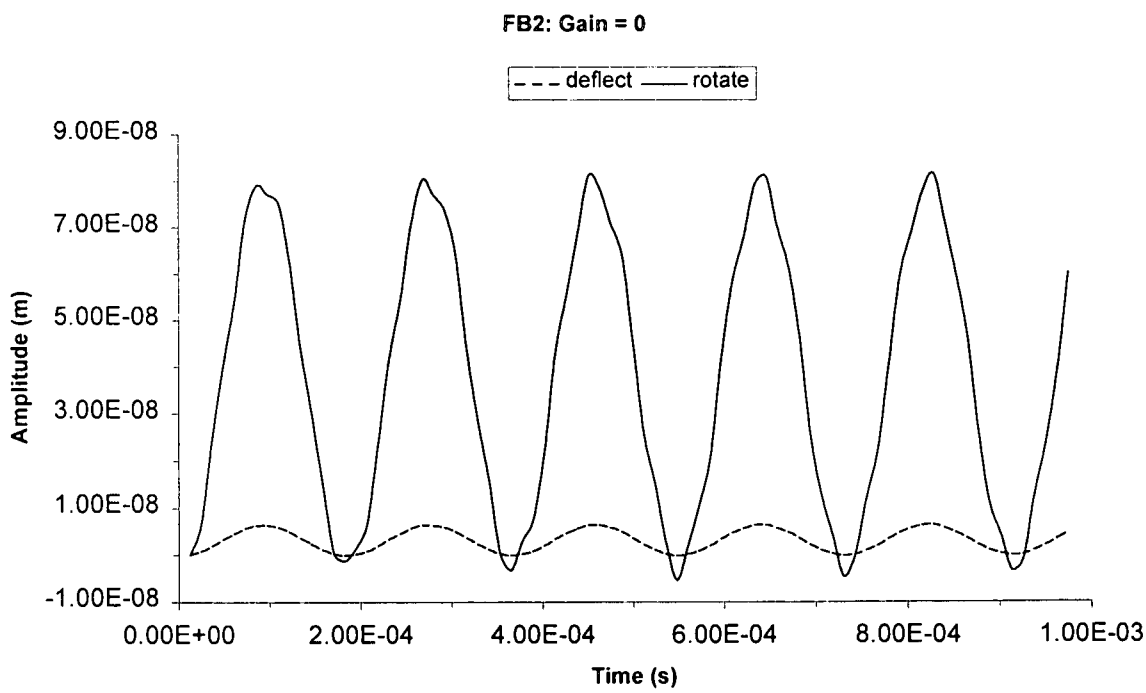

Figure 7.6 *Deflection/rotation vs. time plot for ACF2 at* $A_u = A_{\dot{u}} = 0$.

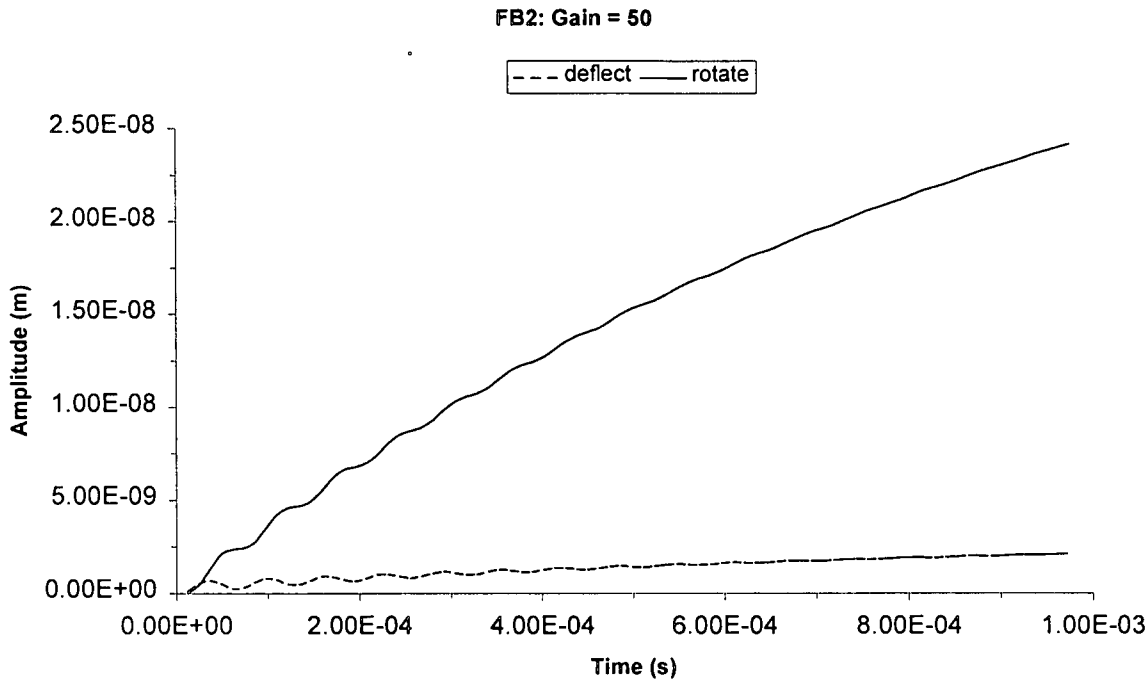

Figure 7.7 *Deflection/rotation vs. time plot for ACF2 at* $A_u = 0$ $A_{\dot{u}} = 50$.

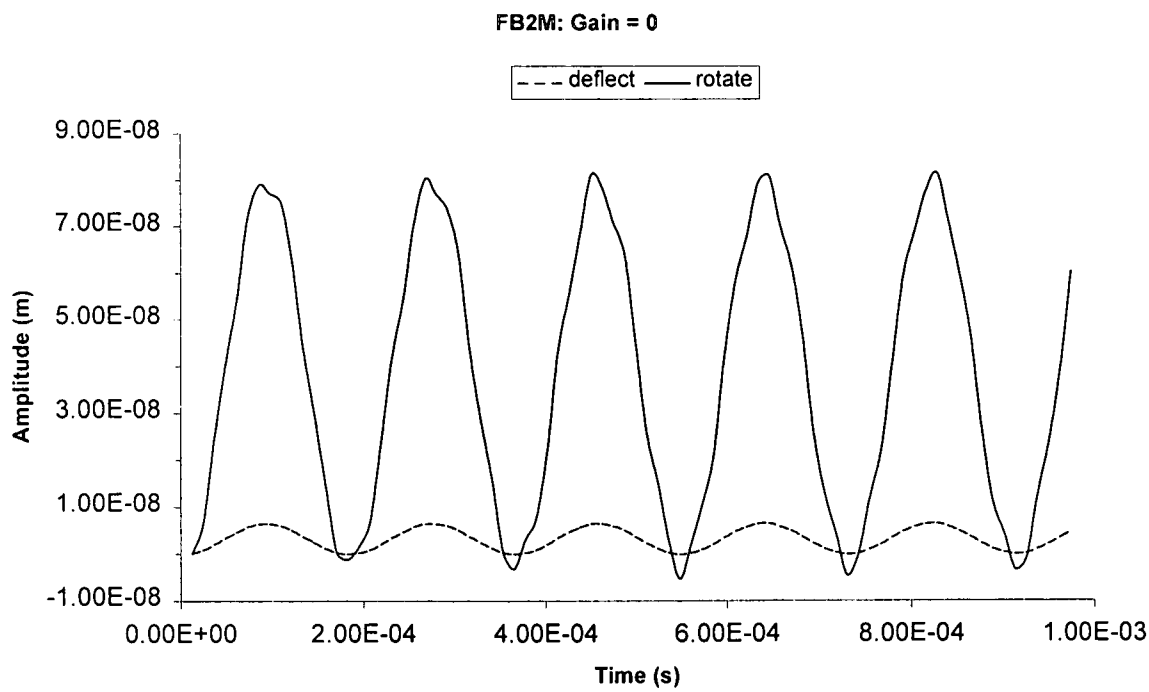

Figure 7.8 *Deflection/rotation vs. time plot for ACF2M at* $A_u = 0$, $A_{\dot{u}} = 0$.

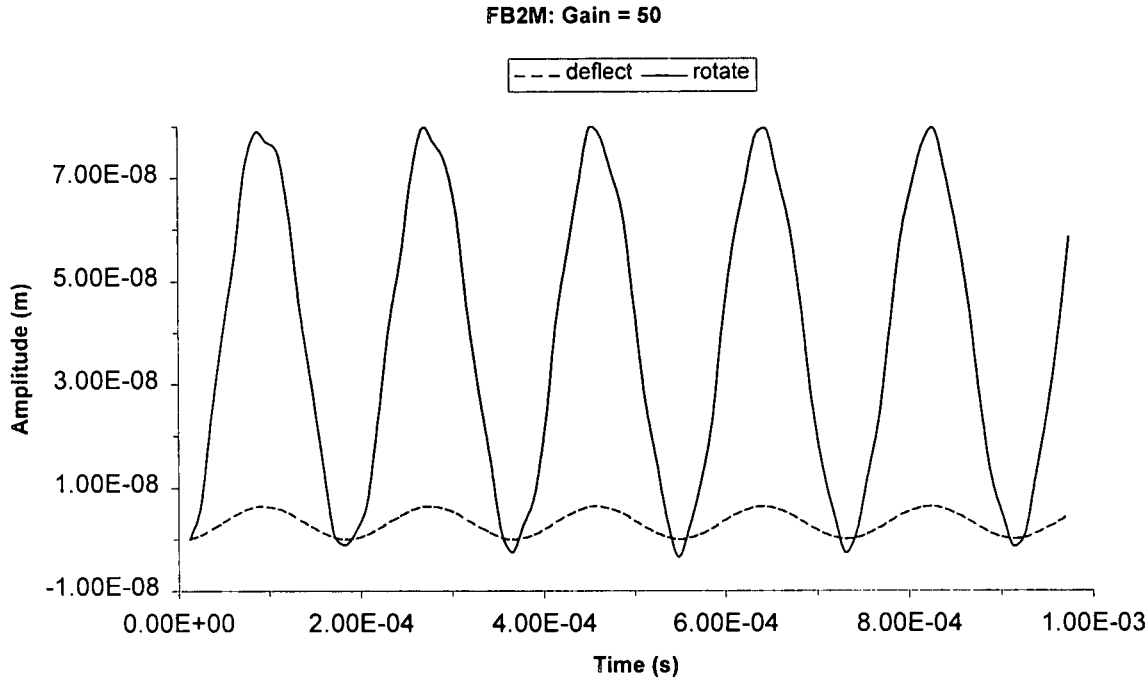

Figure 7.9 *Deflection/rotation vs. time plot for ACF2M at* $A_u = 0,\ A_{ii} = 50$.

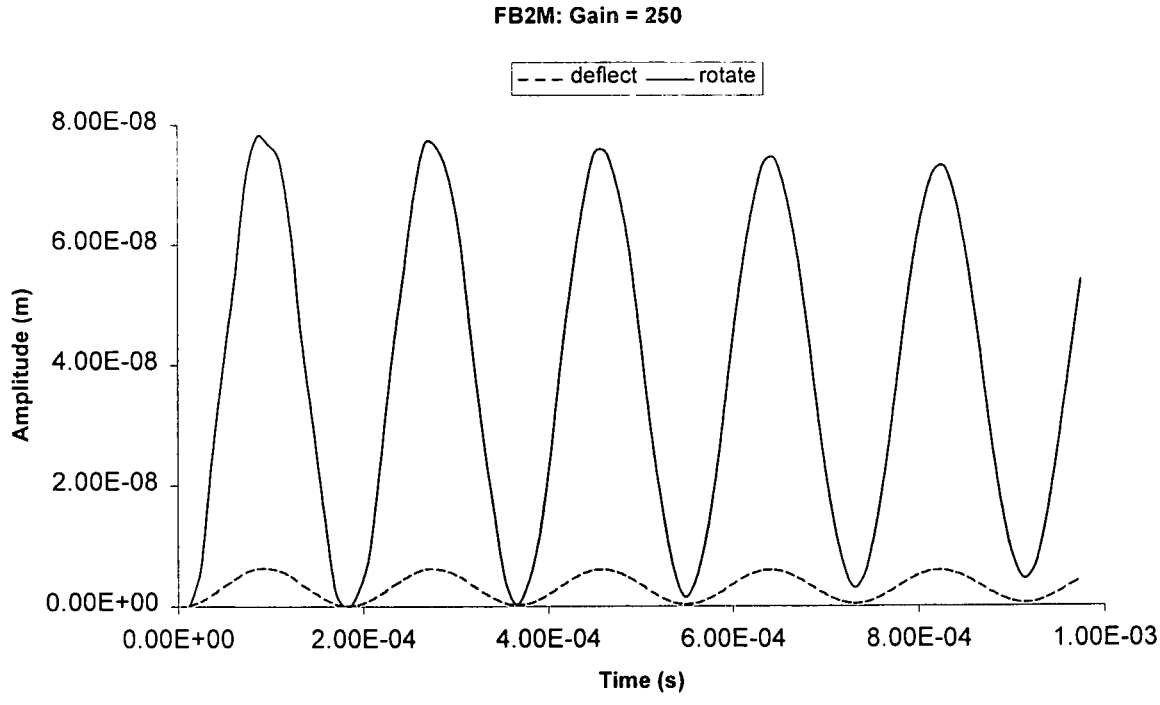

Figure 7.10 *Deflection/rotation vs. time plot for ACF2M at* $A_u = 0,\ A_{ii} = 250$.

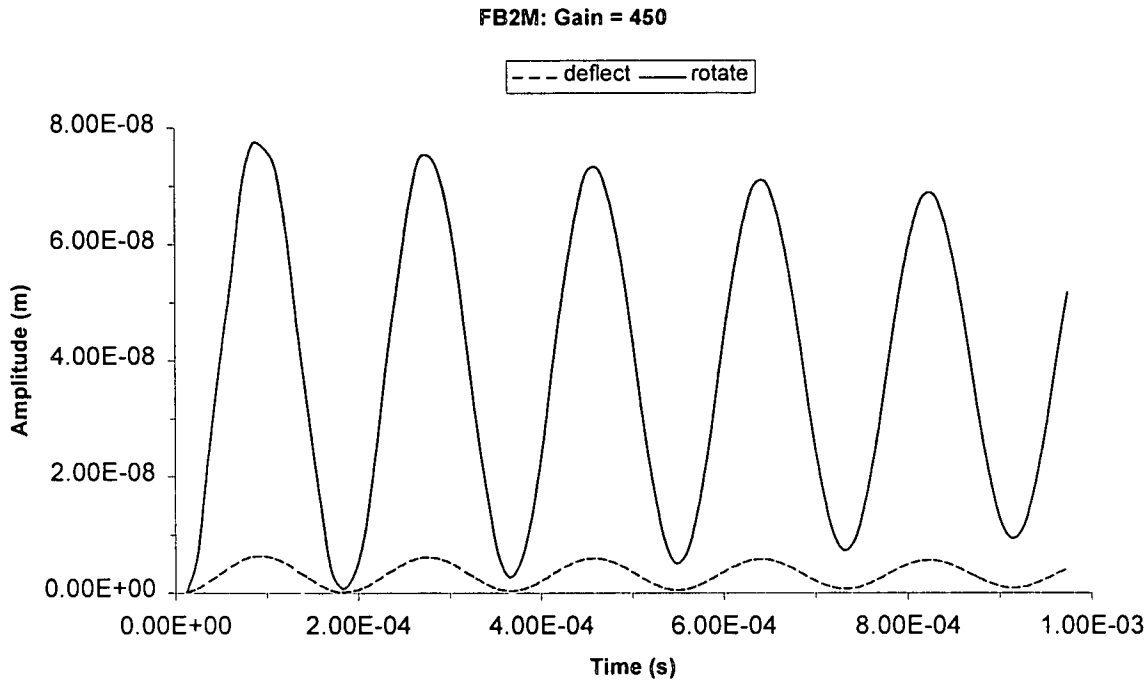

Figure 7.11 *Deflection/rotation vs. time plot for ACF2M at* $A_u = 0,\ A_{\dot{u}} = 450$.

When derivative gain $A_{\dot{u}} > 0$, the solution for ACF1, ACF2 and ACF2M models approaches the equilibrium position as time t approaches infinity. This implies that the models represent an asymptotically stable system. Also, the decay of the transient vibration implies that damping is positive. Damping increases when the feedback gain increases, though at varying degrees per control model. Thus the vibration of piezo-elastic structure can be effectively suppressed by the increase of the feedback gain; in particular, the derivative gain.

Figure 7.7 and Figure 7.9 show that the ACF2 model is stiffer than the ACF2M model. Hence, piezoelectric damping is higher in the ACF2 model than in ACF2M for the same derivative gain. This may be attributed to locking phenomena, as demonstrated in Table 7.3, associated with the discretised potential field. Considering the ACF1, ACF2 and ACF2M

control models, ACF1 model is the stiffest. With hindsight, this may be attributed to the assumptions introduced regarding the charge field as well as locking. As shown in Figure 7.5, the rotations are locked resulting in minute deflection-oscillation occurring indefinitely due to a lack of damping. However, in introducing structural damping, these will gradually subside.

The results obtained using the ACF2M model represent the envisaged behaviour of the piezo-elastic structure. That is, at low feedback gain vibration damping will be equivalently small. An increase in feedback gain will thus lead to an increase in vibration damping (see Figure 7.10 and Figure 7.11). The same phenomenon is observed when using ACF2 except that the results obtained represent a system approaching a critically damped state.

7.3.2 Eigenvalues and mode shapes

Figure 7.12 - Figure 7.15 show the mode shapes obtained using ACF1. Figure 7.16 - Figure 7.19 show the mode shapes obtained using ACF2. Figure 7.20 - Figure 7.23 show the mode shapes obtained using ACF2M. Table 7.6 shows the fundamental frequencies obtained using ACF1, ACF2 and ACF2M. In these cases, the derivative gain was set to zero, i.e. $A_{ii} = 0$. The fundamental frequency, ω_1, of a laminated composite structure without piezoelectric feedback capability was 34471.097 .

A_u	ACF1	ACF2	ACF2M
0	34 471.112	34 471.097	34 471.097
50	99 286.913	34 471.856	34 471.097
150	99 286.913	34 473.374	34 471.097
250	99 286.913	34 474.892	34 471.097

Table 7.6 *Fundamental frequencies at various proportional feedback gain with* $A_{ii} = 0$.

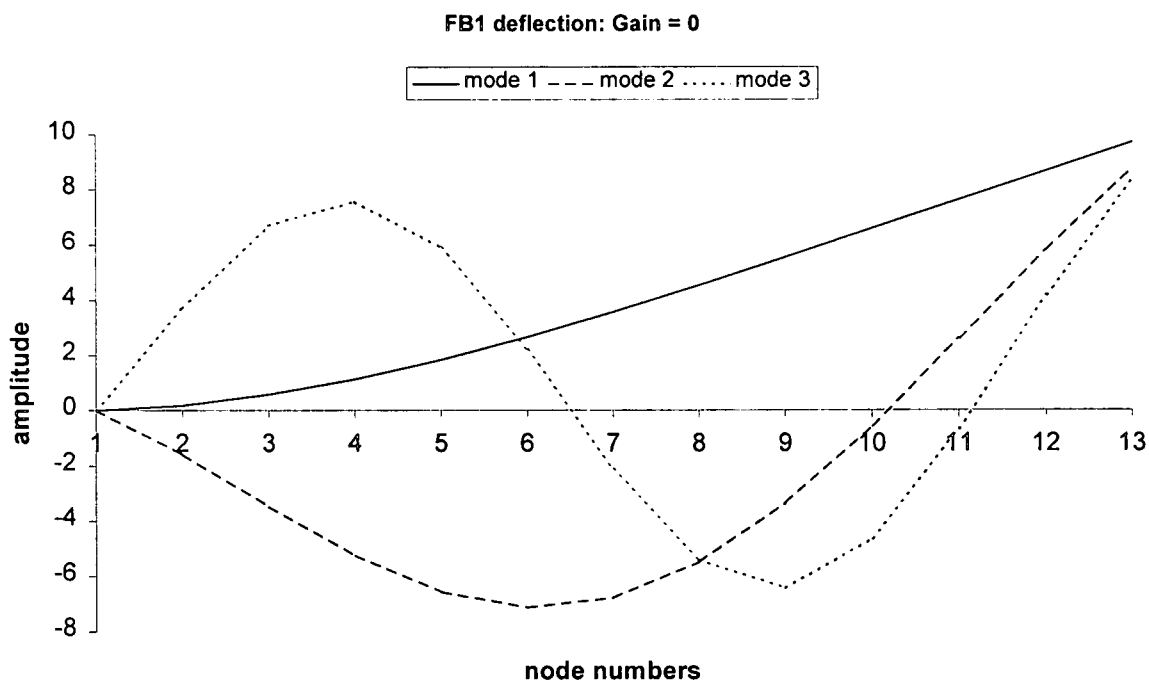

Figure 7.12 *Mode shapes for deflections using ACF1 at* $A_{ii} = 0$, $A_u = 0$.

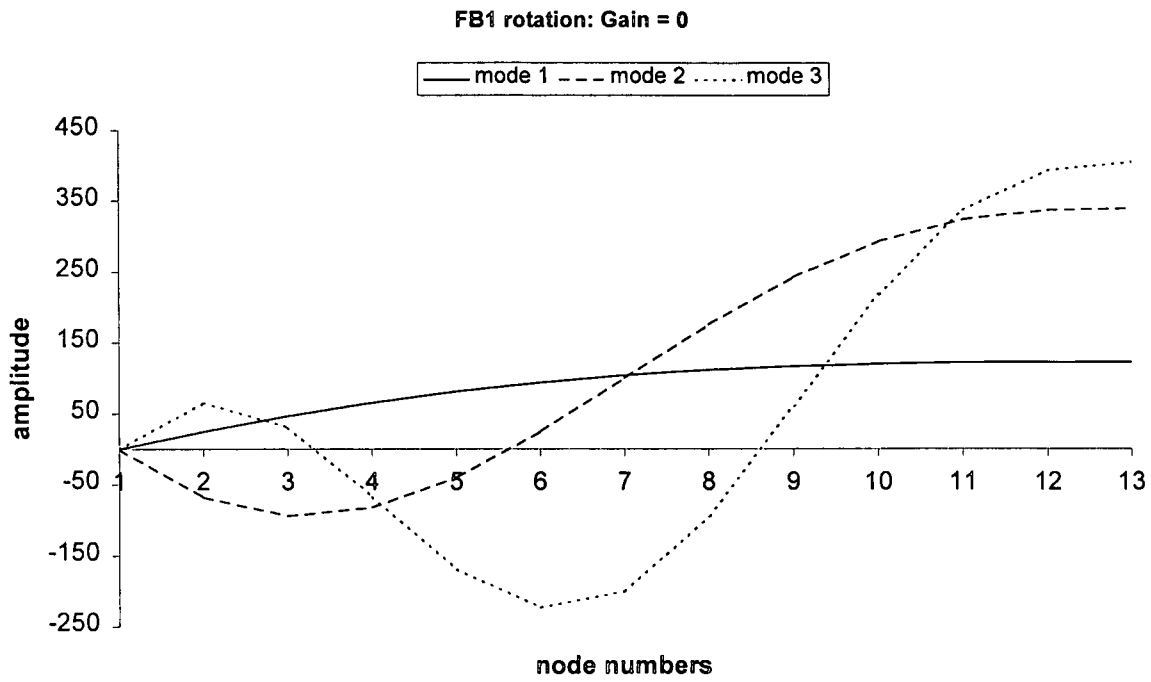

Figure 7.13 *Mode shapes for rotations using ACF1 at* $A_{ii} = 0,\ A_{u} = 0$.

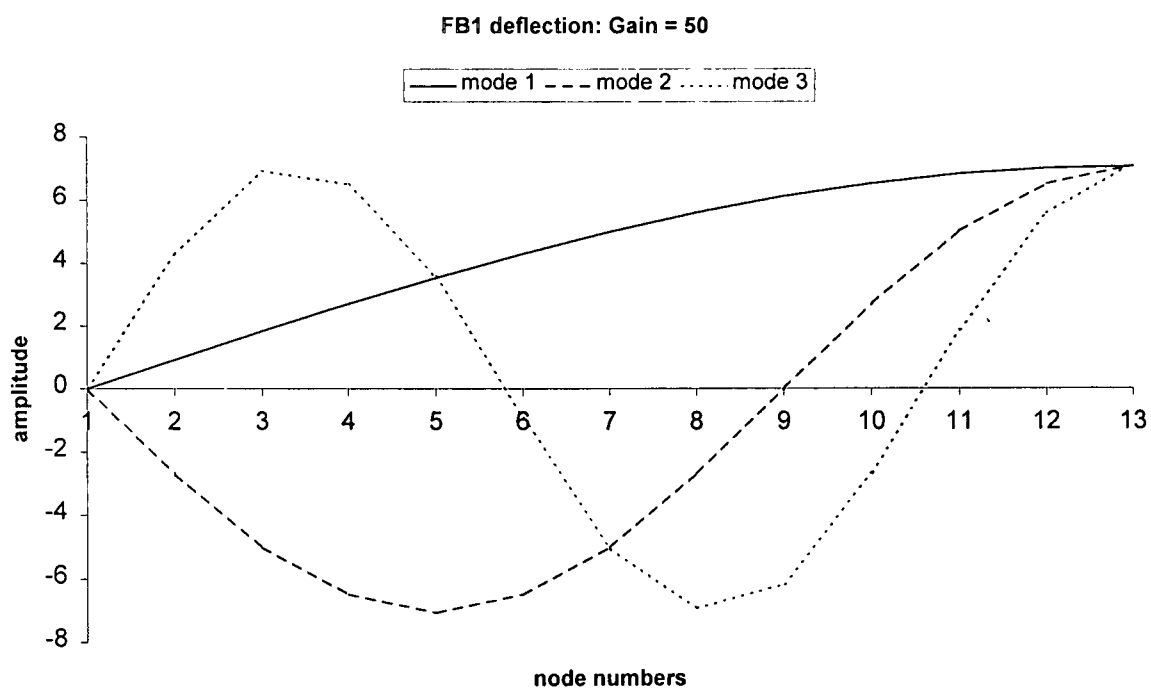

Figure 7.14 *Mode shapes for deflections using ACF1 at* $A_{ii} = 0,\ A_{u} = 50$.

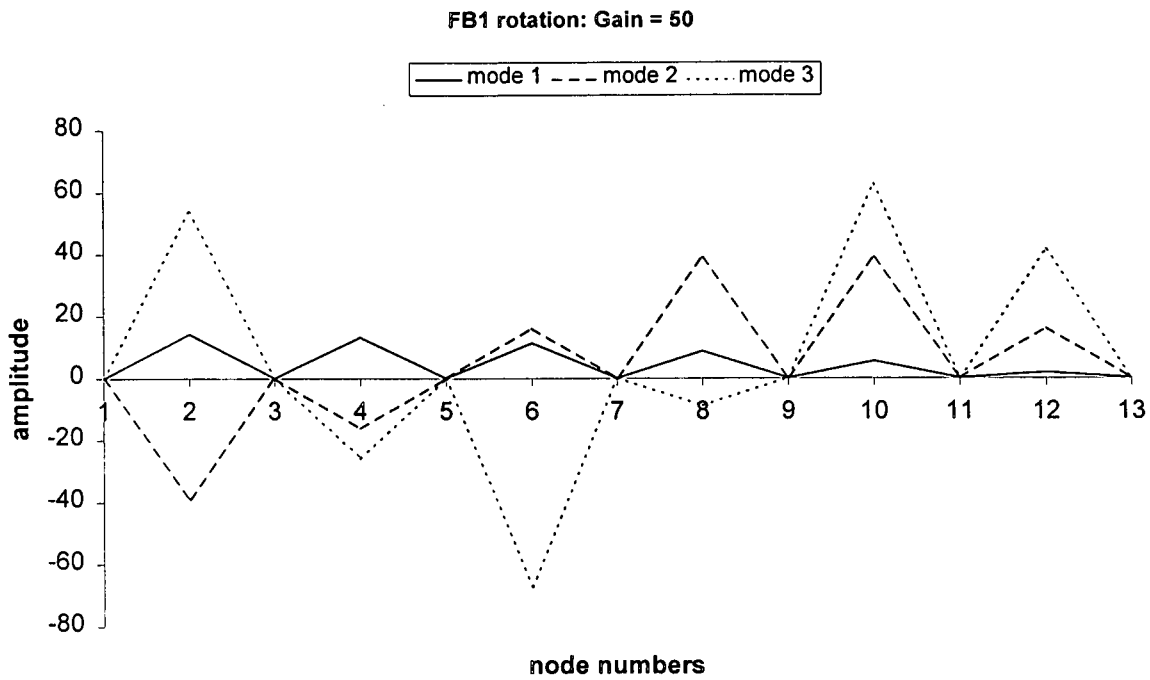

Figure 7.15 *Mode shapes for rotations using ACF1 at* $A_{ii} = 0,\ A_{u} = 50$.

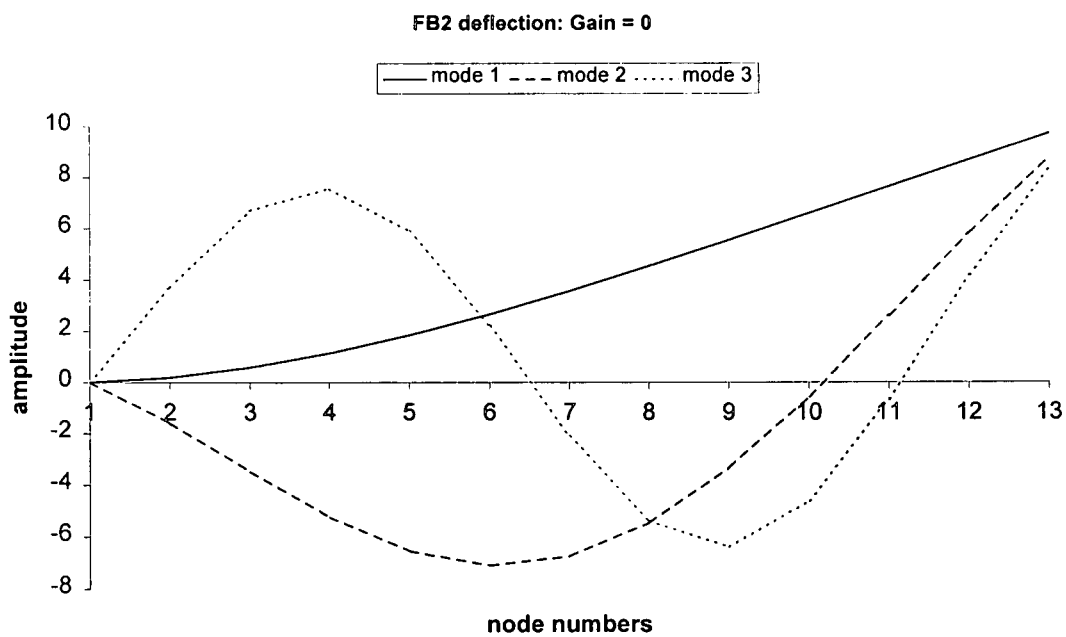

Figure 7.16 *Mode shapes for deflections using ACF2 at* $A_{ii} = 0,\ A_{u} = 0$.

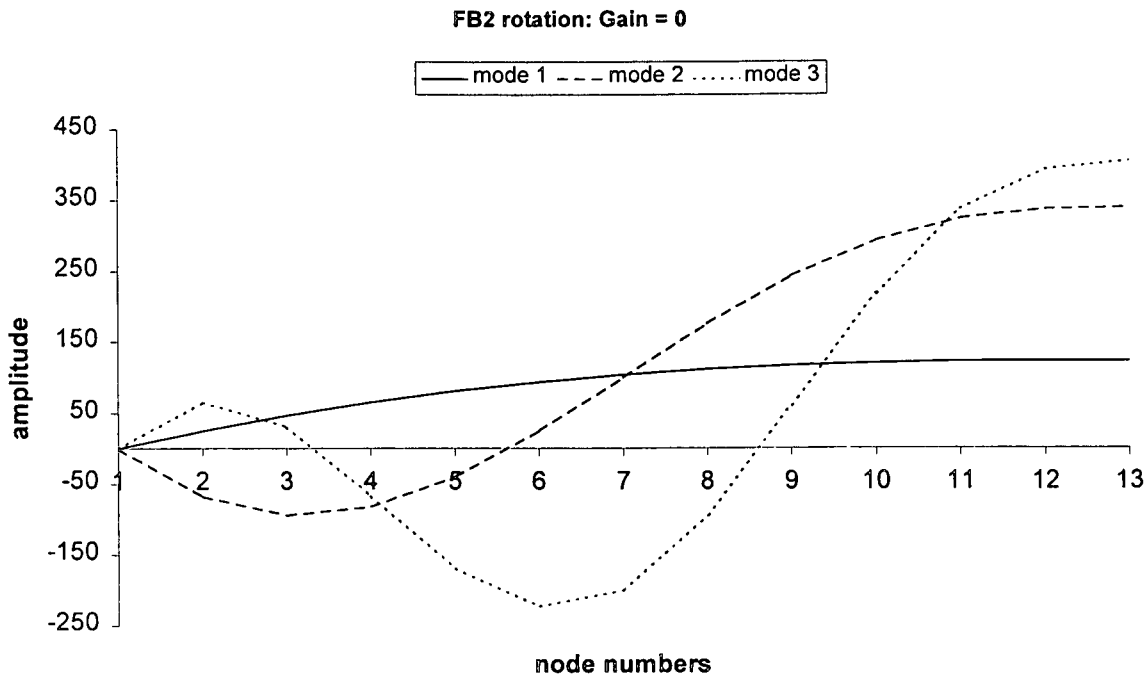

Figure 7.17 *Mode shapes for rotation using ACF2 at* $A_{ii} = 0,\ A_{u} = 0$.

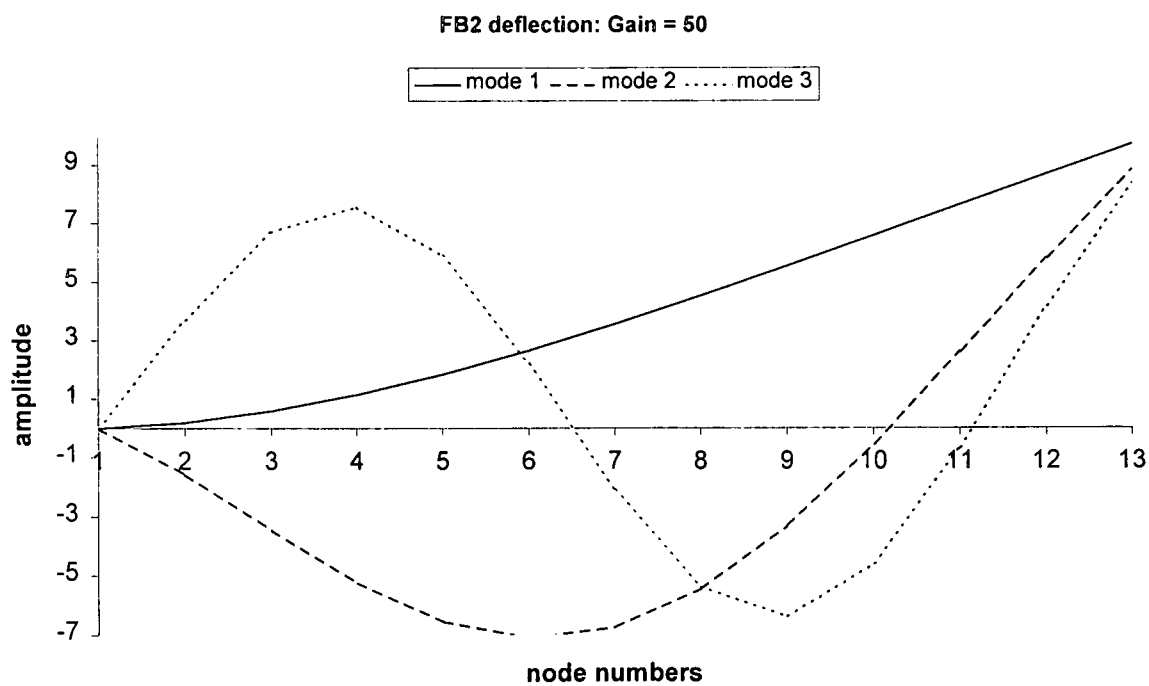

Figure 7.18 *Mode shapes for deflections using ACF2 at* $A_{ii} = 0,\ A_{u} = 50$.

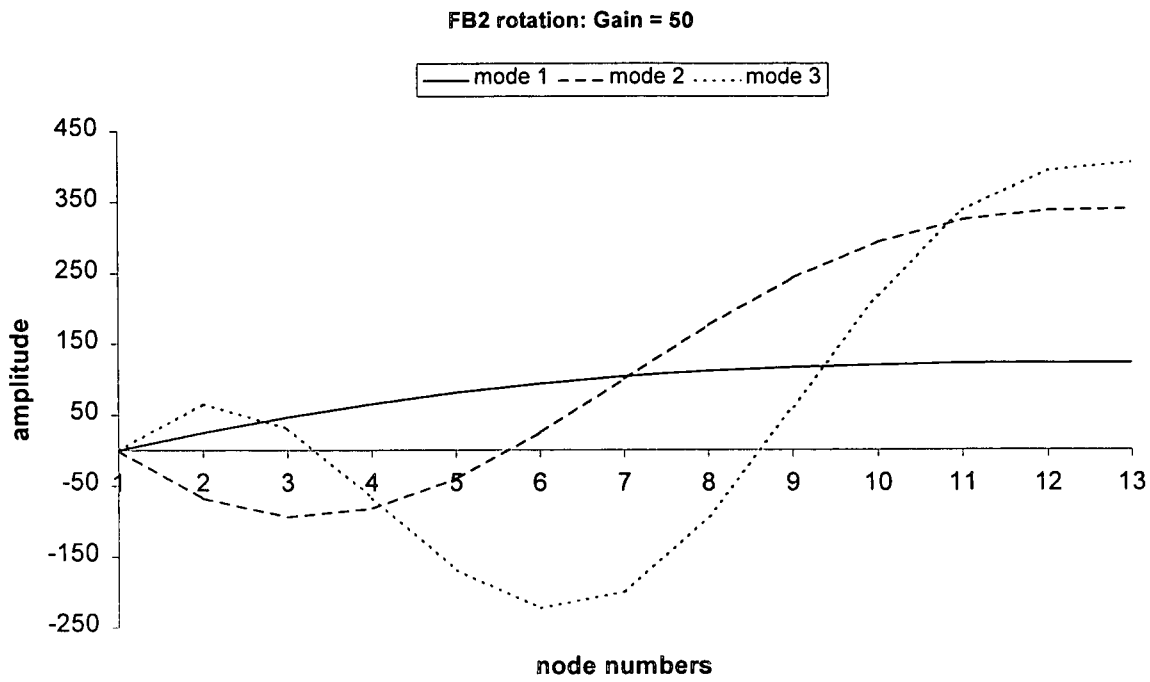

Figure 7.19 *Mode shapes for rotations using ACF2 at* $A_{ii} = 0,\ A_{u} = 50$.

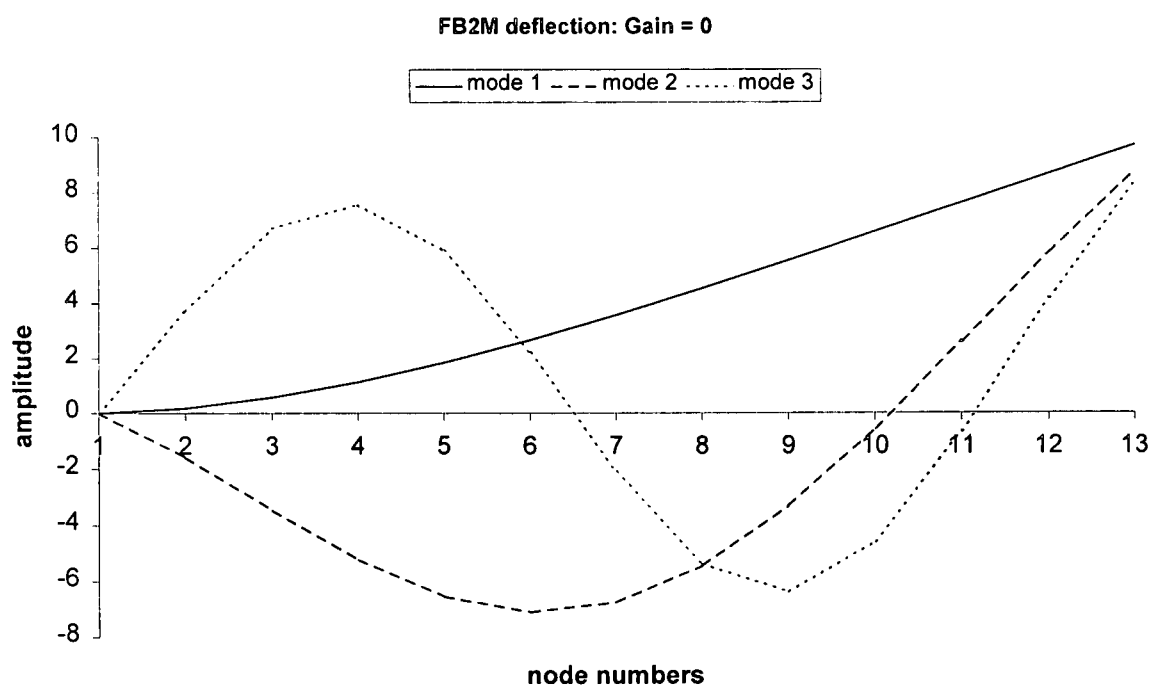

Figure 7.20 *Mode shapes for deflections using ACF2M at* $A_{ii} = 0,\ A_{u} = 0$.

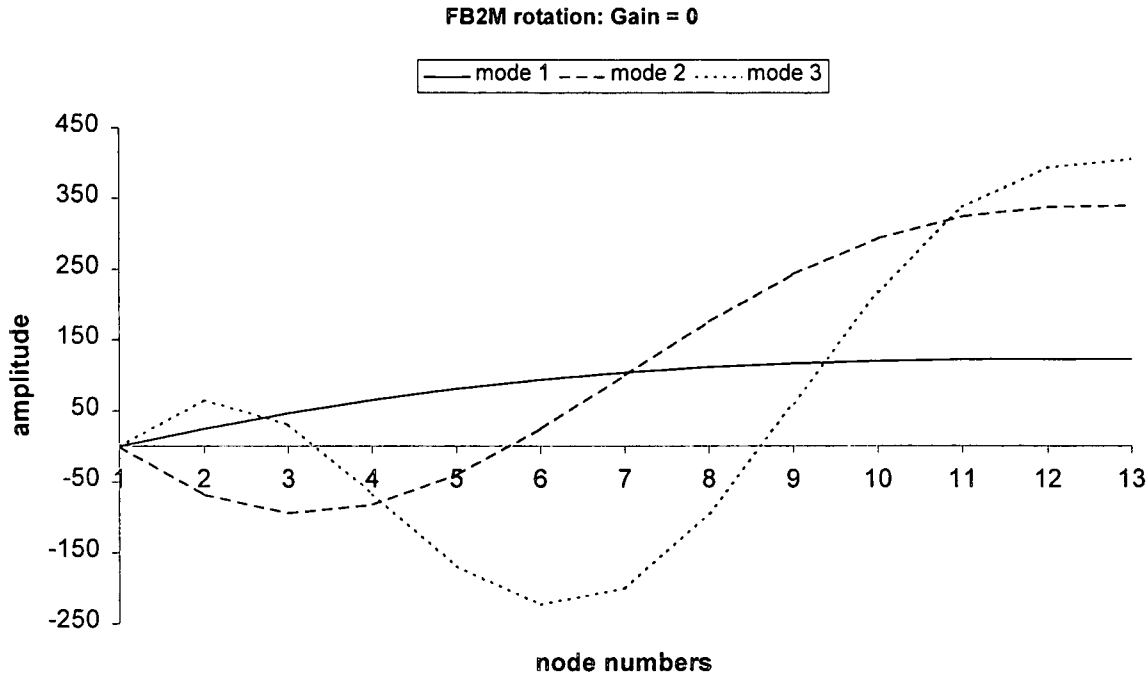

Figure 7.21 *Mode shapes for rotations using ACF2M at* $A_{ii} = 0,\ A_{ii} = 0$.

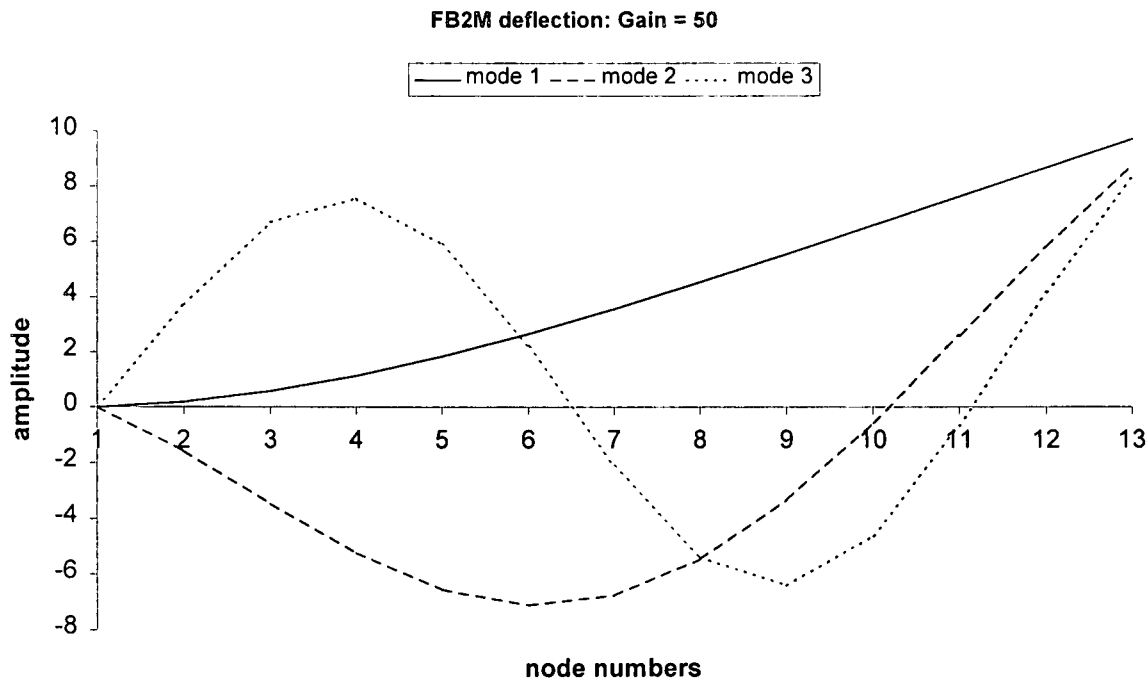

Figure 7.22 *Mode shapes for deflections using ACF2M at* $A_{ii} = 0,\ A_{ii} = 50$.

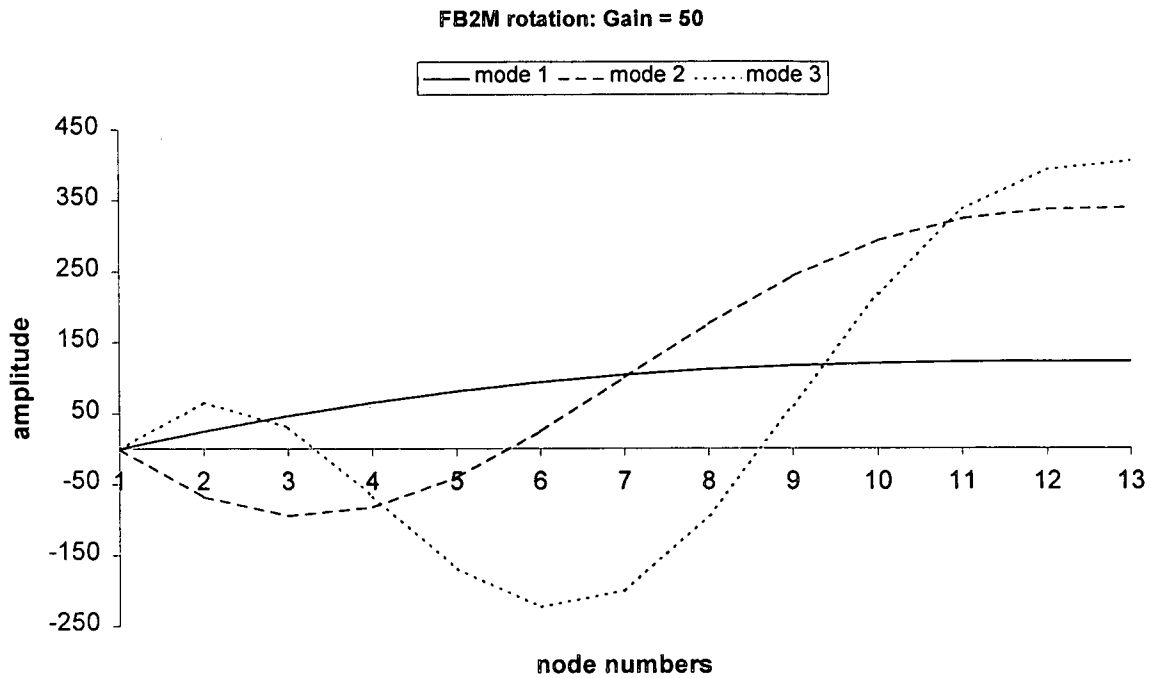

Figure 7.23 *Mode shapes for rotations using ACF2M at* $A_{ii} = 0,\ A_{u} = 50$.

For the condition $A_{u} = 0$, the ACF2 and ACF2M models yielded the same fundamental frequency whereas the ACF1 model yielded a higher fundamental frequency. It follows that the ACF1 model introduced an additional stiffness for this condition. This is a result of piezoelectric effects persisting when $A_{ii} = 0$, a phenomenon characteristic of this model. However, ACF2 and ACF2M models allowed no piezoelectric effects at this condition. Both models resemble a structure without feedback capability for this condition. Hence, the fundamental frequencies for the passive structure, ACF2 and ACF2M are the same.

The condition $A_{ii} = 0,\ A_{u} = 50$, ACF1 yielded a fundamental frequency almost three times the one obtained when $A_{u} = 0$. Referring to Figure 7.14, it can be seen that there is a large influence of rigid body motion on the fundamental frequency. Figure 7.15 shows that the

rotations are locked at inter-element nodes. This behaviour was observed in the time response as well – see Figure 7.5, indicating that the piezoelectric feedback introduces an extremely high stiffness which penalises, i.e. disallowing any movement on, the affected nodal variables. It is worth mentioning at this stage that the piezoelectric effect introduces ill-conditioning in the combined – elastic and piezoelectric – stiffness matrix which is evident in Figure 7.15.

For the ACF2 and ACF2M models, their mode shapes look similar with mode shapes characteristic of an elastic structure. However, their fundamental frequencies are not the same. The ACF2 model yielded a higher fundamental frequency than the ACF2M model. Also, the effects of locking on the ACF2 model are not as large as those observed when using ACF1.

7.4 Conclusion

This report detailed a study conducted to investigate the dynamic stability of the existing active control model (ACF1) of a composite structure embedded with a piezoelectric sensor and actuator for the purpose of vibration measurement and control. Criteria for stability were established based on the second method of Lyapunov which considers the energy of the system. Results showed that ACF1 is asymptotically stable although piezoelectric control effects persist when the feedback gain is set to zero. Meanwhile, it is required that there should be no control effects through the piezoelectric actuator when the gain is set to zero. Hence, a new active control model (ACF2) was developed to satisfy the stability criteria, resulting in the requirement of no piezoelectric control effects when the gain is set to zero.

In ACF1 and ACF2, the displacement and potential fields are discretised using the finite element method. In light of the locking phenomena associated with discrete displacements – which were expected to be pronounced in the case of discrete potentials due to their element geometry, ACF2-mixed was developed. ACF2 and ACF2-mixed control methodologies are similar except that in ACF2 both the displacement and potential field are discretised whereas in ACF2-mixed only the displacement field is discretised.

In addition to stability analysis of the ACF2 and ACF2-mixed, convergence, stability and accuracy analysis of the time integration scheme were investigated. The outcome showed that the numerical integration scheme exhibits second order accuracy. Also, the stability of the numerical scheme does not depend only on the parameters of Newmark, as is the case in the computation of passive structures. The feedback gain also has a role in the stability of the numerical scheme. By satisfying requirements for both the parameters of Newmark and the feedback gain, unconditional stability can be guaranteed.

With these requirements in mind, numerical results were generated for ACF1, ACF2 and ACF2-mixed. These results show that ACF1 exhibits extreme damping effects. This is attributed to mesh locking. In ACF2, this phenomenon is also observed but relaxed in comparison to ACF1. ACF2-mixed yielded the envisaged results in that damping effects were small at low feedback gain and increased with an increase in the feedback gain. Therefore, ACF2(-mixed) is envisaged to provide engineers with an alternative simulation model to solve actively controlled vibration problems hitherto.

7.5 References

1. BATHE K [1996] *Finite element procedures*, pub. Prentice Hall.
2. CHANDRASHEKHARA K AND DONTHIREDDY P [1997], Vibration suppresion of composite beams with piezoelectric devices using a higher order theory, *Eur. J. Mech. A/Solids*, **16**, no. 4, 709-721.
3. D'AZZO J J AND HOUPIS C H [1981], *Linear Control System Analysis and Design: Conventional and Modern*, 2nd ed., pub. McGraw-Hill.
4. D'AZZO J J AND HOUPIS C H [1995], *Linear Control System Analysis and Design: Conventional and Modern*, 4th ed., pub. McGraw-Hill.
5. IRONS B AND SHRIVE N G [1987], *Numerical Methods in Engineering and Applied Science: Numbers are fun*, pub. Ellis Horwood.
6. KEKANA M AND BADUR J [2000], Modelling of Beams using the Reduced Integration Technique: Statics and Free Vibrations, *R & D Journal*, **16**, no. 1, 9-15.
7. RAVEN F H [1995], *Automatic Control Engineering*, 5th ed., pub. McGraw-Hill.
8. WEAVER W JR., TIMOSHENKO S P AND YOUNG D H [1990], *Vibration problems in engineering*, 5th ed., pub. John Wiley & Sons.

A Appendix

A.1 1-D formulation for ACF2-mixed

Consider a composite beam of constant thickness h and width b, as shown in Figure A.1. It is defined in the Cartesian co-ordinates x, y and z with axes x and y laying on the middle surface of the beam. The origin of the co-ordinate system is located on the middle surface of the beam with the z-axis normal to the middle surface. The ACF2-mixed is given in equation (5.22) as

$$\boldsymbol{M}_{uu}\ddot{\tilde{\boldsymbol{u}}} + \left[\boldsymbol{C}_R + \boldsymbol{K}_{u\nabla}\boldsymbol{A}_{\dot{u}}\boldsymbol{K}_{\phi\nabla}\right]\dot{\tilde{\boldsymbol{u}}} + \boldsymbol{K}_{uu}\tilde{\boldsymbol{u}} = \tilde{\boldsymbol{F}} \tag{A.1}$$

In the present study, a first order shear deformable theory is employed to investigate the problem and the following displacement field is assumed

$$\boldsymbol{u}(x,y,z,t) = \boldsymbol{u}_0(x,t) + z\boldsymbol{u}_1(x,t) = \begin{Bmatrix} 0 \\ -w \end{Bmatrix} + z\begin{Bmatrix} \theta_x \\ 0 \end{Bmatrix} \tag{A.2}$$

where w represents the displacement of the reference surface in the z direction and θ_x the rotation of the transverse normal about the y axis.

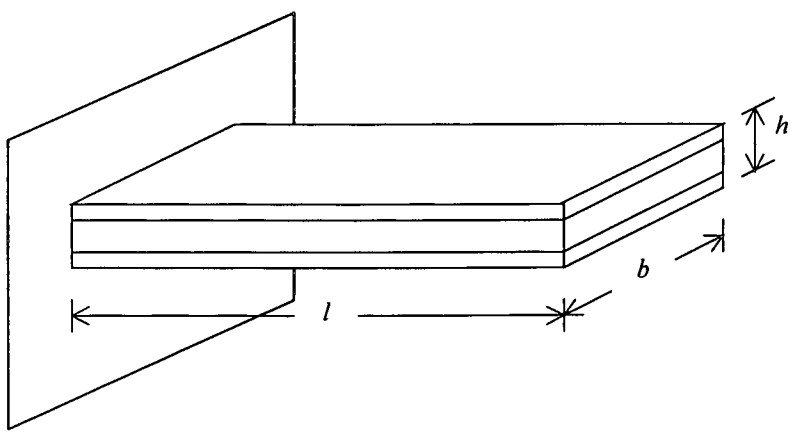

Figure A.1 A *schematic showing the dimensions of the built-in beam.*

The discrete displacements are given as

$$\begin{Bmatrix} -w \\ \theta_x \end{Bmatrix} = \begin{bmatrix} -N_{ui} & 0 \\ 0 & N_{ui} \end{bmatrix} \begin{Bmatrix} \tilde{w}_i \\ \tilde{\theta}_{xi} \end{Bmatrix} = \boldsymbol{N}_u \tilde{\boldsymbol{v}} \tag{A.3}$$

where $i \in 1,2,...,n$ represents the node number of the element associated with the displacement $\boldsymbol{u}$ and n the number of nodes of the displacement element. The strains associated with the displacements are

$$\begin{Bmatrix} \varepsilon_{xx} \\ \gamma_{xz} \end{Bmatrix} = \begin{bmatrix} 0 & z\frac{\partial N_u}{\partial x} \\ -\frac{\partial N_u}{\partial x} & N_u \end{bmatrix} \begin{Bmatrix} \tilde{w}_i \\ \tilde{\theta}_{xi} \end{Bmatrix} = \begin{bmatrix} z\boldsymbol{B}_1 \\ \boldsymbol{B}_2 \end{bmatrix} \{\tilde{\boldsymbol{v}}\} \tag{A.4}$$

Consider the term: $\boldsymbol{M}_{uu}\ddot{\tilde{\boldsymbol{u}}} = \int_{\Omega} \boldsymbol{N}_u^T \rho \boldsymbol{N}_u d\Omega$

The elemental contribution on the domain Ω may be represented as

$$\boldsymbol{M}_{uu}\ddot{\tilde{\boldsymbol{u}}} = \sum_{e=1}^{nelem} \int_{\Omega^e} \boldsymbol{N}_u^T \rho \boldsymbol{N}_u d\Omega^e \tag{A.5}$$

where $e \in 1,2,...,nelem$ represents the element number, *nelem* the number of elements and Ω^e the sub-domain of Ω. Upon substituting the displacements given in equation (A.2)and taking

$$(\rho_1, \rho_{zz}) = \sum_{k=1}^{nlayer} \int_{h_{k-1}}^{h_k} \rho(1, z^2) dz \tag{A.6}$$

where $k \in 1,2,...,nlayer$ represents the layer number and *nlayer* the number of orthotropic layers in a laminate, the elemental mass matrix becomes

$$\boldsymbol{M}_{uu}\ddot{\tilde{\boldsymbol{u}}} = \sum^{nelem} \int_0^b dy \int_{-1}^{1} \begin{bmatrix} N_{ui} & 0 \\ 0 & N_{ui} \end{bmatrix} \begin{bmatrix} \rho_1 & 0 \\ 0 & \rho_{zz} \end{bmatrix} \begin{bmatrix} N_{ui} & 0 \\ 0 & N_{ui} \end{bmatrix} \begin{Bmatrix} \ddot{\tilde{w}}_i \\ \ddot{\tilde{\theta}}_{xi} \end{Bmatrix} J_\xi \, d\xi \tag{A.7}$$

where J_ξ represents the Jacobian transformation in the x direction.

Similarly, the elemental stiffness matrix is given as

$$\boldsymbol{K}_{uu}\tilde{\boldsymbol{u}} = \sum^{nelem} \int_0^h dy \int_{-1}^{1} \begin{bmatrix} \boldsymbol{B}_{1i} \\ \boldsymbol{B}_{2i} \end{bmatrix}^T \begin{bmatrix} \overline{C}_{zz} & 0 \\ 0 & \overline{C}_1 \end{bmatrix} \begin{bmatrix} \boldsymbol{B}_{1i} \\ \boldsymbol{B}_{2i} \end{bmatrix} \begin{Bmatrix} \tilde{w}_i \\ \tilde{\theta}_{xi} \end{Bmatrix} J_\xi \, d\xi \tag{A.8}$$

where $(\overline{C}_1, \overline{C}_{zz}) = \int_{h_{k-1}}^{h_k} (\breve{C}_{55}, z^2 \breve{C}_{11}) dz$ and

$$\begin{aligned} \breve{C}_{11} &= \overline{C}_{11} + \left(\frac{\overline{C}_{16}\overline{C}_{26} - \overline{C}_{12}\overline{C}_{66}}{\overline{C}_{22}\overline{C}_{66} - \overline{C}_{26}^2} \right) \overline{C}_{12} + \left(\frac{\overline{C}_{12}\overline{C}_{26} - \overline{C}_{22}\overline{C}_{16}}{\overline{C}_{22}\overline{C}_{66} - \overline{C}_{26}^2} \right) \overline{C}_{16} \\ \breve{C}_{55} &= \overline{C}_{55} - \frac{\overline{C}_{45}^2}{\overline{C}_{44}} \end{aligned} \tag{A.9}$$

The constants $\breve{C}_{ii}$ are obtained by incorporating the condition $\sigma_y = \tau_{xy} = \tau_{yz} = 0$ in the plate formulation while assuming $\varepsilon_y \neq \gamma_{xy} \neq \gamma_{yz} \neq 0$. Thus reducing the two-dimensional problem to a one-dimensional one (Chandrashekhara and Donthireddy, 1997).

Consider the term: $\boldsymbol{K}_p \ddot{\tilde{\boldsymbol{u}}} = \boldsymbol{K}_{u\nabla} A_{\ddot{u}} \boldsymbol{K}_{\phi\nabla} \ddot{\tilde{\boldsymbol{u}}} = \int_\Omega \boldsymbol{B}_u^T \overline{\boldsymbol{e}}_A A_{\ddot{u}} \overline{\boldsymbol{g}}^{-1} \overline{\boldsymbol{e}}_S{}^T \boldsymbol{B}_u \ddot{\tilde{\boldsymbol{v}}} d\Omega$

where A and S represents the piezoelectric actuator and sensor layers, respectively. The elemental contribution on the domain Ω may be represented as

$$\boldsymbol{K}_p \ddot{\tilde{\boldsymbol{u}}} = \sum_{e=1}^{nelem} \int_{\Omega^e} \boldsymbol{B}_u^T \overline{\boldsymbol{e}}_A A_{\ddot{u}} \overline{\boldsymbol{g}}^{-1} \overline{\boldsymbol{e}}_S{}^T \boldsymbol{B}_u \ddot{\tilde{\boldsymbol{v}}} d\Omega^e \tag{A.10}$$

The coupled elemental piezoelectric matrix becomes

$$\boldsymbol{K}_p \ddot{\tilde{\boldsymbol{u}}} = A_{\ddot{u}} \sum^{nelem} \int_0^h dy \int_{h_{k-1}}^{h_k} z^2 dz \int_{-1}^{1} \begin{bmatrix} \boldsymbol{B}_{1i} \\ \boldsymbol{B}_{2i} \end{bmatrix}^T \begin{bmatrix} \overline{e}_{13} \\ 0 \end{bmatrix} \overline{g}_{33}^{-1} \begin{bmatrix} \overline{e}_{13} & 0 \end{bmatrix} \begin{bmatrix} \boldsymbol{B}_{1i} \\ \boldsymbol{B}_{2i} \end{bmatrix} \begin{Bmatrix} \ddot{\tilde{w}}_i \\ \ddot{\tilde{\theta}}_{xi} \end{Bmatrix} J_\xi \, d\xi \tag{A.11}$$

A.2 1-D formulation for ACF2-mixed

The ACF2, equation (3.47), is rewritten for convenience here as

$$\boldsymbol{M}_{uu}\ddot{\tilde{\boldsymbol{u}}} + \boldsymbol{K}_{u\phi}A_{ii}\boldsymbol{K}_{\phi\phi}^{-1}\boldsymbol{K}_{\phi u}\dot{\tilde{\boldsymbol{u}}} + \boldsymbol{K}_{uu}\tilde{\boldsymbol{u}} = \tilde{\boldsymbol{F}} \tag{A.12}$$

The potential field is approximated by discrete potentials as

$$\phi = N_{\phi j}\tilde{\phi}_j = \boldsymbol{N}_{\phi}\tilde{\boldsymbol{\phi}} \tag{A.13}$$

where $j \in 1,2,...,m$ represents the node number of the element associated with the potential ϕ and m the number of nodes of the potential element. The position in the thickness, i.e. z-direction, is interpolated with the same functions as $z = N_{\phi j}z_j$. The gradient of the potential in the thickness direction is given as $\phi_{,z} = \boldsymbol{N}_{\phi,z}\tilde{\boldsymbol{\phi}} = \boldsymbol{B}_{\phi}\tilde{\boldsymbol{\phi}}$, where the variable after the comma denotes differentiation with respect to the variable.

Consider the matrix: $\boldsymbol{K}_{\phi u} = \int_{\Omega}\boldsymbol{B}_{\phi}^{T}\bar{\boldsymbol{e}}^{T}\boldsymbol{B}_{u}d\Omega = \boldsymbol{K}_{u\phi}^{T}$

The elemental contribution on the domain Ω may be represented as

$$\boldsymbol{K}_{\phi u} = \sum_{e=1}^{nelem}\int_{\Omega^e}\boldsymbol{B}_{\phi}^{T}\bar{\boldsymbol{e}}^{T}\boldsymbol{B}_{u}d\Omega^{e} \tag{A.14}$$

The coupled piezoelectric matrix becomes

$$\boldsymbol{K}_{\phi u} = \sum^{nelem}\int_{0}^{h}dz\int_{-1}^{1}\left[B_{\phi j}\right]^{T}\left[N_{\phi k}\right]\{z_k\}J_{\eta}d\eta\int_{-1}^{1}\begin{bmatrix}\boldsymbol{B}_{1i}\\ \boldsymbol{B}_{2i}\end{bmatrix}J_{\xi}d\xi \tag{A.15}$$

Consider the matrix: $\boldsymbol{K}_{\phi\phi} = \int_{\Omega}\boldsymbol{B}_{\phi}^{T}\bar{\boldsymbol{g}}\boldsymbol{B}_{\phi}d\Omega$

The elemental contribution on the domain Ω may be represented as

$$\boldsymbol{K}_{\phi\phi} = \sum_{e=1}^{nelem}\int_{\Omega^e}\boldsymbol{B}_{\phi}^{T}\bar{\boldsymbol{g}}\boldsymbol{B}_{\phi}d\Omega^{e} \tag{A.16}$$

The elemental dielectric matrix becomes

$$K_{\phi\phi} = \sum^{nelem} \int_0^l dx \int_0^h dy \int_{-1}^{1} [B_{\phi j}]^T \bar{g}_{33} [B_{\phi j}] J_\eta d\eta \tag{A.17}$$

where J_η represents the Jacobian transformation in the z direction.